ABSTRACT

Title of dissertation: A NATURAL EXTENSION OF STANDARD WARPED HIGHER-DIMENSIONAL COMPACTIFICATIONS: THEORY AND PHENOMENOLOGY

Sungwoo Hong, Doctor of Philosophy, 2017

Dissertation directed by: Professor Kaustubh Agashe
Department of Physics

Warped higher-dimensional compactifications with "bulk" standard model, or their AdS/CFT dual as the purely 4D scenario of Higgs compositeness and partial compositeness, offer an elegant approach to resolving the electroweak hierarchy problem as well as the origins of flavor structure. However, low-energy electroweak/flavor/CP constraints and the absence of non-standard physics at LHC Run 1 suggest that a "little hierarchy problem" remains, and that the new physics underlying naturalness may lie out of LHC reach. Assuming this to be the case, we show that there is a simple and natural extension of the minimal warped model in the Randall-Sundrum framework, in which matter, gauge and gravitational fields propagate modestly different degrees into the IR of the warped dimension, resulting in rich and striking consequences for the LHC (and beyond).

The LHC-accessible part of the new physics is AdS/CFT dual to the mechanism of "vectorlike confinement", with TeV-scale Kaluza-Klein excitations of the gauge and gravitational fields dual to spin-0,1,2 composites. Unlike the mini-

mal warped model, these low-lying excitations have predominantly flavor-blind and flavor/CP-safe interactions with the standard model. In addition, the usual leading decay modes of the lightest KK gauge bosons into top and Higgs bosons are suppressed. This effect permits erstwhile subdominant channels to become significant. These include flavor-universal decays to all pairs of SM fermions, and a novel channel decay to a radion and a SM gauge boson, followed by radion decay to a pair of SM gauge bosons. We present a detailed phenomenological study of the latter cascade decay processes.

Remarkably, this scenario also predicts small deviations from flavor-blindness originating from virtual effects of Higgs/top compositeness at O(10) TeV, with subdominant resonance decays into a pair of Higgs/top-rich final states, giving the LHC an early "preview" of the nature of the resolution of the hierarchy problem. Discoveries of this type at LHC Run 2 would thereby anticipate (and set a target for) even more explicit explorations of Higgs compositeness at a 100 TeV collider, or for next-generation flavor tests.

A NATURAL EXTENSION OF STANDARD WARPED HIGHER-DIMENSIONAL COMPACTIFICATIONS: THEORY AND PHENOMENOLOGY

by

Sungwoo Hong

Dissertation submitted to the Faculty of the Graduate School of the
University of Maryland, College Park in partial fulfillment
of the requirements for the degree of
Doctor of Philosophy
2017

Advisory Committee:
Professor Kaustubh Agashe, Chair/Advisor
Professor Zackaria Chacko
Professor Sarah Eno
Professor Rabindra Mohapatra
Professor Raman Sundrum
Professor Richard Wentworth

Dedication

To Yoojin

Acknowledgments

I owe a great debt of gratitude to all those who have made the completion of this work possible and thanks to whom my life as a graduate student has been full of excitement.

To the greatest extent, I would like to express my deep appreciation to my advisor, Professor Kaustubh Agashe for providing me with an invaluable opportunity to work with him on various exciting and thought-provoking projects. The process of learning from him and working with him has been truly amazing and I owe an enormous debt to him. Every discussion with him was fruitful and inspiring. I thank the limitless patience and diligence he has shown during our discussion, answering countless questions I had. Even outside the academic life, he has always been willing to listen to my personal concerns and reach out to help. It has been a great pleasure to be his student and work with him.

I would also like to thank Professor Zackaria Chacko for offering me a precious chance to work with him on several projects and providing great guidance in the early stage of my life at the graduate school. Also, without his help and encouragement, it would have been impossible for me to learn about cosmology and physics of dark matter as much as I have done. His generosity and strong friendship offer me freedom to speculate freely, resulting in unbounded discussion.

I would like to acknowledge priceless learning, help and advice from Professor Raman Sundrum. Undoubtedly, his extraordinarily deep understanding of everything has been a strong inspiration throughout my time here at the University of

Maryland. He has demonstrated conceivably the highest level of standards for the way particle physicists think and I have been so lucky to be able to learn quantum field theory and theories beyond it from him. Moreover, his great leadership and friendship will be unforgettable.

Thanks are due to Professor Rabindra Mohapatra, Professor Sarah Eno and Professor Richard Wentworth for agreeing to serve on my thesis committee and for sparing their invaluable time reviewing the manuscript.

Interactions with other members of the Maryland Center for Fundamental Physics has also been indispensable in reaching my goal. I thank Professor Ted Jacobson, Professor Rabindra Mohapatra, Professor Tom Cohen, Professor Paulo Bedaque, and Professor Sarah Eno for active interactions, discussions and their considerations.

I have been so lucky to have many wonderful people to collaborate with. Their interactions, corrections, patience, and sharing their expertise and passion with me are greatly appreciated. They include Professor Takemichi Okui, Yanou Cui, Yuhsin Tsai, Luca Vecchi, Roberto Franceschini, Doojin Kim, Jack Collins, Rashmish Mishra and Peizhi Du.

Many fellow graduate students and post-docs have had very important influences and interactions with them has been very fruitful. I would like to thank David Curtin, Kaustubh Deshpande, Majid Ekhterachian, Anton de la Fuente, Michael Geller, Soubhik Kumar, Chang Hun Lee, Arif Mohd, Simon Riquelme, Prashant Saraswat, Antony Speranza, and Christopher Verhaaren.

I would also like to acknowledge help and financial support from Maryland

Center for Fundamental Physics (MCFP), National Science Foundation (NSF), and The Kwanjeong Educational Foundation in South Korea.

I appreciate my parents and parents-in-law for their unlimited spiritual, emotional, and financial support.

I owe my deepest thanks to my wife Yoojin. It is an obvious fact that without her support, in every aspect, I would have never been able to get to the point where I am standing. In every single moment in my life as a graduate student, it has been her heartwarming encouragement and strong friendship that make my achievement possible.

I apologize to those I have inadvertently left out.

Thanks to all.

Table of Contents

List of Figures

List of Abbreviations

AdS	Anti-de Sitter
BSM	Beyond the Standard Model
CFT	Conformal Field Theory
DM	Dark Matter
EFT	Effective Field Theory
EW	Electroweak
EWPT	Electroweak Precision Test
EWSB	Electroweak Symmetry Breaking
GeV	Giga electron-volt
GIM	Glashow-Iliopoulos-Maiani mechanism
IR	Infrared (= low energy or long distance)
KK	Kaluza-Klein
LEP	Large Electron-Positron
LHC	Large Hadron Collider
MeV	Mega electron-volt
PNGB	Pseudo-Nambu-Goldstone-Boson
QCD	Quantum Chromodynamics
QED	Quantum Electrodynamics
QFT	Quantum Field Theory
QM	Quantum Mechanics
RS	Randall-Sundrum
SM	Standard Model (of Particle Physics)
SR	Special Relativity
UV	Ultraviolet (= high energy or short distance)
VEV	Vacuum Expectation Value
YM	Yang-Mills
4(5)D	four(five) dimensional

Chapter 1: Introduction

Particle physics is about understanding fundamental laws of nature in a unified fashion. To this end, it is required to figure out what constitutes the Universe we live in and what interactions cause the dynamics responsible for the phenomena we observe. Over the past decades, we have learnt that seemingly elementary particles, such as hydrogen atom or pion, are secretly composite states, having substructures on even smaller length scales, i.e. made up of even more fundamental particles, like electron or quarks. We have also understood that different forces are responsible for binding constituent particles for different composite particles. For hydrogen atom, it is electromagnetic force that binds a proton and an electron. For pion, it is strong nuclear force that binds quarks together. For nuclei of heavy atoms, it is the remnant of strong nuclear force that holds protons and neutrons together. Revelation of such surprising truths has been pursued by zooming in on smaller and smaller length scales and by observing what happens at such length scale. This, in turn, is achieved by colliding two particles at higher and higher energies and by measuring outcomes in a systematic way. Physics at such small length scales with very high energy is full of both *quantum mechanical* and *relativistic* effects. For this reason, development of unified framework of quantum mechanics (QM) and special

relativity (SR) was the crucial step in making progress in particle physics. The special relativity requires physics to respect Poincaré invariance: rotation, translation, and Lorentz boost. The quantum mechanics, on the other hand, asks information about a physical state, e.g. mass, momentum, and spin, to be encoded as a state in the physical Hilbert space and the time evolution of such state to be dictated by unitary transformation. In quantum mechanics, the output of the theory is a set of probabilities for a given physical state to have non-trivial overlaps with eigenstates of observable operators in question. The unitarity of the time evolution operator is, then, the requirement of the conservation of probability. By the same token, the symmetry transformations of Poincaré group should be realized as either linear and unitary or anti-linear and anti-unitary operators in the physical Hilbert space. The synthesis of relativity and quantum mechanics[1], however, turned out to be much more challenging and tighter than simply representing Lorentz transformations as unitary operators. The ultimate product was the *relativistic quantum field theory* (QFT) [1]. Among many astonishing features that QFT predicts are the existence of anti-particles: particles that possess the same mass and spin as the corresponding particles, but have opposite charges. In other words, consistency with principles of QM and SR requires anti-particles to exist. This is one example that shows how robust the progress of particle physics has been.

In QFT, a *particle* at a spacetime point is realized as local quantum fluctuations of the corresponding quantum field at that point. *Interactions* among particles

[1]To be more precise, it is the union of relativity, quantum mechanics and principle of cluster decomposition. The principle of cluster decomposition is a notion of *locality*. Intuitively, this states that the probability of two events occurring with large enough separation should be factorized into probabilities for each event to happen. See [1] for more details.

are represented as local, Lorentz invariant product of corresponding quantum fields. For example, as proposed by Enrico Fermi in 1933 [2], the beta decay, i.e. decay of a neutron (n) to a proton (p), an electron (e) and an electron anti-neutrino ($\bar{\nu}_e$), can be effectively explained by the local interaction

$$G_F \, (\bar{u}d) \, (\bar{\nu}_e e) \, , \tag{1.1}$$

where u (d) denotes up (down) quark inside proton (neutron) and G_F, called the Fermi constant, parametrizes the strength of the interaction. In the same way, we can describe the decay of muon to an electron, an electron anti-neutrino, and a muon neutrino, $\mu^- \to e^- \bar{\nu}_e + \nu_\mu$, and the measurement of the muon lifetime provides a way of determining the Fermi constant very precisely: $G_F = 1.1663787(6) \times 10^{-5}$ GeV^{-2} [3]. Above described four-fermion operators can also describe scattering process of two incoming fermions into two outgoing fermions. The probability for such a scattering to happen is understood in terms of a cross section (σ). In weakly coupled QFT, the computation is performed perturbatively. That is, for a given process, one finds connected Feynman diagrams for the process using interaction vertices in the theory, order by order in coupling constant(s), and computes the amplitude using Feynman rules. The largest contribution comes from the diagram(s) of lowest order in coupling(s). For the above Fermi's theory, the leading order cross section is given by[2]

$$\sigma \sim G_F^2 E^2 \approx \frac{E^2}{(293 \text{ GeV})^4}, \tag{1.2}$$

[2]We neglect $\mathcal{O}(1)$ constants, which is irrelevant for the discussion.

where E is the center of mass energy. It is clearly seen from Eq. (1.2) that the odds for the process to occur increases indefinitely (quadratic in E) and as the energy approaches $G_F^{-1/2} \approx 293$ GeV the prediction of the theory reveals internal inconsistency. Namely, either the unitarity of quantum mechanics is violated (since the probability increases arbitrarily) or the theory becomes strongly coupled at high energies (since the perturbative computation based on the assumption of weak coupling gives wrong answer). One way or the other, this signals the breakdown of the theory. This is one good example of *effective field theory* (EFT). Provided that the physics is described by local interactions and that there is no correlation among vastly different length scales, one can construct an EFT valid up to some energy scale, often called cut-off of the EFT. The idea is that, in order to describe physics at an energy scale of interest, one does not need to know every physics at much higher energy scale. Instead, one can obtain a reliable and consistent coarse-grained description, in which the physics on much smaller length scale is effectively captured in a series of local operators among degrees of freedom appearing at a low energy. Therefore, one obtains an EFT by first identifying relevant degrees of freedom and by writing down all possible local operators consistent with the symmetries of the theory. Effective field theory is a very powerful way of studying physics. After all, one would not want to know every interactions among quarks and electrons in order to compute and understand thermodynamic properties of water. EFT may or may not be renormalizable. Renormalizable QFTs are field theories in which every ultraviolet (UV) divergence appearing in the loop calculations can be absorbed into existing finite number of parameters of the theory. This is equivalent

to the statement that the theory does not encounter any kind of inconsistency as the cut-off sent to infinity. As we saw from the example of Fermi's theory, non-renormalizable EFTs, on the other hand, break down at some cut-off scale. Around the cut-off scale, new physics must appear in order to recover validity of the theory. Such a new theory, embedding the low energy EFT, extends the validity of EFT and is called UV-completion of infrared (IR) EFT. UV-completion of an EFT may be another EFT, which in turn may or may not be renormalizable. The Fermi's theory of four-fermion interaction discussed above turned out to be the IR EFT of the weak interaction of standard model (SM) of particle physics. Before the energy scale reaches the cut-off scale, the local four fermion operator gets resolved by the physical exchange of massive vector bosons, known as $W^{\pm}$ (for charged vector current) or Z (for neutral vector current), between fermion currents. It is a well-known fact that a manifestly Lorentz invariant and unitary description of *massless* spin-1 particle should be in the form of gauge theory. This is true for both abelian, i.e. $U(1)$, and non-abelian, i.e. Yang-Mills (YM), gauge theories. If we make the gauge field *massive*, however, things get a bit subtler. In both cases, gauge invariance is lost. However, given that gauge invariance is merely a redundancy of description to keep manifest Lorentz invariance and unitarity, this is not a real problem. In order to figure out the trouble caused by the bare mass term, we focus on additional degree of freedom generated by the mass term, i.e. the longitudinal modes, and study processes among them. Namely, we consider $2 \to 2$ scattering process of longitudinal modes. For the $U(1)$ case, due to the lack of self-interactions, there is no amplitude for such scattering. For the YM case, considering $W_L^+ W_L^- \to W_L^+ W_L^-$ scattering as

a concrete example, one finds that the tree-level amplitude for the elastic scattering grows as E^2 and this is a clear indication that perturbative unitarity will break down at some scale. A careful partial wave amplitude analysis shows that the loss of perturbative unitarity in the s-wave scattering occurs at $\sqrt{s} \approx 3$ TeV. What we learn from this is that the theory of massive W's and Z gauge bosons, as a UV-completion of Fermi's theory, breaks down around TeV scale and calls for yet another UV-completion. The very same situation can be phrased differently in terms of electroweak (EW) symmetry breaking as follows. In the limit that W's and Z are massless, together with photon, the theory respects a gauge invariance: EW symmetry $SU(2)_L \times U(1)_Y$. We know, on the other hand, that W's and Z are massive in reality and adding mass terms by hand triggers breakdown of the theory at some high scale. Thus, explicitly breaking EW symmetry via mass terms seems to the source of the problem. We need a different way of breaking electroweak symmetry. Therefore, studying UV-completion of theory of massive W's and Z is nothing but understanding the nature of electroweak symmetry breaking (EWSB).

1.1 The Higgs Boson

The UV-completion of the theory of massive EW gauge bosons may be done in a weakly coupled fashion at the scale somewhat below the actual cut-off scale. Or, it may well happen that the UV theory is strongly coupled and new strong dynamics appears near the actual cut-off scale. Logically, both are equally possible options. For the former, EWSB is triggered by the vacuum expectation value (VEV) of

elementary scalar field and, for the latter, it is induced by confinement of some new strong dynamics. Interestingly, the nature has chosen the second path once in the context of quantum chromodynamics (QCD)[3]: the quark condensate spontaneously breaks approximate flavor symmetry of quark sector diagonally, $SU(3)_L \times SU(3)_R \to SU(3)_V$, and as a result eight Pseudo-Nambu-Goldstone Bosons (PNGB) appear ($\pi^{\pm}, \pi^0, K^{\pm}, K^0$, and η). It may be a natural guess that this would happen again for EWSB. However, the discovery of a new scalar particle, the Higgs boson, at the Large Hadron Collider (LHC) in 2012 [4,5] seems to say otherwise. The mass of the Higgs is about $M_H \approx 125$ GeV [6] and so far its properties are consistent with the SM prediction that the Higgs is *elementary* particle, has no spin, is its own anti-particle, is CP-even, and has zero electric and color charge [7–9]. If this turns out to be ultimately true, then EW symmetry is broken by VEV of elementary scalar particle of mass about 125 GeV, and the theory of massive weak gauge bosons is UV-completed by a weakly coupled theory of elementary scalar.

1.2 The Naturalness

Achieving precise understanding of the properties of the Higgs boson is an extremely important goal: whether it is elementary or composite, whether it is CP-even or CP-odd, whether it precisely has the couplings predicted by the SM, and so on. If the Higgs boson is really an elementary scalar, it is the first fundamental scalar particle we have ever discovered. And it is this fact that surprises us and, at

[3] As a matter of fact, the confinement of QCD strong dynamics does induce spontaneous breaking of EW symmetry. It is just that this is a sub-dominant effect.

the same time, makes us feel uncomfortable. This is because very light (compared to the cut-off scale) elementary scalar particle signals large amount of fine-tuning in order to explain the smallness of its mass, unless the theory is secretly embedded in a larger theory with specific structure to make the small mass natural. The SM, from a pure field theory viewpoint, is well-defined all the way up to the Planck scale, where gravity becomes strongly coupled and quantum gravity effects start becoming significant.[4] If no physics beyond-the-SM (BSM) exists between the weak scale ($\sim$ Higgs mass) and the Planck scale of $M_{\rm Pl} \sim 10^{19}$ GeV, i.e. the SM is truly valid up to the Planck scale, then the hierarchy in mass squared between the weak scale and the Planck scale is about 10^{34}. This can be translated into the hierarchy in the strength of gravitational interaction and the weak interaction. Namely, the ratio of the Newton's constant, $G_N \sim M_{\rm Pl}^{-2}$, to the Fermi constant, $G_F \sim M_H^{-2}$, is given by $G_N/G_F \sim 10^{-34}$: gravity is weaker than the weak interaction, the weakest one among all three gauge interactions, by 34 orders of magnitude!

In order to demonstrate the seriousness of the problem, consider the following situation.[5] Suppose we have a thermodynamic system of a large number of particles at a temperature T. A particle in this system will repeat the processes of propagating freely and colliding with others, eventually setting in thermal equilibrium with its total energy of the order of T. Now, let us imagine adding one particle, called "Higgs boson", to the system and it is initially at rest with total energy equal to its mass.

[4] Of course, there are other reasons to believe that the SM is not complete and is only an EFT. For example, the SM does not provide explanations for the origin of neutrino masses, the dark matter (DM), and the asymmetry between baryons and anti-baryons. Moreover, gravity is not part of the SM, whether classical gravity or quantum one.

[5] I found this very nice analogy in Gian Giudice's article [10].

Assume that the mass is much smaller than the temperature of the system. Like any other particles do, collisions of "Higgs boson" with other particles will bring the "Higgs boson" in the thermal equilibrium and hence will set its energy to be of the order of T. Now, if we replace thermal fluctuations with quantum fluctuations, T with the cut-off scale Λ, and particles in the thermal bath with particles in the quantum vacuum, we can see how 'unnatural' the 125 GeV mass of the Higgs boson it is. The quantum vacuum is full of pair creation and annihilation of virtual particles. Just like "Higgs boson" in thermal bath gets interrupted and brought into thermal equilibrium by surrounding particles, as the Higgs boson propagates through the vacuum, it interacts with virtual particles and gets "equilibrated" in a sense that its mass gets quantum corrected. This tends to lift the mass of the Higgs close to the maximum amount of energy that virtual particles can borrow from the vacuum for short period of time (as long as it is allowed by Heisenberg's uncertainty principle), i.e. close to the cut-off scale of the theory.

In QFT, this phenomenon is understood from the fact that loop corrections to the Higgs mass from other particles are quadratically sensitive to the UV cut-off. One important lesson is that even if we accept that nature may set up parameters in a hierarchical way, quantum effects usually "wash" out such hierarchy and restore validity of naive dimensional analysis. In the case of the Higgs mass, then, the SM alone does not explain why the Higgs is so light compared to the cut-off scale and the only explanation is the fine-tuning (in mass squared) between the bare mass term and quantum corrections by one part in 10^{34}. If you do not find this suspicious, you should also not be surprised to see a solar system long pencil standing on a

table on its tip a millimeter wide, since it is the same amount of fine-tuning! [10] Although this issue of *naturalness* is certainly not a problem of logical inconsistency, it makes us think that something must be going on in order to stabilize the Higgs mass. However, precisely for the same reason, it is not obvious how to define and quantify the notion of naturalness. 't Hooft [11] provided a concrete formulation of naturalness criterion based on concepts of *symmetry* and *effective theory*. It says that it is natural for a parameter of the theory to be much smaller than unity only if setting it to zero enhances the symmetry of the theory. This concept of naturalness, often termed as technical naturalness, being based on the notion of effective theory, rules out the possibility of correlation of low energy dynamics (e.g. the Higgs mass) with physics at very short distances (via parameters appearing in the theory) and it looks for the reason behind the naturalness within low energy effective theory. 't Hooft's naturalness criterion applies well to a broad class of examples. For example, chiral symmetry emerges as we set the mass of fermion to zero. Similarly, setting the mass of spin-1 particle to zero make the theory respect gauge invariance. Finally, setting the mass of PNGB, e.g. pions and kaons, to zero enhances the shift symmetry. For all these cases, masses are protected by symmetries and as long as symmetries are not anomalous, this continues to be true even at quantum level. The problem with the fundamental scalar is that there is no symmetry that protects its mass from quantum corrections. A slightly non-trivial case is that of the mass splitting between charged and neutral pions induced by electromagnetic interaction. Up to

$\mathcal{O}(1)$ factor, the splitting in mass squared is given by

$$M_{\pi^+}^2 - M_{\pi^-}^2 \approx \frac{3\alpha}{4\pi}\Lambda^2 \tag{1.3}$$

where α is the fine structure constant. The measured value is $M_{\pi^+}^2 - M_{\pi^-}^2 = (35.5\text{MeV})^2$ [12]. Imagining that we are living in a time where we just discovered pions and measured the mass splitting without having an access to much higher energy, this question is qualitatively the same as the hierarchy problem of the Higgs mass. The splitting is quadratically sensitive to the cut-off scale and if the cut-off is much higher than GeV, then we will need to argue that there must be fine-tuning in order to match the measured value. On the other hand, if we believe the theory is natural and hence Eq. (1.3) is smaller than the measured value, we expect new physics to show up below 850 MeV. Indeed, a "new" particle, namely, the ρ meson, shows up at $M_\rho = 770$ MeV, and for energies above this, pion's composite substructure gets resolved, softening the electromagnetic effects. If we set the splitting to zero, then all pions are degenerate and isospin symmetry is restored (forgetting about other pseudoscalar mesons for now): symmetry of the theory increases as we set the splitting to zero. This is a great case in which nature has chosen the (technical) naturalness, instead of fine-tuning. We may hope that similar thing happens for the Higgs.

For decades, a vast array of work has been done exploring ideas beyond the SM that can explain naturalness of the Higss mass. These include technicolor [13], supersymmetric extension of the SM [14, 15], composite Higgs models [16–21], large

extra dimensions [22,23], warped extra dimensional models [24,25], and little Higgs models [26,27]. At the same time, there have been enormous amount of effort on the experimental side, including the Large Electron-Positron (LEP) collider (for e^+e^- collisions) and LHC (for hadron collisions) as high energy frontiers and electroweak precision test (EWPT) and flavor experiments as low energy precision frontiers, trying to test those ideas. Discovery of physics beyond the SM with the properties predicted by any of the above ideas will be a decisive evidence for the naturalness of the EW scale. Unfortunately, as of today, there has been no conclusive signals for new physics. In addition, low energy precision experiments tend to impose strong constraints on the allowed parameter space of the theories. Partly inspired by such circumstances, recently several conceptually new ideas have been put forward. These include twin Higgs models [28], folded supersymmetry [29], and cosmological relaxation [30]. A different direction, called split supersymmetry, was proposed [31] in which the lightness of the Higgs mass is attributed to anthropic principle and the existence of supersymmetry is motivated instead by the gauge coupling unification and dark matter.

1.3 Outline of Thesis

In this thesis, in the context of warped extra dimensional framework of Randall-Sundrum (RS) type (and composite Higgs as its 4D dual via the AdS/CFT correspondence [32]), we propose yet another logical possibility and explore theoretical and phenomenological consequences. To be more specific, we first noticed the follow-

ing facts: (1) there has been no discovery of new physics beyond the SM at the LHC and (2) without having extra structures, low energy constraints from electroweak precision and flavor/CP violation tests push the mass scale of the Kaluza-Klein (KK) particles[6] (well) beyond the reach of the LHC. Such circumstances inspire the possibility that although it is still a good guiding principle, the naturalness may not be realized 100 % and the central players (e.g. top partner) of the naturalness may lie out of current and near-future experimental reach. One immediate question is then if there exists a suitable/natural extension in which light states are allowed and can be produced at the LHC, permitting us to learn about solution to the hierarchy problem, albeit indirectly. Indeed, we found such an extension in the context of Randall-Sundrum model. In this case, the low energy constraints are easily satisfied by the geometric localization of fields, and a few TeV KK scale for gauge boson and gravity is still allowed. In this framework, the scale of the Higgs/top compositeness is still tied to the flavor scale and hence much higher than TeV, making the weak scale meso-tuned. Phenomenologically, our extension leads to changes in the strength of the couplings of $\sim$ TeV mass KK modes. We show that these features can lead to, rather remarkably, a significant deviation of the decay branching fractions of KK gauge bosons, e.g. KK Z and KK gluon, to pairs of the SM particles, compared to the minimal/standard setup. Moreover, it can also lead to $\mathcal{O}(1)$, but still noticeable, deviation compared to the flavor universal limit, when the Higgs/top compositeness physics is realized around $\mathcal{O}(10)$ TeV as suggested by

[6]Loosely speaking (and as will be explained in detail in Chap. 2, KK particles are extra dimensional excitation of the SM particles.

the flavor bound. Furthermore, it can give rise to other channels, which used to be subdominant and hence have not been searched for as yet in the minimal/standard setup, acquire significant rate. Discovering such signal processes in the predicted topology, therefore, will provide prominent evidence for the extended framework and a hint for the ultimate fate of the naturalness of the weak scale.

The rest of the thesis is organized as follows. In Chap. 2, we provide a brief review of the standard Randall-Sunrum model and its 4D dual description. Chap. 3 is devoted to our theoretical development of the *extension*. The detailed LHC phenomenological study of the extended framework is presented in Chap. 4. For the purpose of making this chapter self-contained and also in order to provide a collection of knowledges directly relevant to the phenomenological study, at the risk of repetition, we provide rather detailed review on the theory presented in Chap. 3. We think that readers mainly interested in LHC signals of the extended framework can skip to Chap. 4 directly. Chap. 5 provides the conclusion to the thesis.

Chapter 2: Review of Standard Randall-Sundrum Model

In this Chapter, we provide a brief review of the standard Randall-Sundrum model [24, 25] and its dual description [33–36] in terms of strongly coupled (broken) 4D conformal field theory (CFT) coupled to dynamical gravity. As we show below, in the case where the SM gauge and fermion fields propagate in the bulk of the warped 5D spacetime, the dual 4D CFT is also weakly coupled to the dynamical gauge fields and external/elementary fermions. Since most of the discussion in Chap. 3 and Chap. 4 of the thesis, where our original work is presented, is using 4D CFT language, our review of the 5D aspects of the RS model will be brief and mostly qualitative. For more details, see [37–42].

2.1 Randall-Sundrum Model

In the RS model, the spacetime is described by a slice of 5D Anti-de Sitter (AdS) space with curvature scale k. The metric of this spacetime is described by

$$ds^2 = e^{-2k|y|} dx^\mu dx^\nu \eta_{\mu\nu} - dy^2, \tag{2.1}$$

where $\eta_{\mu\nu} = \mathrm{diag}(+,-,-,-)$ is the flat 4D Minkowski metric, x^μ are the 4D coordinates and y is the coordinate for the fifth dimension and is constrained to $0 \leq y \leq \pi r_c$. The boundaries of the fifth dimension are 4D branes: the UV brane at $y = 0$ and the IR brane at $y = \pi r_c$. In order for this metric to solve the Einstein's equation, the tension of the two branes needs to be tuned to

$$\tau_0 = 12kM_5^3, \qquad \tau_1 = -12kM_5^3, \tag{2.2}$$

where $\tau_{0(1)}$ is the tension of UV (IR) brane and M_5 is the 5D Planck mass. As is evident, the UV (IR) brane is the brane with positive (negative) tension. Up on integrating the 5D Einstein-Hilbert action over the extra dimension and by matching the result to 4D gravity action, one obtains the effective 4D Planck scale in terms of 5D parameters:

$$M_{\mathrm{Pl}}^2 = \frac{M_5^3}{k}\left(1 - e^{-2k\pi r_c}\right). \tag{2.3}$$

Provided $k\pi r_c$ is moderately larger than unity and assuming no sizable hierarchy between M_5 and k, we see that $M_{\mathrm{Pl}} \approx M_5 \approx k$. Namely, 5D gravity in AdS_5 with the Planck sized fifth dimension with 5D fundamental scale of $\sim M_{\mathrm{Pl}}$ is reduced to 4D gravity on large scale (i.e. distances larger than the radius of curvature).

In order to see how the hierarchy problem is solved in the RS model, consider a case with the SM Higgs localized on the IR brane.[1] The action for the Higgs field

[1] Perfect localization of the Higgs field is not strictly necessary, and it is mainly for the simplicity of the discussion. 5D Higgs field with IR-localized zero mode will result in the same results.

is described by

$$S_{\text{Higgs}} = \int d^4x \sqrt{g^{\text{ind}}} \left\{ g^{\text{ind}}_{\mu\nu} D^\mu H^\dagger D^\nu H - V(H) \right\}, \quad V(H) = \lambda \left(H^\dagger H - v^2 \right)^2, \tag{2.4}$$

where $g^{\text{ind}}_{\mu\nu}|_{y=\pi r_c} = e^{-2k\pi r_c} \eta_{\mu\nu}$ is the induced metric on the IR brane and v is the VEV of the Higgs, whose natural size will be $M_5 \sim M_{\text{Pl}}$. Plugging the induced metric in the above action, the action for the Higgs becomes

$$S_{\text{Higgs}} = \int d^4x e^{-4k\pi r_c} \left\{ e^{2k\pi r_c} \eta_{\mu\nu} \partial^\mu H^\dagger \partial^\nu H - \lambda \left(H^\dagger H - v^2 \right)^2 \right\}. \tag{2.5}$$

The Higgs field is not canonically normalized and we need to do field redefinition $\tilde{H} = e^{-k\pi r_c} H$ for correct normalization. After the redefinition, the action becomes

$$S_{\text{Higgs}} = \int d^4x \left\{ \eta_{\mu\nu} \partial^\mu \tilde{H}^\dagger \partial^\nu \tilde{H} - \lambda \left(\tilde{H}^\dagger \tilde{H} - \left(e^{-k\pi r_c} v \right)^2 \right)^2 \right\}. \tag{2.6}$$

We see that, after canonically normalizing the Higgs field, the effective VEV (which corresponds to the weak scale at the end) is *warped down*: $\tilde{v} = e^{-k\pi r_c} v$. In other words, due to the curvature of the geometry, there is an exponential redshift of the mass scale from the UV to the IR brane. This, in turn, implies that if the fundamental scale at the UV brane is the 4D Planck scale, then for the proper radius of compactification πr_c of about $35 - 40$ times larger than the curvature radius $1/k$, the fundamental scale at the IR brane is the weak scale. The radius of the extra dimension can be stabilized by Goldberger-Wise mechanism [43]. Therefore, strong gravitational redshift of the AdS space combined with the radius stabilization solves

the electroweak hierarchy problem.

The rest of the SM fields may either be localized on the IR brane with the Higgs (as in the original RS1 model [24]) or propagate in the bulk with couplings to the Higgs on the IR brane. It turns out that the latter case is very attractive since it provides an elegant way to resolve flavor hierarchy problem. Therefore, we consider the bulk SM scenario in this thesis. The compactness of the extra dimension allows one to decompose a 5D field into a tower of 4D fields, known as Kaluza-Klein (KK) decomposition. If $\Phi(x, y)$ denotes a 5D field of any spin, then one can write

$$\Phi(x, y) = \sum_n f_n(y)\phi_n(x) \tag{2.7}$$

where $\phi_n(x)$ represents an infinite tower of 4D fields and $f_n(y)$ is the extra dimensional wavefunction (or profile) for the field $\phi_n(x)$. The 4D field $\phi_n(x)$ is required to satisfy the 4D equation of motion (relevant one for the spin of the field) and the 5D equation of motion is then reduced to the differential equation for the profile. If the 5D field satisfies Neumann boundary condition on *both* UV and IR brane, the KK spectrum contains the massless mode, called zero mode. For the other cases, the corresponding KK tower does not include zero mode and contains only massive modes, the mass of the first KK mode and the mass separation being roughly of the order of the warped down AdS curvature scale, i.e. $ke^{-k\pi r_c} \sim \mathcal{O}(\text{TeV})$.

The localization of the zero mode, i.e. whether localized near the UV/IR brane or even flat, is determined by the 5D bulk mass. For fermion, writing the 5D mass in units of curvature scale as $m = ck$, the fermion zero mode is localized near the

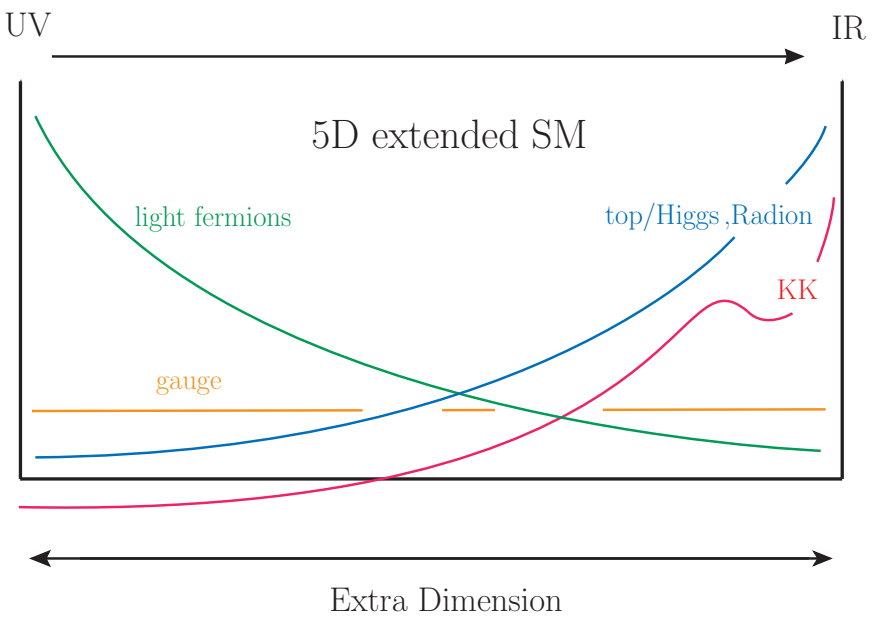

Figure 2.1: Warped extra dimensional model with SM fields in bulk (standard framework). Schematic shapes of extra-dimensional wavefunctions for various particles (zero modes and a generic KK mode) are shown.

UV (IR) brane if $c > 1/2$ ($c < 1/2$). For $c = 1/2$, the zero mode profile is flat. The zero mode profile of the gauge field is flat and the gravity zero mode is localized near the UV brane. (see Fig. 2.1)[2]

The zero modes are identified with the 4D SM fields. For example, the gravity zero mode corresponds to the 4D gravity and the fact that it is localized near the UV brane, where the fundamental scale is $\sim M_{\rm Pl}$, explains why the effective Planck scale is much higher than the weak scale (recall that the Higgs is localized on the IR brane where the fundamental scale is $\sim$ TeV). For fermions, assuming anarchic 5D Yukawa couplings, the 4D effective Yukawa couplings, and hence its mass, are

[2]Also shown in Fig. 2.1 is a scalar particle called radion. Intuitively, radion describes the fluctuation of the overall size of the extra dimension. Since we will have detailed discussion about radion, or dilaton as its 4D dual, in subsequent chapters, we will not discuss about it any more in this chapter.

determined by products of the values of zero mode profiles on the IR brane for left-handed and right-handed fermions. For light fermions, we can simply choose the mass parameter c in such a way that the profiles are localized near the UV brane and hence having exponentially small tail on the IR brane. For the heavy fermions like top quark, we do the exactly the opposite, i.e. make them be localized near the IR brane. The required hierarchy in the mass parameter c is exponentially reduced compared to the original fermion mass hierarchy and $\mathcal{O}(1)$ difference in c suffices to explain the entire flavor hierarchy. It may be worthwhile to emphasize that the SM is now fundamentally 5D, and the required 5D parameters to explain the measured fermion spectrum are not tuned and thus natural.

Other 4D effective couplings of the SM particles can be obtained by integrating involved particles' zero modes profiles over the extra dimensions. For example, for the SM gauge coupling among, say photon, electron and positron, one simply integrate product of zero mode profiles of these three particles along the fifth direction. For the KK particle - SM particle 1 - SM particle 2 coupling, one again integrates the product of KK profile, zero mode profile for the first and the second along the fifth dimension. In this way, the effective couplings are overlap integral of product of relevant profiles.

We already mentioned that light SM fermions are localized near the UV brane and heavy SM fermions are leaning toward the IR brane. All KK modes, regardless of spin and charges, are localized near the IR brane (see Fig. 2.1). One intuitive explanation for this can be obtained from 4D dual description, which we now discuss.

2.2 4D holographic dual description

We begin with the 4D CFT dual description of the 5D gravity theory in RS background of Eq. (2.1). Via AdS/CFT correspondence [32], the gravity theory in the 5D spacetime which is asymptotically AdS_5 (i.e. without branes) is dual to a strongly coupled CFT. Since the UV brane of the RS model corresponds to a big modification of the pure AdS geometry at small y and small y is dual to high energy in CFT, the UV brane is dual to the UV cut-off of the CFT. The zero mode graviton localized near the UV brane is dual to the fundamental spin-2 field external to the CFT. At this point, i.e. without having IR brane yet, the 5D gravity theory is dual to a strongly coupled CFT with a UV cut-off and the CFT is (weakly) coupled to 4D gravity. In the absence of the IR brane, the KK spectrum is continuum and when we add the IR brane at finite y, the KK spectrum becomes gapped. Moreover, adding the IR brane into the theory represents a deviation from the AdS at large y. Hence it must correspond to confinement of the CFT in the IR and this confinement breaks conformal invariance spontaneously, leading to the generation of bound states. KK modes in the 5D side are then dual to these composite resonances of CFT confinement and the fact that such composite states emerging in the IR of the CFT is dual to the feature that *all* KK profiles are localized near the IR brane. Physics external to the CFT is dual to states leaning towards the UV brane. In this 4D picture, the Higgs is a composite state and is dual to it being localized near the IR brane. The hierarchy problem is then solved simply by the fact that the Higgs is only formed as a bound state of strongly coupled preons at $\sim$ TeV scale.

The existence of the holographic dual description and the fact that low energy EFT in 5D is a weakly coupled theory of KK modes then suggests that the low energy theory of composite states of the broken CFT is weakly coupled as is true in the large-N limit. To summarize, the RS model is dual to a strongly coupled 4D CFT with a UV cut-off and with the scale invariance being spontaneously broken at a IR scale, producing gapped composite resonances which are weakly coupled.

The dual picture of the gauge fields in bulk (assuming zero mode exists) is that the CFT has a conserved global symmetry current and it is coupled to a 4D gauge field external to the CFT:

$$\mathcal{L} = \mathcal{L}_{\rm CFT} + A_\mu J^\mu_{\rm CFT} - \frac{1}{4g^2} F_{\mu\nu} F^{\mu\nu}. \tag{2.8}$$

where $F_{\mu\nu}$ is the field strength tensor of A_μ. Note that the conserved current has zero anomalous dimension and hence the operator $A_\mu J^\mu_{\rm CFT}$ is marginal. When the CFT confines in the IR (at $\Lambda_{\rm IR}$), generating composite states, the conserved current interpolates the massive spin-1 composite states of the CFT:

$$J^\mu_{\rm CFT} \sim \frac{\Lambda^2_{\rm IR}}{g_\star} \rho^\mu \tag{2.9}$$

where $g_\star$ is the composite coupling among three composites and ρ^μ is the vector "meson" of the CFT.[3] In this way, the operator $A_\mu J^\mu_{\rm CFT}$ describes the mixing between elementary A_μ and composite ρ_μ and upon diagonalization, we get one massless

[3]The appearance of $\Lambda^2_{\rm IR}$ in Eq. (2.9) is purely dimensional one. A less trivial $\frac{1}{g_\star}$-dependence can be understood as follows. The current-current correlator in large-N is schematically given by $\langle JJ \rangle \sim \frac{N}{16\pi^2}$ and as we show below, $g_\star \sim \frac{4\pi}{\sqrt{N}}$. Therefore, J is parametrically proportional to $1/g_\star$.

(corresponding to unbroken, SM gauge boson) and one massive (corresponding to the KK mode) spin-1 state. Also, due to the marginality, the operator $A_\mu J^\mu_{\rm CFT}$ does not RG run from UV to IR and this is dual to the fact that gauge zero mode has a flat profile. In order to understand the duality of couplings, notice first that the coupling among three composite states in the CFT, assuming CFT being large-N $SU(N)$ gauge theory, is given by to leading order in large-N expansion,

$$g_\star \sim \frac{4\pi}{\sqrt{N}}. \tag{2.10}$$

Recalling that heavy composites are dual to KK modes in 5D, we get the duality map by looking at, for instance, coupling of two KK gauge bosons with the Higgs on the IR brane. Explicit 5D calculation shows that this coupling is

$$\sqrt{g_5^2 k} \approx \sqrt{g^2 k \pi r_c} \tag{2.11}$$

where g_5 (g) is the 5D (4D) gauge coupling and we used $g = g_5/\sqrt{\pi r_c}$ for the equality. Therefore, from this, we obtain the dual relation for the couplings

$$\sqrt{g_5^2 k} \sim \frac{4\pi}{\sqrt{N}}. \tag{2.12}$$

One sanity check that this relation passes is obtained by considering RG running of

the SM gauge coupling. The dominant contribution from the CFT is given by[4]

$$\frac{1}{g^2} \sim \frac{N}{16\pi^2} \log\left(\frac{k}{\text{TeV}}\right) \sim \frac{1}{g_\star^2} k\pi r_c \tag{2.13}$$

and this agrees with what we obtained above.

The dual interpretation of the bulk fermion (assuming zero mode exists) can be understood similarly. It is dual to an external fermion (ψ) coupled weakly and linearly to the CFT fermion operator ($\mathcal{O}_{\text{CFT}}$),

$$\mathcal{L} = \mathcal{L}_{\text{CFT}} + \lambda \psi \mathcal{O}_{\text{CFT}}. \tag{2.14}$$

The bulk mass parameter c is dual to the scaling dimension (d) of $\mathcal{O}_{\text{CFT}}$ via $d = 2+c$. Therefore, for 5D fermion with $c > 1/2$ ($c < 1/2$), whose zero mode is localized near the UV (IR) brane, the operator $\psi\mathcal{O}_{\text{CFT}}$ is irrelevant (relevant). When the CFT confines, similarly to the case of gauge boson, the operator $\mathcal{O}_{\text{CFT}}$ creates massive composite fermion when acting on the vacuum, and $\lambda\psi\mathcal{O}_{\text{CFT}}$ describes the mixing of the elementary fermion with the composite fermion. The size of the mixing is determined by the size of λ in the IR. For $d > 5/2$ (dual to $c > 1/2$), the coupling decreases as it flows to the IR (since it is irrelevant operator), resulting in suppressed mixing. For $d < 5/2$ (dual to $c < 1/2$), it is opposite and we get unsuppressed mixing. The SM fermion is then identified as the massless states after diagonalizing the mixing between external and composite fermions. For $c > 1/2$, the SM fermion

[4]This is obtained from RG running of the coefficient of the gauge kinetic term.

is mostly elementary and for $c < 1/2$, it is mostly composite. Namely, the SM states are the admixture of elementary and composite states. This is known as *partial compositeness* [44]. This feature explains the flavor hierarchy as follows. In the CFT dual description, the Higgs is one of the composite states of the CFT and thus the coupling of the SM fermion to the Higgs has to proceed via the fermion's compositeness. For $c > 1/2$, due to exponentially suppressed composite component, the effective Yukawa is very small, i.e. the corresponding SM fermion is light. In 5D, this corresponds to the zero mode being localized near the UV brane, leaving exponentially suppressed tail on the IR brane, and hence tiny Yukawa coupling. For $c < 1/2$, the story is exactly the opposite. In this way, we see that solving the flavor hierarchy via partial compositeness in the 4D CFT is the holographic dual of solving it via field localization in the 5D.

Chapter 3: Flavor Universal Resonances and Warped Gravity

In this Chapter, we develop an extension of the standard Randall-Sundrum framework. For a detailed review on the standard Randall-Sundrum framework, see Chap. 2. For the sake of completeness, this chapter contains discussion on the review of the standard framework. We think this makes the motivation for the extension more apparent and the comparison of the two (standard and the extension) frameworks manifest.

3.1 Introduction

The scenario of Higgs compositeness [45] offers a powerful resolution to the Hierarchy Problem. The Standard Model (SM) Higgs degrees of freedom remain much lighter than the Planck scale in the face of radiative corrections because they are only assembled at $\sim$ TeV scale, as tightly bound composites of some new strongly interacting "preons". This is in close analogy to how the ordinary charged pion remains much lighter than the Planck scale in the face of QED radiative corrections, by being assembled as a quark-gluon composite at $\sim$ GeV. But despite the simple plot, composite Higgs dynamics is notoriously difficult to model in detail because it requires understanding a new strongly-coupled dynamics, operating outside

perturbative control.

Remarkably, Higgs compositeness has an alternate "dual" formulation [33–36, 46] in the form of "warped" higher-dimensional theories of Randall-Sundrum type [24, 25], related to the purely 4D formulation via the famous AdS/CFT correspondence [32]. In the warped framework there can exist a regime of weakly-coupled higher-dimensional effective field theory, allowing more detailed phenomenological modeling as well as a prototype for UV completion, say within string theory [47, 48]. Fig. 2.1 shows a schematic representation of particle physics in the simplest such setting, with a single microscopic extra-dimensional interval. The SM is now fundamentally 5-dimensional [37–42], but its lightest modes appear as the familiar 4D SM particles, with phenomenological properties deriving from their extra-dimensional wavefunctions. In particular, the SM fermions naturally have disparate wavefunctions, which lead to an attractive mechanism for the origin of SM flavor structure, AdS/CFT dual to the robust mechanism of Partial Compositeness [44].

On top of the lightest modes are Kaluza-Klein (KK) excitations of the SM (Fig. 3.1), which effectively cut off quantum corrections to the Higgs mass and electroweak symmetry breaking (EWSB). Naturalness then implies that these KK states should have masses of the order TeV scale.[1] This is the basis of ongoing LHC searches for KK-excited tops and bottoms ("top partners") and KK gauge bosons and spin-2 KK gravitons. Because of their strong extra-dimensional wavefunction-overlap with the top quark and Higgs, these KK resonances predominantly decay to

[1] An elegant realization in warped extra dimension of the composite Higgs mechanism, i.e., where it is a PNGB like the pion, is via gauge-Higgs unification [36, 46]. It is in this case that the cutoff of Higgs quantum corrections is the KK scale. However, this aspect plays little role in this chapter. So, for brevity, we simply suppress this extra structure of the Higgs field.

t, h, W_L, Z_L [49]. From the viewpoint of 4D Higgs compositeness, the KK excitations are simply other composites of the same preons inside the Higgs (and the closely-related top quark).

Lower-energy experiments are also sensitive to KK states via their *virtual* exchanges. Electroweak precision tests, now including the rapidly developing body of precision Higgs measurements, robustly constrain the KK spectrum, but are still consistent with KK discoverability at the LHC [50–54]. However, as in the supersymmetric paradigm, the constraints from tests of flavor and CP violation are extremely stringent. Although the warped extra-dimensional framework (and partial compositeness) enjoys a powerful generalization of the SM GIM mechanism suppressing FCNCs [55–58], it is imperfect. Typically in parameter space flavor and CP constraints imply $M_{\rm KK} \gtrsim O(10)$ TeV for the KK threshold [59–62]!

What are we to make of this situation? While flavor and CP tests have very high virtual reach for the warped/composite scenario, they do not appear as robust as electroweak constraints. It is indeed plausible that a more refined mechanism for flavor structure is occurring within Higgs compositeness so as to relax the bounds significantly, and admit KK states within LHC reach [63–68]. Because of this, it is imperative that LHC experiments continue to search for KK resonances along the lines of Fig. 2.1 and 3.1, in tandem with ongoing low-energy searches for new sources of flavor and CP violation. But it is also possible that the hierarchy problem is imperfectly solved by Higgs compositeness at a scale $\gtrsim O(10)$ TeV, leaving a *Little Hierarchy Problem* between $\sim O(10)$ and $\sim O(1)$TeV. We simply do not understand fundamental physics and the principle of Naturalness underlying the SM hierarchy

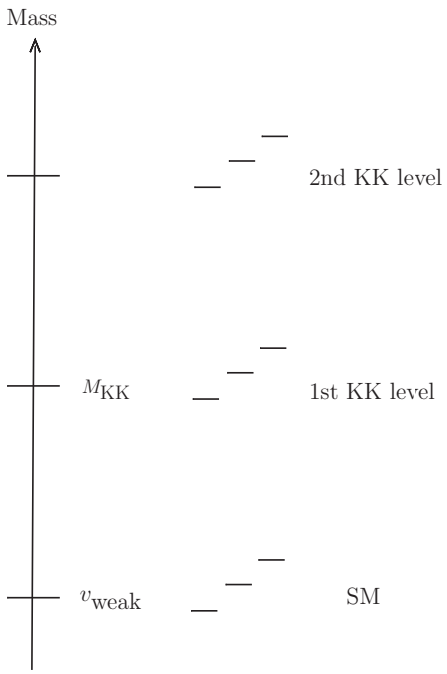

Figure 3.1: General spectrum of model of Fig. 2.1.

problem deeply enough to know if they should reliably predict the threshold of new physics to better than a decade in energy. Of course, such a possibility leads to the practical problem that $M_{\rm KK} \gtrsim O(10)$ TeV is outside LHC reach and yet frustratingly close! (It is noteworthy however that such new physics might be within reach of proposed 100 TeV colliders).

In this thesis, we will pursue the scenario of Higgs compositeness at $\gtrsim O(10)$ TeV. This straightforwardly suppresses all virtual KK-mediated electroweak, flavor and CP violating effects enough to be robustly consistent with all precision experiments to date. But we will ask what natural forms of new physics might lie *within LHC reach* if we go beyond the minimal structure of Fig. 2.1 and 3.1, without reintroducing conflict with precision tests. We can think of such non-minimal physics lying below the scale at which the hierarchy problem is solved as "vestiges of natu-

ralness". If the LHC cannot reach the states central to solving the dominant part of the hierarchy problem (such as KK tops), the search for light vestiges, related to the central players but not among them, are the best hope for the LHC.

In particular, we study *literally* a straightforward extension of Fig. 2.1 which exploits the fact that different types of fields can propagate different amounts into the IR of a warped extra dimension, as schematically depicted in Fig. 3.2. For simplicity, we focus on three categories of fields: (i) SM matter, including the Higgs, (ii) gauge fields, (iii) gravity. Gravity is the dynamics of all spacetime and therefore must be present in the entire length of the extra dimension in the form of 5D General Relativity. Gauge fields and matter can however reside in a smaller region. Matter fields can live in an even smaller region of the extra dimension than the gauge fields, but not the other way around because charged matter always radiate gauge fields. This explains the ordering shown in Fig. 3.2. The different regions are separated by "3-branes", $(3+1)-$dimensional defects in the 5D spacetime. Fig. 3.2 is a simple, robust and interesting generalization of the minimal structure of Fig. 2.1, 3.1. A quite different proposal using an intermediate brane in warped spacetime was made in [69] in the context of explaining 750 GeV diphoton excess at the LHC [70, 71]. Different matter fields propagating from the UV brane to different intermediate branes were studied in [72,73]. Also, a set-up with (only) *two* branes, but a departure from pure AdS near the infrared brane, can result in the Higgs profile being peaked a bit away from the IR brane [74].

The new physics to the IR of Higgs compositeness is (AdS/CFT dual to) that of "Vectorlike Confinement", proposed in references [75–77] as a phenomenologically

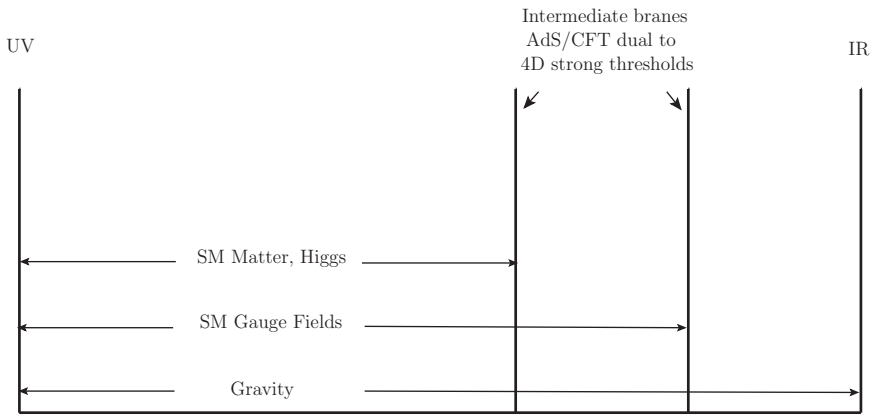

Figure 3.2: Model with two intermediate branes/thresholds.

rich structure that is remarkably safe from precision tests, and is a natural candidate for a light vestige of a more general dynamics that solves the hierarchy problem. In the framework of Fig. 3.2, vectorlike confinement incarnates as the extension of the IR of the extra dimension beyond Fig. 2.1, resulting in different KK thresholds for matter, gauge fields and gravity as depicted schematically in Fig. 3.3. A simple but important result we will demonstrate is that the Goldberger-Wise (GW) mechanism [43, 78] for brane/radion stabilization very naturally results in "little" hierarchies $M_{\mathrm{KK}_{\mathrm{matter,Higgs}}} \geq M_{\mathrm{KK}_{\mathrm{gauge}}} \geq M_{\mathrm{KK}_{\mathrm{grav}}}$.

From the purely 4D perspective of strong dynamics, the sequence of KK thresholds, $M_{\mathrm{KK}_{\mathrm{matter,Higgs}}} \geq M_{\mathrm{KK}_{\mathrm{gauge}}} \geq M_{\mathrm{KK}_{\mathrm{grav}}}$, is dual to a sequence of strong confinement scales [79, 80], $\Lambda_{\mathrm{Higgs}} \geq \Lambda_{\mathrm{meson}} \geq \Lambda_{\mathrm{glueball}}$. Over the large hierarchy from the far UV (the Planck or unification scale) down to Λ_{Higgs} the strong dynamics is only slowly evolving. At Λ_{Higgs} the strong dynamics confines "preons" into composites, among which is the light SM-like Higgs. This is analogous to the emergence of pions and heavier hadrons as composites of quarks and gluons upon QCD confinement.

But unlike QCD, the strong dynamics does not end at this point, but rather is reorganized into a new set of strongly interacting preons, *now approximately decoupled from Higgs and flavor physics*. The IR preons do however carry SM gauge charges.

At $\Lambda_{\rm meson}$ there is a second stage of preon confinement, into "mesons" also carrying SM gauge charges. Without direct couplings to the Higgs and SM fermions, this second stage of confinement does not break the SM electroweak chiral symmetries, hence the name "vectorlike" confinement. Again, the strong dynamics need not end at this threshold, but can continue with a set of far-IR SM-neutral preons, which ultimately confine into SM-neutral "glueballs" at $\Lambda_{\rm glueball}$.

Since the new physics below $\Lambda_{\rm Higgs}$ couples to the SM states predominantly via flavor-blind gauge forces, it is naturally safe from the host of electroweak, flavor and CP tests. Phenomenologically, production and decay of the new states below $\Lambda_{\rm Higgs}$ will be mediated by on- and off-shell SM gauge bosons. It is very important that experiments search broadly for this kind of physics. In this way, vectorlike confinement appears as set of "aftershocks" of Higgs compositeness, immune to earlier detection but plausibly lying within grasp of the LHC. We will study several aspects of this strongly motivated scenario in this thesis.

In references [75], vectorlike confinement was modeled on QCD-like dynamics as the simplest way of illustrating the rich possibilities, using real-world understanding of the strong interactions to stay in non-perturbative theoretical control. A feature of these models is that they typically contain several pseudo Nambu-Goldstone bosons (PNGBs) in the IR of the new physics related to the large chiral symmetry,

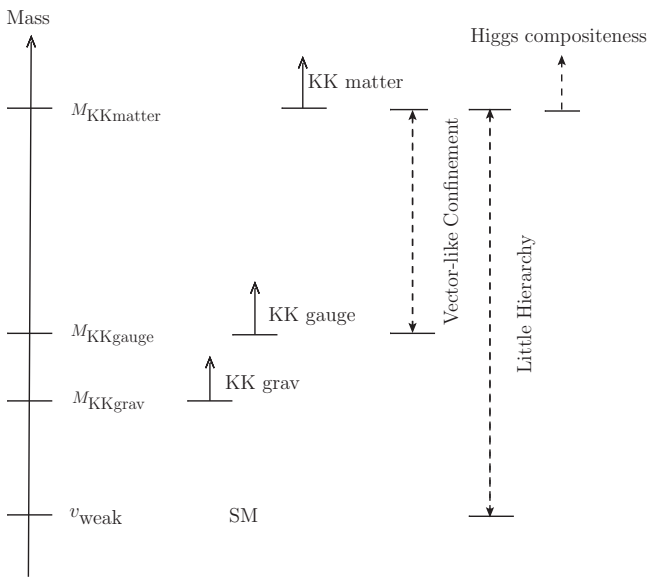

Figure 3.3: Full spectrum of model of Fig. 3.2.

which can dominate the phenomenology.[2] However, the specific phenomenological implications are model-dependent. Although QCD-like dynamics do not have a very useful AdS/CFT dual extra-dimensional description, they are in the same "universality class" as extra-dimensional models of the type depicted in Fig. 3.4, where the 5D gauge group is extended beyond the SM. If UV and IR boundary conditions break some of the gauge symmetry generators, they result in physical extra-dimensional components of the gauge field, "A_5", which are 4D scalars, AdS/CFT dual to PNGB's [36].[3] We will return to study this class of vectorlike confining physics more closely in future work. Unlike in QCD-like constructions, in warped 5D effective field theory we can suppress the existence of A_5's by construction, allowing us to focus on other possibilities for the new phenomenology.

[2]For recent applications of vector-like confinement for explaining the 750 GeV diphoton excess at the LHC, see, for example, the early references [81–86].

[3]Such states tend to be lighter than the typical KK scale and thus can be within LHC reach even in the minimal model of Fig. 2.1 with the IR brane at the flavor/CP bound of $\sim O(10)$ TeV [87, 88].

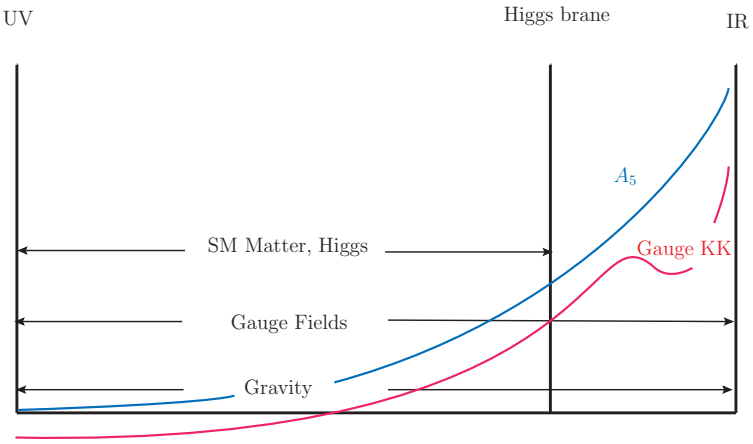

Figure 3.4: Model with an extended gauge group beyond SM and one intermediate brane, resulting in some number of A_5 4D scalars dual to composite PNGB's.

One focus of this chapter will be the possibility that lightest new states are the universal ones arising from 5D General Relativity, the scalar "radion" measuring the (dynamical) size of the final IR segment of the extra-dimensional interval, and spin-2 KK gravitons. These are the hallmarks of warped extra-dimensional physics. Via the AdS/CFT correspondence these states are dual to special "glueballs" interpolated by the conserved energy-momentum tensor of the strong dynamics, the universal composite operator of any quantum field theory. In particular, this symmetric tensor naturally interpolates spin-2 glueballs dual to KK gravitons, while its Lorentz-trace interpolates the "dilaton", a glueball dual to the radion. We will derive and discuss their phenomenological implications, pointing out (i) when they are likely to be the first discovered new states beyond the SM, (ii) their special distinguishing features and the contrast with more QCD-like vectorlike confinement and other beyond-SM physics, (iii) how we can experimentally test whether the new physics is well-described by higher-dimensional dynamics.

In table 3.1, we highlight a couple of signals from the gravity sector, namely radion in the model with one intermediate brane of Fig. 3.4 and KK graviton in the model with two intermediate branes of Fig. 3.2: further details will be provided in the relevant parts of the chapter. For now, it is noteworthy that the decays in these cases dominantly occur to pairs of SM gauge bosons, cf. top/Higgs playing this role in the minimal model of Fig. 2.1. Also, we see that radion and KK graviton are allowed to be lighter than gauge KK modes[4].

A second focus of this chapter will be connecting the new physics the LHC can discover to the solution of the hierarchy problem beyond its reach. We will show that low-lying KK modes, though mostly decoupled from the Higgs and flavor, will have subdominant decay channels into t, h, W_L, Z_L, the traditional signatures of Higgs compositeness. In this way, the LHC would have a valuable resonance-enhanced "preview" of the solution to the hierarchy problem by compositeness, only fully accessible to more energetic future colliders. In particular, we find that spin-1 KK *gauge* bosons are well-suited for this task. Note that these are dual to composite vector "ρ" mesons, which arise as a robust feature in the framework of vector-like confinement also.

A representative sample of the above novel probe of top/Higgs compositeness is shown in table 3.1: we will of course explain in later sections how we obtained these numbers (including assumptions made therein), but let us convey our main message using them for now.

[4]It might be also possible to make KK graviton lighter than gauge KK using large brane-localized kinetic terms (BKT) for gravity [89]. For recent applications of this idea for explaining the 750 GeV diphoton excess at the LHC using KK graviton, see [90–95]. However, with too large BKT for gravity, the radion might become a ghost [89].

Radion / KK Graviton			
		Radion (φ)	KK Graviton
Framework		one intermediate brane (Fig. 3.4)	two intermediate branes (Fig. 3.2)
Parameters		inter-KK gravity coupling = 1	inter-KK gravity coupling = 3
		inter-KK gauge coupling = 3	inter-KK gauge coupling = 3
		$M_{\text{KKgauge}} = 3$ TeV; $m_\varphi = 1$ TeV	$M_{\text{KKgauge}} = 3$ TeV; $M_{\text{KKgrav}} = 1$ TeV
σ_{LHC13} ($pp \to$ Radion/KK Graviton)		~ 80 fb	~ 3.9 fb
BR	gg	$\sim 95\%$	$\sim 95\%$
	ZZ	$\sim 1\%$	$\sim 1\%$
	WW	$\sim 3\%$	$\sim 3\%$
	$\gamma\gamma$	$\sim 0.7\%$	$\sim 0.7\%$

Table 3.1: Estimates for production cross section (at $\sqrt{s} = 13$ TeV LHC) and decay BR's of radion (left) and KK graviton (right) for a given choice of framework and parameters. For radion, model with one intermediate brane is considered with radion mass 1 TeV, $M_{\text{KKgauge}} = 3$ TeV, and inter-KK gravity(gauge) coupling of 1(3) [composite gravity ($g_\star^{\text{grav}}$) and gluon ($g_\star^{\text{QCD}}$) couplings, respectively, which we define in section 3.2.1]. For KK graviton, we instead considered model with two intermediate branes, in which KK graviton is naturally lighter than KK gauge boson. In this case, both inter-KK couplings are taken to be 3.

KK Z				
$\sigma_{\text{LHC13}}\,(pp \to \text{KK Z}) \sim 2.5$ fb for 3 TeV mass and inter-KK coupling of 3				
Λ_{Higgs} / Final state	3 TeV (Fig. 2.1)	10 TeV	15 TeV	∞
di-leptons ($e + \mu$)	~ 0	$\gtrsim 6 - 4\%$	$\gtrsim 6\%$	6%
di-bosons (Higgs/W/Z)	65%	$\sim 0 - 28\%$	$\sim 0 - 4\%$	4%
di-tops	35%	$9 - 20\%$	$9 - 10\%$	10%
di-jets	~ 0	$63 - 36\%$	$63 - 59\%$	59%
KK Gluon				
$\sigma_{\text{LHC13}}\,(pp \to \text{KK gluon}) \sim 151$ fb for 3 TeV mass and inter-KK coupling of 3				
Λ_{Higgs} / Final state	3 TeV (Fig. 2.1)	10 TeV	15 TeV	∞
di-jets (light quarks $+b$)	~ 0	$83 - 91\%$	$86 - 91\%$	83%
di-tops	100%	$17 - 9\%$	$14 - 9\%$	17%

Table 3.2: Estimates for decay BR's of KK Z (top) and KK gluon (bottom) for various values of top/Higgs compositeness scale (Λ_{Higgs}), for fixed spin-1 mass scale of 3 TeV and inter-KK Z/gluon coupling [$g_\star^{Z/\text{gluon}}$, which we define in section 3.2.1] of 3, corresponding to cross-section (at $\sqrt{s} = 13$ TeV LHC) of ~ 2.5 fb (for KK Z) and ~ 151 fb (for KK gluon).

We focus on KK – excited (dual to composite) Z and gluon, where we fix their mass and coupling to light quarks, hence production cross-section (as shown). However, decay branching ratios (BR's) to various final states still vary for the *same* framework as we vary $\Lambda_{\rm Higgs}$: the left-most column corresponds to the standard composite Higgs model (i.e., single IR brane/scale, Fig. 2.1), whereas right extreme is the flavor-blind limit, i.e., Higgs compositeness scale is decoupled (large $\Lambda_{\rm Higgs}$). Remarkably, we see that decay BR's might be sensitive to $\sim 10-15$ TeV Higgs compositeness scale [in the sense that such values of Higgs compositeness scale can result in $\sim O(1)$ deviations from *both* flavor-blind and standard limits], which is the ball park of the generic *lower* limit on the Higgs compositeness scale from flavor/CP violation!

This chapter is organized as follows. We begin in section 3.2 with laying out the structure of the model with gauge and gravity propagating in the same bulk, but matter/Higgs in a subspace, i.e., with the usual UV and IR branes along with a single intermediate brane de-marking the matter/Higgs endpoint. In section 3.3, we then describe salient features of the LHC signals of this framework. In section 3.4, we discuss more general framework with two intermediate branes, in which gravity extends even beyond the gauge bulk. Some technical details are relegated to the appendices.

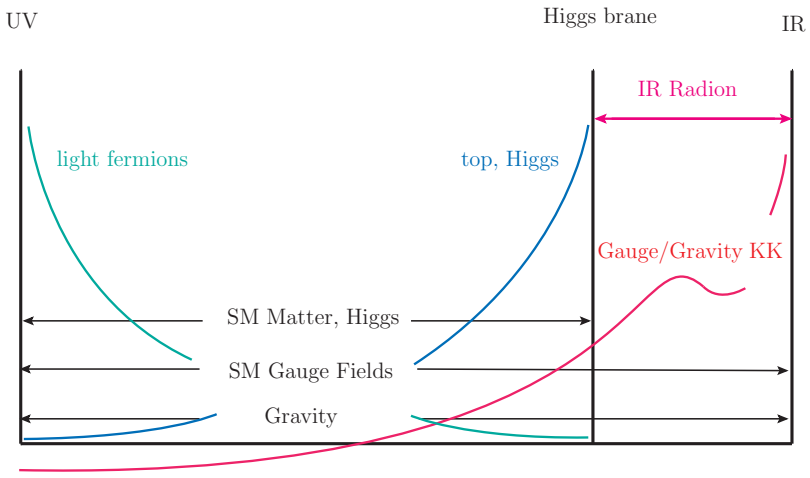

Figure 3.5: Model with one intermediate brane showing light IR radion degree of freedom.

3.2 Model with *one* intermediate brane

We consider gauge and gravity living in the *same* bulk starting at the UV brane, with scale $\Lambda_{\rm UV} \lesssim M_{\rm Pl}$ and ending at the IR brane, with scale $\Lambda_{\rm IR}$, which can be as low as $\sim$ a couple of TeV: see Fig. 3.5. In the notation used in section 3.1, both $\Lambda_{\rm meson}$ and $\Lambda_{\rm glueball}$ are $\sim \Lambda_{\rm IR}$, which are also (roughly) the gauge and graviton KK scales in the 5D model. For now, we will assume the gauge symmetries to be only the SM throughout the bulk so that we do not have A_5's; we will briefly discuss the latter possibility in section 3.2.4. The rest of the SM propagates from the UV brane to an intermediate brane (dubbed "Higgs" brane), taken to be $\sim O(10)$ TeV consistently with (anarchic) flavor bounds. We will discuss more details below, showing that even with contribution from composite states of strong dynamics below $\sim \Lambda_{\rm Higgs}$, our framework is indeed safe from EW and flavor/CP violation precision tests. As usual, the lighter SM fermions are assumed to be peaked near the UV

brane.

3.2.1 Parameters

We use the usual notation where M_5 is the 5D Planck scale and k is the AdS curvature scale. The cubic self-coupling of graviton *KK* modes (or that of one graviton KK to any two modes localized near IR brane, for example, KK gauge) is then given (roughly) by

$$g_\star^{\rm grav} \equiv \sqrt{\frac{k^3}{M_5^3}} \tag{3.1}$$

Also, $g_\star^{\rm grav}$ is dual to coupling of three composites, one of which being spin-2 (and for which we will use the *same* notation).

Similarly, g_5 is the (dimension*ful*) 5D gauge coupling, with the coupling between (three) 4D modes (one of which is gauge KK) localized near IR brane (or three composites, with one being spin-1) given (roughly) by

$$g_\star^{\rm gauge} \equiv g_5\sqrt{k} \tag{3.2}$$

As usual, the sizes of both $g_\star$'s are constrained by perturbativity and fitting observed/4D SM couplings (i.e., of *zero* modes).

However, in the model at hand, there is a *new* ingredient, namely, the intermediate (Higgs/matter) brane which has tension, i.e., is gravitating, resulting in

(i) k being different on the two sides of this brane and

(ii) a new perturbativity constraint associated with branon (brane-bending) degree of freedom.

We will discuss these issues in detail in Appendix A; here we simply summarize. The following choices of couplings (in the far IR) suffice for having a *finite* regime of validity of 5D effective field theory (including the branon degree of freedom):

$$\begin{aligned} g^{\rm grav}_{\star\,{\rm UV}} &< g^{\rm grav}_{\star\,{\rm IR}} \lesssim 3 \\ g^{\rm gauge}_{\star\,{\rm UV}} &\sim g^{\rm gauge}_{\star\,{\rm IR}} \sim 3 \end{aligned} \tag{3.3}$$

while giving observable signals.

3.2.2 Spectrum

We expect to have two radions (dual to dilatons in the CFT description), roughly corresponding to fluctuations of Higgs brane relative to UV (heavier mode) and that of IR brane relative to Higgs brane. We now work out some of the details of this picture. We first give a schematic review of the GW mechanism in the CFT language for the minimal model of Fig. 2.1 [34]. We start in the UV with

$$\mathcal{L}\left(\Lambda_{\rm UV}\right) \ni \mathcal{L}_{\rm CFT} + \lambda\, \Lambda_{\rm UV}^{\epsilon}\, \mathcal{O}_{\rm GW} \tag{3.4}$$

where $\mathcal{O}_{\rm GW}$ is scalar operator with *scaling* dimension $(4-\epsilon)$ (with $\epsilon > 0$): we also use the convention where its naive/engineering dimension is the same so that the

coupling constant λ above is dimension*less*. We assume that $\mathcal{O}_{\rm GW}$ acquires a VEV in the IR, breaking the conformal symmetry spontaneously; this scale can be thought of as the VEV of the dilaton field (denoted by Φ of mass dimension +1). So, we get the dilaton potential

$$\mathcal{L}\left(\Lambda_{\rm IR}\right) \;\ni\; (\partial_\mu \Phi)^2 + \lambda' \Phi^4 + d\,\lambda\,\Phi^4 \left(\frac{\Phi}{\Lambda_{\rm UV}}\right)^{-\epsilon} \tag{3.5}$$

where the second term on the RHS is consistent with conformal symmetry and in the third term, d is an $O(1)$ factor in the interpolation of Φ by $\mathcal{O}_{\rm GW}$. Here, we assume that the scaling dimension of $\mathcal{O}_{\rm GW}$ remains $(4-\epsilon)$ even in the IR and we have dropped subleading terms, i.e. $O\left(\lambda^2 \left(\frac{\Phi}{\Lambda_{\rm UV}}\right)^{-2\epsilon}\right)$.

Minimizing above potential in the IR, we see that the radius is stabilized, i.e., IR scale is fixed as

$$\Lambda_{\rm IR}(\sim \langle\Phi\rangle) \;\sim\; \Lambda_{\rm UV}\left(-d\frac{\lambda}{\lambda'}\right)^{\frac{1}{\epsilon}} \tag{3.6}$$

$$\ll\; \Lambda_{\rm UV},\ \text{assuming } \epsilon < 1 \tag{3.7}$$

where $\sim$ above (and henceforth) indicates validity up to $O(1)$ factors. In particular (and as is well-known), we see that $\epsilon \sim O(0.1)$ (i.e., a mild tuning) together with $(-d\lambda/\lambda') \sim O\Big[1/\left(\text{a few}\right)\Big]$ suffices to generate the enormous Planck-weak hierarchy.

Once again, in the model at hand, we will have two copies of above module, roughly speaking corresponding to the two hierarchies, i.e., $\Lambda_{\rm Higgs}/\Lambda_{\rm UV}$ (roughly the

usual one) and $\Lambda_{\rm IR}/\Lambda_{\rm Higgs}$.[5] As shown in more detail in the Appendix B, the two stabilizations can be done "sequentially", giving a heavy dilaton (mass dictated by $\Lambda_{\rm Higgs}$) and lighter one (mass $\propto \Lambda_{\rm IR}$): for the purpose here (i.e., LHC signals), we will focus on the latter, for which $\Lambda_{\rm Higgs}$ can be simply taken to be a "fixed/UV" scale. The physical dilaton (denoted by φ) corresponds to fluctuations around the VEV, i.e.,

$$\Phi \sim \Lambda_{\rm IR} + a g_\star^{\rm grav} \varphi \tag{3.8}$$

where a is an $O(1)$ factor. Plugging this into the above potential, the *lighter* dilaton mass is then given by [96–99]

$$m_\varphi^2 \sim \epsilon\, \lambda'\, \Lambda_{\rm IR}^2 \tag{3.9}$$

where ϵ is then (roughly) set (as above) to logarithm of hierarchy (the one relevant here is between Higgs and IR branes) and λ' is dual, in 5D, to the amount of detuning of IR brane tension. So, to summarize the various scales, we consider the case:

$$m_\varphi \lesssim \Lambda_{\rm IR} \ll \Lambda_{\rm Higgs}. \tag{3.10}$$

[5] Note that we envisage the new, second hierarchy to be at most $O(10)$, i.e., it is (much) smaller than the usual/first one, thus requiring an even more natural value of ϵ, i.e., $\sim 1/$ a few , cf. $\sim O(0.1)$ for the Planck-weak case.

3.2.3 Couplings

3.2.3.1 Radion/Dilaton

Once again, we treat the separation between UV and Higgs brane to be fixed, thus reducing the (light) radion/dilaton analysis to the usual minimal case with only two branes. We then simply drop the label "IR" on dilaton and $\mathcal{O}_{\rm GW}$.

Coupling to SM gauge fields

These can be deduced from the running of the SM gauge couplings as follows. We start with value $g_{\rm UV}$ at $\Lambda_{\rm UV}$ and pass through various thresholds all the way to M_Z [100]:

$$\begin{aligned}\frac{1}{g_{\rm SM}^2} \approx \frac{1}{g_{\rm UV}^2} &+ b_{\text{strong UV}} \log\left(\frac{\Lambda_{\rm UV}}{\Lambda_{\rm Higgs}}\right) + b_{\text{strong IR}} \log\left(\frac{\Lambda_{\rm Higgs}}{\Lambda_{\rm IR}}\right) + \\ &(b_{\rm SM} - b_{\text{top, Higgs}}) \log\left(\frac{\Lambda_{\rm UV}}{\Lambda_{\rm Higgs}}\right) + b_{\rm SM} \log\left(\frac{\Lambda_{\rm Higgs}}{M_Z}\right) \end{aligned} \tag{3.11}$$

where $b_{\text{strong UV (IR)}}$ are the contributions of UV and IR 4D strong dynamics (including, in the former case, the SM top quark and Higgs, which are composites), respectively, to the running of the SM gauge coupling and $b_{\rm SM}$ is the usual SM contribution.

We expect

$$\begin{aligned} b_{\rm strong} &= \frac{O\left(N_{\rm strong}\right)}{16\pi^2} \\ &\sim \frac{1}{\left(g_\star^{\rm gauge}\right)^2} \end{aligned} \tag{3.12}$$

where in second line, we have used the standard large-N relation that coupling of three composites, i.e., $g_\star^{\rm gauge}$ (in this case, one being spin-1/gauge) is given by $\sim 4\pi/\sqrt{N_{\rm strong}}$. In fact, the 5D result is:

$$b_{\rm strong} \;=\; \frac{1}{g_5^2 k} \tag{3.13}$$

which (as expected) is a good match to the second line of Eq. (3.12) above [using Eq. (3.2)].

The dilaton can be considered to be fluctuations around TeV scale, i.e., $\Lambda_{\rm IR} \to \Lambda_{\rm IR} + a g_\star^{\rm grav}\varphi$ [see Eq. (3.8)]. We plug this into the gauge field kinetic term in the form $F_{\mu\nu}F^{\mu\nu}/\left(4\, g_{\rm SM}^2\right)$, with $g_{\rm SM}$ as in Eq. (3.11). We thus get, after canonically normalizing the gauge field, the dilaton coupling to SM gauge bosons [99, 101, 102]:

$$\begin{aligned}
\delta\mathcal{L} \;&\sim\; g_{\rm SM}^2 b_{\rm strong}\varphi F_{\mu\nu}F^{\mu\nu}\frac{g_\star^{\rm grav}}{\Lambda_{\rm IR}} + ... \\
&\sim\; \left(\frac{g_{\rm SM}}{g_{\star\,\rm IR}^{\rm gauge}}\right)^2 \varphi F_{\mu\nu}F^{\mu\nu}\frac{g_\star^{\rm grav}}{\Lambda_{\rm IR}}.
\end{aligned} \tag{3.14}$$

Coupling to top quark/Higgs

For simplicity, we assume that the top quark/Higgs are *strictly* localized on the Higgs brane, which (as already mentioned) we are treating (effectively) as "UV" brane for the purpose of obtaining couplings of the light radion. In the 5D model, we can couple the Higgs and top quarks to the 5D GW field (used for stabilization) evaluated at the Higgs brane, thereby generating a coupling of radion to the top quark/Higgs. We will work out the size of this induced coupling in the compositeness

picture, the above coupling in the 5D model being dual to:

$$\delta\mathcal{L}\left(\Lambda_{\rm Higgs}\right) \sim \frac{\kappa\Lambda_{\rm Higgs}^{\epsilon}}{\Lambda_{\rm Higgs}^{4}}\mathcal{O}_{\rm GW}\mathcal{O}_{t/H} \tag{3.15}$$

where $\mathcal{O}_{t/H}$ is an operator (of mass dimension 4) containing top quark and Higgs fields (to be discussed more below). Since $\mathcal{O}_{\rm GW}$ obtains a VEV at scale $\Lambda_{\rm IR}$ (fluctuations around which correspond to the dilaton), we can interpolate it in the IR as

$$\mathcal{O}_{\rm GW} \quad \sim \quad \Lambda_{\rm IR}^{3-\epsilon} g_{\star\,\rm IR}^{\rm grav}\varphi \tag{3.16}$$

i.e., (as above) we can choose derivatives to *not* appear on φ, which implies that we must allow the most general form of $\mathcal{O}_{t/H}$ (i.e. we can*not* integrate by parts to get rid of derivatives on top quark and Higgs fields):

$$\mathcal{O}_{t/H} \quad \ni \bar{t}\,\not{\partial}\,t - \left(\partial^{\mu}\bar{t}\right)\gamma_{\mu}t + c_1 y_t \bar{t}tH + c_2\left(\partial_{\mu}H^{\dagger}\right)\partial^{\mu}H + c_3 H^{\dagger}\Box H + \frac{\left(y_t, g_{\rm EW}\right)^2\Lambda_{\rm Higgs}^2}{16\pi^2}H^{\dagger}H \tag{3.17}$$

where c's are *independent/arbitrary* coefficients.

Let us consider dilaton decay from each term in turn. A quick, *explicit* computation shows that amplitude for $\varphi \to \bar{t}t$ from the top quark "kinetic"[6] term in $\mathcal{O}_{t/H}$ is $\propto m_t$: a simple argument based on angular momentum conservation for scalar decay into a fermion-antifermion pair shows that it must be so. So, the first two

[6] quotes are used here since these are actually multiplied by φ.

terms actually contribute similarly to the third term, i.e., "mass" term (where we have included y_t, i.e., SM top Yukawa, as flavor spurion in the power counting).

On the other hand, for $\varphi \to H^\dagger H$, i.e., decay into scalars, there is no such constraint from angular momentum conservation: indeed, we explicitly find that kinetic term for H gives amplitude $\propto p_{H\,1}.p_{H\,2} \approx m_\varphi^2/2$ (in the limit of $m_H \ll m_\varphi$). Note that contribution of the $\Box H$ term (for on-shell H) *is* $\propto m_H^2$, i.e., *actual* mass term, which is $\ll m_\varphi^2$, thus is sub-dominant to the contribution of the Higgs kinetic term. In the last term in $\mathcal{O}_{t/H}$, we have assumed that the SM Higgs complex doublet H is a PNGB so that its "mass squared" is SM loop factors smaller than $\Lambda_{\rm Higgs}^2$. Given our choices of $\Lambda_{\rm Higgs} \sim O(10)$ TeV and $\Lambda_{\rm IR} \sim$ a few TeV, we see that this contribution is – roughly and numerically – comparable to that from the Higgs kinetic term.

So, we can just keep top quark *mass* and Higgs *kinetic* terms in $\mathcal{O}_{t/H}$ above. We then get

$$\delta\mathcal{L}\left(\Lambda_{\rm IR}\right) \sim \kappa \left(\frac{\Lambda_{\rm IR}}{\Lambda_{\rm Higgs}}\right)^{4-\epsilon} g_{\star\,\rm IR}^{\rm grav} \frac{\varphi}{\Lambda_{\rm IR}} \left[m_t \bar{t} t + \left(\partial_\mu H\right)^\dagger \partial^\mu H\right] \tag{3.18}$$

which gives a (much) smaller decay width for dilaton into top/Higgs as compared to SM gauge bosons in final state.[7]

We conclude from the above analyses that the production of the radion/dilaton is dominated by gluon fusion; dilaton decays mostly to two SM gauge bosons, all via Eq. (3.14).

[7] We have checked that other possible contributions to the radion couplings to top/Higgs are comparable to or smaller than the above.

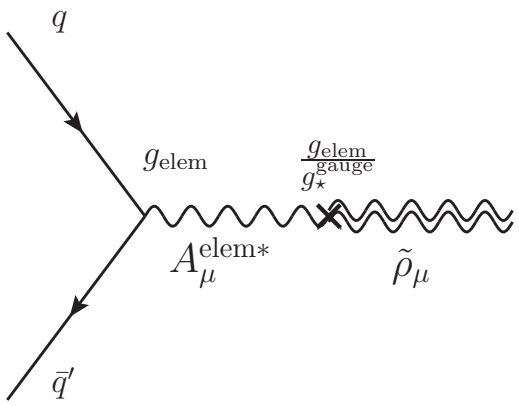

Figure 3.6: Universal spin-1 couplings via elementary-composite mixing (generalization of well-known $\gamma - \rho$ mixing).

3.2.3.2 Spin-1/Gauge KK

We focus here on the lightest spin-1 composite, denoted by $\tilde{\rho}$ (reserving ρ for the mass eigenstate: see below).

Flavor universal coupling

The flavor universal part of coupling of ρ (to matter/Higgs fields) is given by a generalization of the well-known phenomenon of $\gamma - \rho$ mixing from QCD [103] (see also Fig. 3.6), which we briefly review here.

We start with the kinetic and mass terms

$$\begin{aligned}\mathcal{L} \ \ni \ & -\frac{1}{4}\left(\tilde{\rho}^{\mu\nu}\tilde{\rho}_{\mu\nu} + F^{\text{elem }\mu\nu}F_{\text{elem }\mu\nu}\right) + \\ & \frac{1}{2}\Lambda_{\rm IR}^2\left[\tilde{\rho}_\mu\tilde{\rho}^\mu - 2\frac{g_{\rm elem}}{g_\star^{\rm gauge}}\tilde{\rho}^\mu A_\mu^{\rm elem} + \left(\frac{g_{\rm elem}}{g_\star^{\rm gauge}}\right)^2 A_\mu^{\rm elem}A^{\text{elem }\mu}\right] + \\ & g_{\rm elem}\bar{q}A_\mu^{\rm elem}\gamma^\mu q + g_\star^{\rm gauge}\bar{\psi}\tilde{\rho}_\mu\gamma^\mu\psi \end{aligned} \tag{3.19}$$

where $A_\mu^{\rm elem}$ denotes gauge field *external* to the 4D strong dynamics (thus often called

"elementary"): *all* SM matter (fermions and Higgs boson, denoted generically by q above) couple to it with strength $g_{\rm elem}$. Similarly, all composite fermions of strongly coupled sector are denoted by ψ and composite vector meson $\tilde{\rho}_\mu$ couples to them with strength $g_\star^{\rm gauge}$. Note that the second term in the second line of Eq. (3.19), $\sim \tilde{\rho}_\mu A_\mu^{\rm elem}$, is obtained by starting from $A_\mu^{\rm elem} J^\mu_{\text{strong IR}}$ and then using the usual interpolation for (the lightest) spin-1 composites (ρ mesons):

$$J^\mu_{\text{strong IR}} \sim \frac{\Lambda_{\rm IR}^2}{g_\star^{\rm gauge}} \rho^\mu_{\rm IR}. \tag{3.20}$$

As we will see, even though the above mass terms break *elementary* gauge symmetry, there *is* a residual gauge invariance (corresponding to a massless field) which we identify with the final SM gauge symmetry [103]. We diagonalize the mass terms by defining the physical states (admixtures of $\tilde{\rho}$ and $A_\mu^{\rm elem}$):

$$A_\mu = \cos\theta A_\mu^{\rm elem} + \sin\theta \tilde{\rho}_\mu \tag{3.21}$$

$$\rho_\mu = \cos\theta \tilde{\rho}_\mu - \sin\theta A_\mu^{\rm elem} \tag{3.22}$$

and

$$\sin\theta = \frac{g_{\rm elem}}{\sqrt{g_{\rm elem}^2 + g_\star^{\rm gauge\ 2}}}. \tag{3.23}$$

This gives

$$\begin{aligned}\mathcal{L} \;\ni\; & -\frac{1}{4}\left(\rho^{\mu\nu}\rho_{\mu\nu} + F^{\mu\nu}F_{\mu\nu}\right) + \\ & \frac{1}{2}\Lambda_{\rm IR}^2\rho^\mu\rho_\mu + g_{\rm SM}\bar{\psi}A^\mu\gamma_\mu\psi + g_\star^{\rm gauge}\bar{\psi}\rho^\mu\gamma_\mu\psi + \\ & g_{\rm SM}\bar{q}A^\mu\gamma_\mu q + \frac{g_{\rm SM}g_{\rm elem}}{g_\star^{\rm gauge}}\bar{q}\rho^\mu\gamma_\mu q + \cdots \end{aligned} \tag{3.24}$$

where the last term is the (universal) coupling of SM fermions to ρ. Also, as anticipated above, A_μ is massless (thus corresponds to the SM gauge field), with

$$g_{\rm SM} \;=\; \frac{g_\star^{\rm gauge}g_{\rm elem}}{\sqrt{g_{\rm elem}^2 + g_\star^{\rm gauge\ 2}}} \tag{3.25}$$

being the SM gauge coupling. Henceforth, we will assume $g_{\rm elem} \ll g_\star^{\rm gauge}$ so that

$$g_{\rm SM} \;\approx\; g_{\rm elem} \tag{3.26}$$

and coupling of SM fermions to ρ is $\approx g_{\rm SM}^2/g_\star^{\rm gauge}$.

Couplings to radion/dilaton

As discussed above, couplings of dilaton/radion can be obtained by using it as a "compensator" for $\Lambda_{\rm IR}$, giving Eq. (3.14) from dependence of $g_{\rm SM}$ [8] on $\Lambda_{\rm IR}$ (via RG evolution of the gauge coupling) *and* a coupling to two $\tilde{\rho}$'s (which gets converted

[8] More precisely, dependence of $g_{\rm SM}$ on $\Lambda_{\rm IR}$ originates from dependence of $g_{\rm elem}$ on $\Lambda_{\rm IR}$ via the relation $\frac{1}{g_{\rm SM}^2} = \frac{1}{g_{\rm elem}^2} + \frac{1}{g_\star^{\rm gauge\ 2}}$.

mostly into two ρ's):

$$\begin{aligned}\delta\mathcal{L} &\sim \Lambda_{\rm IR}^2\tilde{\rho}_\mu\tilde{\rho}^\mu \\ &\to \Phi_{\rm IR}^2\tilde{\rho}_\mu\tilde{\rho}^\mu \\ &\ni g_{\star\,\rm IR}^{\rm grav}\Lambda_{\rm IR}\varphi\rho^\mu\rho_\mu \end{aligned} \tag{3.27}$$

which however is not relevant for collider signals. Note that using $\gamma-\rho$ mixing in first line of Eq. (3.27), one *naively* obtains couplings of φ to $A_\mu A^\mu$ or $A_\mu\rho^\mu$; however, after properly adding contributions from the other two terms in the second line of Eq. (3.19), we can see that these terms vanish.

In addition, *after* radius stabilization/explicit breaking of conformal symmetry, we get a mixed coupling of dilaton, i.e., to ρ and SM gauge field as follows. In the IR, we can interpolate the GW operator as

$$\mathcal{O}_{\rm GW} \ni \Lambda_{\rm IR}^{-\epsilon}\tilde{\rho}^{\mu\nu}\tilde{\rho}_{\mu\nu}. \tag{3.28}$$

Plugging above in Eq. (3.4), RG-running down to $\Lambda_{\rm IR}$ and then promoting $\Lambda_{\rm IR}\to\Lambda_{\rm IR}+ag_{\star\,\rm IR}^{\rm grav}\varphi$, we get

$$\begin{aligned}\delta\mathcal{L}\left(\Lambda_{\rm IR}\right) &\sim \lambda\left(\frac{\Lambda_{\rm IR}}{\Lambda_{\rm Higgs}}\right)^{-\epsilon}\tilde{\rho}^{\mu\nu}\tilde{\rho}_{\mu\nu} \\ &\sim \lambda\epsilon g_{\star\,\rm IR}^{\rm grav}\left(\frac{\Lambda_{\rm IR}}{\Lambda_{\rm Higgs}}\right)^{-\epsilon}\frac{\varphi}{\Lambda_{\rm IR}}\tilde{\rho}^{\mu\nu}\tilde{\rho}_{\mu\nu}. \end{aligned} \tag{3.29}$$

Finally, plugging the mass eigenstates from Eq. (3.22) into above gives[9]:

$$\delta\mathcal{L}\left(\Lambda_{\rm IR}\right) \;\sim\; \lambda\epsilon g^{\rm grav}_{\star\,\rm IR}\left(\frac{\Lambda_{\rm IR}}{\Lambda_{\rm Higgs}}\right)^{-\epsilon}\frac{g_{\rm elem}}{g^{\rm gauge}_{\star\,\rm IR}}\rho^{\mu\nu}F^{\mu\nu}\frac{\varphi}{\Lambda_{\rm IR}}. \tag{3.30}$$

From Eq. (3.7), here we have $\epsilon \sim 1/\log\left(\Lambda_{\rm Higgs}/\Lambda_{\rm IR}\right) \sim 1/$ a few, since the relevant hierarchy is $\Lambda_{\rm Higgs}/\Lambda_{\rm IR}$ as indicated (again, it is *not* the large one: $\Lambda_{\rm UV}/\Lambda_{\rm IR}$), and from this we also see that $\left(\Lambda_{\rm IR}/\Lambda_{\rm Higgs}\right)^{-\epsilon}$ is an $O(1)$ factor. Thus, the ρ-dilaton-SM gauge boson coupling in Eq. (4.11) can be (roughly) comparable to the last term in Eq. (3.24), i.e., universal ρ coupling (assuming $g^{\rm grav}_{\star\,\rm IR} \sim 1$). Note that *decay* of ρ to two φ (cf. spin-2 below) is *not* allowed by a combination of Bose-Einstein statistics and angular momentum conservation arguments.

Flavor *non*-universal couplings to top/Higgs

On the other hand, the flavor non-universal part of the ρ couplings (relevant only for top quark/Higgs: negligible for light fermions, at least for LHC signals) arises from

$$\delta\mathcal{L}\left(\Lambda_{\rm Higgs}\right) \sim \frac{\left(g^{\rm gauge}_{\star\,\rm UV}\right)^2}{\Lambda^2_{\rm Higgs}}J^{\mu}_{\rm strong\;IR}\left(\bar{t}\gamma_\mu t + H^\dagger D_\mu H\right) \tag{3.31}$$

where this coupling of top/Higgs to IR strong dynamics is generated by integrating out physics of top/Higgs compositeness at scale $\sim \Lambda_{\rm Higgs}$, with a coupling characteristic of gauge sector of the *UV* strong dynamics (see appendix B for further

[9]The same procedure also results in couplings of the form $\varphi\rho^{\mu\nu}\rho_{\mu\nu}$ or $\varphi F^{\mu\nu}F_{\mu\nu}$, i.e., *corrections* to the couplings of dilaton/radion to *pairs* of SM gauge fields *from radius stabilization* [99, 102] and ρ's; however, these are *sub*-dominant to the pre-existing ones, hence we will not discuss them further.

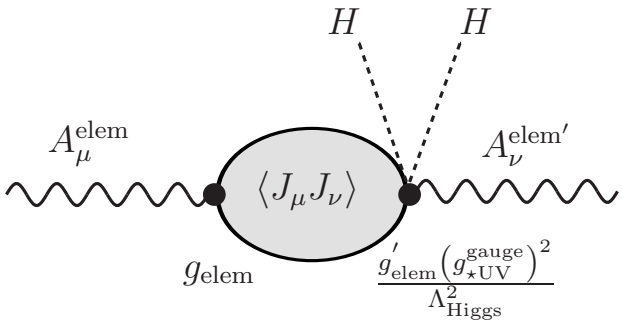

Figure 3.7: Contribution to the S-parameter from the IR strong dynamics.

explanation of the UV and IR CFT's with stabilization mechanism). This runs down to the IR:

$$\delta\mathcal{L}\left(\Lambda_{\rm IR}\right) \;\sim\; \frac{\left(g^{\rm gauge}_{\star\,\rm UV}\right)^2}{g^{\rm gauge}_{\star\,\rm IR}}\left(\frac{\Lambda_{\rm IR}}{\Lambda_{\rm Higgs}}\right)^2 \rho^\mu_{\rm IR}\left(\bar{t}\gamma_\mu t + H^\dagger D_\mu H\right) \tag{3.32}$$

where we have used the interpolation relation of Eq. (3.20).

Clearly, the production of ρ at the LHC proceeds via light quark coupling in last term in Eq. (3.24), while decays occur via same coupling *and* that in Eq. (4.10) and (4.11), assuming φ is lighter than ρ.

Electroweak and flavor/CP violation precision tests

The physics of top/Higgs compositeness with characteristic mass scale $\sim \Lambda_{\rm Higgs}$ (where the UV strong dynamics confines) contributes to EW and flavor/CP violation precision tests. However, as we already indicated at the beginning of section 3.2, these contributions are safe from experimental constraints for the choice of $\Lambda_{\rm Higgs} \sim \mathcal{O}(10)$ TeV. Notice that the (small) flavor non-universal parts of the couplings of spin-1 resonances of the *IR* strong dynamics [see Eq. (4.10)] – which are

suppressed by $\sim \Lambda_{\rm Higgs}$ – *also* give contributions (via their virtual exchange) to EW and flavor/CP violation precision tests. However, as we will show now, such effects are comparable to the *direct* (albeit still virtual) effects of $\Lambda_{\rm Higgs}$ scale physics hence are safe/on the edge (just like the latter).

We begin our discussion by considering contributions of IR strong dynamics to precision tests observables using the above non-universal coupling only *once*, for example, the operator corresponding to the S-parameter:

$$\begin{aligned} \delta\mathcal{L} &\sim C\, W^3_{\mu\nu} B_{\mu\nu} H^\dagger H, \text{ with} \\ C &\equiv \frac{g g' S}{16\pi v^2}, \end{aligned} \tag{3.33}$$

W_3 and B being the neutral $SU(2)$ and hypercharge gauge fields and g (g') are the respective gauge couplings. Integrating out physics at and above the scale $\sim \Lambda_{\rm Higgs}$ generates in the IR effective theory the above operator with coefficient $C_{\rm UV} \sim g g'/\Lambda^2_{\rm Higgs}$ (based on usual, naive dimensional analysis). The contribution from the IR strong dynamics can be obtained by computing the diagram shown in Fig. 3.7. Such a diagram can be generated by sewing together Eq. (3.31) (non-universal coupling) and the (universal) coupling $A_\mu J^\mu_{\text{strong IR}}$ [mentioned below Eq. (3.19)], via the common $J^\mu_{\text{strong IR}}$.

$$g_{\rm elem}\, (g^{\rm gauge}_{\star\ \rm UV})^2\, A^{\rm elem}_\mu \langle J^\mu_{\text{strong IR}} J^\nu_{\text{strong IR}} \rangle \frac{J^{\rm t/H}_\nu}{\Lambda^2_{\rm Higgs}}. \tag{3.34}$$

The current-current correlator $\langle J^\mu(p) J^\nu(-p)\rangle$ contains the piece $\left(\eta^{\mu\nu} - \frac{p^\mu p^\nu}{p^2}\right) p^2 \log p^2$

which contributes to the S-parameter operator. We thus find a log-divergence in the S-parameter in the theory below $\Lambda_{\rm Higgs}$. Finally, matching to the S-parameter operator and using Eq. (3.12) for overall size of correlator, we get $C_{\text{strong IR}} \sim gg' \log\left(\Lambda_{\rm Higgs}/\Lambda_{\rm IR}\right)/\Lambda^2_{\rm Higgs}$.[10] As already mentioned above, the *total* contribution of the IR strong dynamics to S-parameter is then comparable to that from physics at $\Lambda_{\rm Higgs}$. However, there is an important feature we want to emphasize. Namely, the contribution of IR strong dynamics to S-parameter shows a mild *logarithmic* enhancement! This enhancement, however, is not harmful because, with custodial symmetry protection, the constraint from EW precision test on the Higgs compositeness scale in the minimal model of Fig. 2.1 can be as low as ~ 3 TeV [50] so that, even with the above enhancement in the extension in Fig. 3.5, the overall size is small enough with $\Lambda_{\rm Higgs} \sim O(10)$ TeV.

Next, we consider cases where *two* non-universal couplings are involved, giving (for example) a 4-top quark operator, which after rotation to mass basis for quarks will give flavor-violating effects even for light fermions such as $K-\bar{K}$ mixing [55,59]. Clearly, the contribution of UV strong dynamics to such effects is $\propto 1/\Lambda^2_{\rm Higgs}$ (just like for S-parameter above). For the IR strong dynamics contribution, we combine Eq. (3.31) with itself in this case. Here, the current-current correlator can instead give a *quadratic* divergence, which reduces the initial $\sim 1/\Lambda^4_{\rm Higgs}$ suppression by two powers. That is, the contribution from the entire IR strong dynamics to such flavor/CP violating processes are comparable to that of the physics of the UV strong

[10] We have also checked explicitly that the contribution to the S-parameter from the *sum* over tree-level exchanges of composite resonances (in the 4D picture with strong dynamics) or gauge KK modes (from the 5D model) gives a log-divergence.

dynamics, hence safe.

We stress that, for a *fixed* $\Lambda_{\rm Higgs}$, the contribution to precision tests from IR strong dynamics is (roughly) *independent* of $\Lambda_{\rm IR}$ so that there is no relevant constraint on $\Lambda_{\rm IR}$ from here; instead the bound on $\Lambda_{\rm IR}$ is dominated by the direct LHC searches which will be discussed in section 3.3.2.1.

3.2.3.3 Spin-2/Graviton KK

We denote the composite spin-2 by $H^{\mu\nu}$. In general, $H^{\mu\nu}$ couples to not only $T_{\mu\nu}$ of composites, but also other possible Lorentz structures built out of the latter fields [104]. Here, for simplicity and because it dominates in warped 5D effective field theory, we will use (only) $T_{\mu\nu}$ as a representative structure (others will anyway give roughly similar size for coupling/amplitude). If experiments show spin structures other than $T_{\mu\nu}$, it would point to strong dynamics without a good 5D dual.

Coupling to SM gauge bosons

The coupling of $H^{\mu\nu}$ to *SM* gauge bosons is obtained (see Fig. 3.8) by first coupling it to $\tilde{\rho}$'s with strength $g^{\rm grav}_{\star\,{\rm IR}}$ (i.e., a 3-composite vertex), followed by mixing of $\tilde{\rho}$'s with external gauge field (as outlined above), i.e.,

$$\begin{aligned} \delta\mathcal{L}\left(\Lambda_{\rm IR}\right) &\sim \frac{g^{\rm grav}_{\star\,{\rm IR}}}{\Lambda_{\rm IR}} H^{\mu\nu} T^{(\tilde{\rho})}_{\mu\nu} \\ &\to \left(\frac{g_{\rm SM}}{g^{\rm gauge}_{\star\,{\rm IR}}}\right)^2 \frac{g^{\rm grav}_{\star\,{\rm IR}}}{\Lambda_{\rm IR}} H^{\mu\nu} T^{({\rm gauge})}_{\mu\nu}. \end{aligned} \tag{3.35}$$

Coupling to radion/dilaton

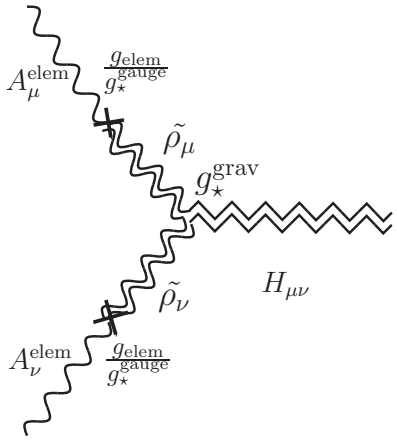

Figure 3.8: Spin-2 KK graviton couplings to SM gauge bosons

In addition, we have the coupling to two dilatons/radions:

$$\delta\mathcal{L}\left(\Lambda_{\rm IR}\right) \sim \frac{g_{\star\,{\rm IR}}^{\rm grav}}{\Lambda_{\rm IR}} H^{\mu\nu} T_{\mu\nu}^{(\varphi)}. \tag{3.36}$$

Of course, this is relevant for decay of composite spin-2/KK graviton only if $m_\varphi \lesssim \Lambda_{\rm IR}/2$ and in this case, dominates over other decays: see, for example, [95].

Flavor *non*-universal coupling (to top/Higgs)

Finally, coupling to top quark/Higgs follows from a procedure similar to spin-1 above, i.e., we have

$$\delta\mathcal{L}\left(\Lambda_{\rm Higgs}\right) \sim \frac{\left(g_{\star\,{\rm UV}}^{\rm grav}\right)^2}{\Lambda_{\rm Higgs}^4} T^{\mu\nu\,(t/H)} T_{\mu\nu}^{(\text{strong IR})} \tag{3.37}$$

where $T^{\mu\nu\,(t/H)}(T_{\mu\nu}^{(\text{strong IR})})$ is energy-momentum tensor made of top/Higgs fields (preons of IR strong dynamics) and this coupling of top/Higgs to IR strong dynamics is generated by integrating out physics at the scale $\sim \Lambda_{\rm Higgs}$, with a coupling characteristic of gravity sector of the UV strong dynamics. After IR theory

hadronizes, Eq. (3.37) becomes

$$\delta\mathcal{L}\left(\Lambda_{\rm IR}\right) \sim \left(\frac{\Lambda_{\rm IR}}{\Lambda_{\rm Higgs}}\right)^4 \frac{\left(g^{\rm grav}_{\star\,\rm UV}\right)^2}{g^{\rm grav}_{\star\,\rm IR}} \frac{H^{\mu\nu}}{\Lambda_{\rm IR}} T^{(t/H)}_{\mu\nu} \tag{3.38}$$

using the interpolation

$$T^{\rm strong\ IR}_{\mu\nu} \sim \frac{\Lambda^3_{\rm IR}}{g^{\rm grav}_{\star\,\rm IR}} H_{\mu\nu}. \tag{3.39}$$

Production of composite spin-2/KK graviton occurs via coupling to gluons in Eq. (3.35). Decays of composite spin-2/KK graviton is dominated by the same couplings, i.e., into *all* SM gauge bosons *and* to pair of dilatons via Eq. (3.36), assuming $m_\varphi < \Lambda_{\rm IR}/2$. We give a summary of relevant couplings in table 3.2.4.

Given the above flavor non-universal couplings of KK graviton of the IR strong dynamics (cf. those of gauge KK discussed earlier), it is clear that contributions from KK graviton exchange to precision tests are suppressed compared to those of gauge KK by $\sim E^2/\Lambda^2_{\rm Higgs}$, where E is the characteristic (low) energy of the corresponding test. Hence, there is no additional constraint here from the KK graviton sector.

3.2.4 Extended Bulk Gauge Symmetries/Dual to PNGBs of Vector-Like Confinement

Relation to vector-like confinement

We can enlarge the bulk gauge symmetries beyond the SM.

Resonance \ Type of coupling	Higgs compositeness-sensitive	flavor-blind
radion/dilaton	$\frac{g^{\rm grav}_{\star\,\rm IR}}{\Lambda_{\rm IR}}\left(\frac{\Lambda_{\rm IR}}{\Lambda_{\rm Higgs}}\right)^{4-\epsilon}\left[m_t\bar{t}t+(\partial H)^2\right]$	$\frac{g^{\rm grav}_{\star\,\rm IR}}{\Lambda_{\rm IR}}\left(\frac{g_{\rm SM}}{g^{\rm gauge}_{\star\,\rm IR}}\right)^2 F^{\mu\nu}F_{\mu\nu}$
KK Z	$\frac{\left(g^{\rm gauge}_{\star\,\rm UV}\right)^2}{g^{\rm gauge}_{\star\,\rm IR}}\left(\frac{\Lambda_{\rm IR}}{\Lambda_{\rm Higgs}}\right)^2\left(\bar{t}\gamma^\mu t+H^\dagger\partial^\mu H\right)$	$\frac{g^2_{\rm EW}}{g^{\rm gauge}_{\star\,\rm IR}}\left(\bar{q}\gamma^\mu q+\bar{l}\gamma^\mu l\right)$ (*all* generations)
KK gluon	$\frac{\left(g^{\rm gauge}_{\star\,\rm UV}\right)^2}{g^{\rm gauge}_{\star\,\rm IR}}\left(\frac{\Lambda_{\rm IR}}{\Lambda_{\rm Higgs}}\right)^2\bar{t}\gamma^\mu t$	$\frac{g^2_{\rm QCD}}{g^{\rm gauge}_{\star\,\rm IR}}\bar{q}\gamma^\mu q$ (*all* generations)
KK graviton	$\frac{\left(g^{\rm grav}_{\star\,\rm UV}\right)^2}{g^{\rm grav}_{\star\,\rm IR}}\frac{1}{\Lambda_{\rm IR}}\left(\frac{\Lambda_{\rm IR}}{\Lambda_{\rm Higgs}}\right)^4 T^{(t/H)}_{\mu\nu}$	$\frac{g^{\rm grav}_{\star\,\rm IR}}{\Lambda_{\rm IR}}\left(\frac{g_{\rm SM}}{g^{\rm gauge}_{\star\,\rm IR}}\right)^2 T^{(\rm gauge)}_{\mu\nu}$

Table 3.3: Summary of universal and non-universal couplings of various composites for the model with one intermediate brane. $T^{(t/H)}_{\mu\nu}(T^{(\rm gauge)}_{\mu\nu})$ is energy-momentum tensor made of top/Higgs (SM gauge bosons) fields.

We then consider breaking them down to the smaller groups (while preserving the SM subgroup of course) on the various branes by simply imposing Dirichlet boundary condition, i.e.,

$$G_{\rm UV} \overset{\Lambda_{\rm Higgs}}{\to} G_{\rm IR} \overset{\Lambda_{\rm IR}}{\to} H_{\rm IR} \supset {\rm SM} \tag{3.40}$$

where each stage of gauge symmetry breaking delivers (scalar) A_5's, localized at the corresponding brane (including possibly the SM Higgs boson in the first step). Such a framework is shown in Figs. 3.4 and 3.9. These A_5's are dual to PNGBs arising from spontaneous breakdown of global symmetries of the strong dynamics corresponding to the gauged ones shown in Eq. (3.40) [36]. In particular, the 4D physics dual to the last stage of breaking (rightmost bulk in Figs. 3.4 and 3.9), i.e., SM symmetries being unbroken, is known in the literature as vector-like confinement [75]. While from the 5D viewpoint, presence of A_5's seems rather "non-minimal", it is quite natural to have PNGB's in 4D strong dynamics as illustrated by ordinary QCD. In fact, QCD-like strong dynamics was first used to realize the general idea of vector-like confinement.

Note that A_5's are massless at tree-level (in the presence of only the above boundary condition breaking), acquiring a potential via loops, with mass scale being set by corresponding Λ. Thus they are naturally light, as expected from them being dual to PNGB's. Gauge and graviton KK modes (and even possibly the radion) can then decay into pairs of A_5's, drastically modifying the LHC signals of the gauge and graviton KK (or radion) based only on the couplings shown earlier. In

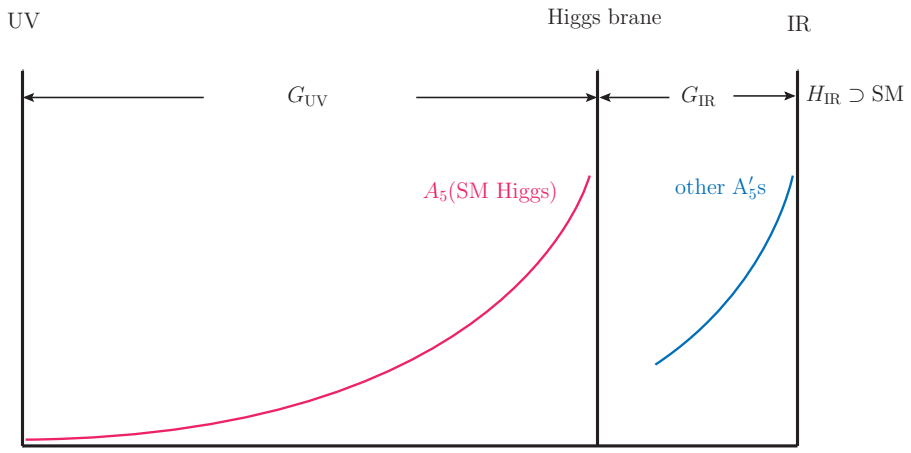

Figure 3.9: Extended bulk gauge symmetries, with rightmost bulk segment being dual to vector-like confinement

this chapter, we take the *minimal* 5D perspective in assuming that A_5's are absent, cf. the expectation based on QCD-like 4D strong dynamics. Hence, gauge KK will decay dominantly into pairs of SM fermions, while SM gauge bosons will be the search channel for KK graviton and radion, as mentioned earlier. Remarkably, the flexibility afforded by 5D leads to broader class of models, with more diverse phenomenology than contemplating just 4D QCD-like strong dynamics.

Coupling to two SM gauge bosons

There is an interesting comparison with dilaton/radion that we would like to draw by considering the simplest mechanism for production and decay of (single) A_5 (dual to PNGB). Namely, PNGB famously has a coupling to two weakly-coupled gauge bosons via the (gauged) Wess-Zumino-Witten term, for example, we have $\pi^0 F_{\mu\nu}\tilde{F}^{\mu\nu}$ leading to the decay $\pi^0 \to \gamma\gamma$ in real-world QCD. This interaction is dual to the one originating for the A_5 from the Chern-Simons term in the 5D model (see

also discussions in [81, 105]):

$$\begin{aligned} \mathcal{L}_{5\mathrm{D}} \;&\ni\; K f_{abc} \epsilon^{MNRST} A^a_M F^b_{NR} F^c_{ST} + ... \\ &\sim\; K f_{abc} A^a_5 F^{b\,\mu\nu} \tilde{F}^c_{\mu\nu} + ... \end{aligned} \tag{3.41}$$

where a, b, c are gauge adjoint indices.

Crucially, we see that, *ir*respective of considerations of parity as a fundamental symmetry, the coupling of A_5 to two SM gauge bosons via Chern-Simons term has "CP-odd" structure, i.e., involves $F_{\mu\nu}\tilde{F}^{\mu\nu}$. This feature is in *contrast* to the "CP-even" coupling, i.e., to $F_{\mu\nu}F^{\mu\nu}$, of dilaton/radion as we see in Eq. (3.14). Let us compare to vector-like confinement, in particular, QCD-like dynamics: this theory respects parity even in the IR and PNGB's are parity-odd (as per the Vafa-Witten theorem [106, 107]), which enforces a coupling to pairs of SM gauge bosons to be to the combination $F_{\mu\nu}\tilde{F}^{\mu\nu}$. However, we see that there is a more general (than parity) argument for such a structure from Chern-Simons term in 5D.

Moreover, the 5D Chern-Simons term is *dual* to anomalies in global currents of the 4D strong dynamics, i.e., K of Eq. (3.41) – appropriately made dimensionless – is related to the coefficient of the *chiral* anomaly in 4D. In this sense, we see that there is actually a *similarity* in the couplings of A_5 (PNGB) and dilaton to two SM gauge bosons, i.e., both are driven by anomalies: chiral for former vs. *scale* anomaly for dilaton [as seen clearly in first line of Eq. (3.14), i.e., the "b_{strong}"-form].

3.3 Phenomenology

General features

We first discuss some overall points, before studying each particle in detail. Assuming $\Lambda_{\rm Higgs} \gg \Lambda_{\rm IR}$, the couplings of the (lightest) KK/composite spin-1 gauge bosons to the SM matter (fermions and Higgs) are *significant* (albeit mildly suppressed relative to the SM values) and (approximately) flavor-*blind*: see last term in Eq. (3.24) and Eq. (4.10). On the other hand, radion and KK/composite graviton couple predominantly to pairs of SM gauge bosons and *negligibly* to SM matter: see Eqs. (3.35), (3.38), (3.14) and (4.5). This feature is in sharp contrast to *standard* minimal model of Fig. 2.1, where couplings to heavy SM (top quark/Higgs/longitudinal W/Z) dominate as far as decays are concerned. So, dilepton, diphoton and dijet final states are usually – and correctly – *neglected*, but now they acquire significance or even the dominant role. At the same time, the (small) flavor non-universality arising in these couplings (i.e., Higgs/top compositeness scale) can be probed by *precision* studies of these *flavor-universal resonances* (of mass $\sim \Lambda_{\rm IR}$), thereby distinguishing it from (purely) vector-like confinement (which corresponds to decoupling of top/Higgs compositeness scale), rather experimentally one can see the latter as a vestige of a full solution to the Planck-weak hierarchy. Finally, in the case of a unified bulk gauge symmetry, i.e., *entire* SM gauge group is subgroup of *simple* IR bulk gauge group ($H_{\rm IR}$ of Eq. (3.40)), we should of course also find that resonances come in complete degenerate unified multiplets. This is dual to the IR strong dynamics having a simple global symmetry partially gauged

by SM.

3.3.1 Radion/dilaton

Dilaton Production

Note that dilaton can be somewhat lighter than higher spin composites [see Eq. (4.1)], thus possibly the first particle to be discovered. Rough estimates of the (total) cross-section (from gluon fusion) for $g_\star^{\rm grav} = 1$; $g_\star^{\rm QCD} = 3$, $\Lambda_{\rm IR} = 3$ TeV and m_φ =1 (2) TeV are $\sigma_{\rm tot} \sim 80$ (~ 4.4) fb.[11] One of these sample points was mentioned as part of table 3.1 in introduction.

Dilaton Decay

Moving onto decays of dilaton, these are dominantly to two SM gauge bosons (based on the couplings discussed earlier, assuming $\Lambda_{\rm Higgs} \gg \Lambda_{\rm IR}$). It is noteworthy that in the unified case, i.e., SM gauges a subgroup of a simple global symmetry group of 4D strong dynamics, considering $SU(5)$ unification as an example here, we obtain the following relation [see Eq. (3.14)]:

$$\frac{C_{\varphi\gamma\gamma}}{g_\gamma^2} : \frac{C_{\varphi ZZ}}{g_Z^2} : \frac{C_{\varphi WW}}{g_W^2} : \frac{C_{\varphi gg}}{g_{QCD}^2} = \frac{8}{3} : \frac{5}{8} : 1 : 1 \tag{3.42}$$

where $C_{\varphi VV}$ denotes the coupling of the dilaton to two corresponding SM gauge bosons and g_V's are corresponding SM gauge couplings, both being renormalized at a relevant energy scale (roughly at $\mu \sim m_\varphi$). This striking feature can be checked by measuring dilaton BR's. Numerically, BR's to $\gamma\gamma$, ZZ, WW and gg (in this

[11] All cross-section numbers are for LHC13 and have been obtained using implementations of above models into Madgraph.

unified case) are $\approx 0.7\%$, 1%, 3% and 95%, respectively. However, note that the above universality (among the SM gauge groups) feature applies for *any* $H_{\rm IR}$-singlet composite scalar. In this sense dilaton is not unique. The current bounds on cross-section $\times$ BR to di-photons from resonant di-photon searches at the LHC [108,109] are ~ 0.5 (0.2) fb for 1 (2) TeV mass. Similarly, di-jet searches [110] give a bound of ~ 200 fb (1 pb) for 2 (1) TeV mass. Both of these are satisfied for the above illustrative choice of parameters, although the 1 TeV case is on the edge of the di-photon bound. Note that values of $g_\star^{\rm grav}$ larger than 1 would then be ruled out (keeping other parameters the same). However, for the model with two intermediate branes to be discussed in section 3.4, we will show that such values of $g_\star^{\rm grav}$ can indeed satisfy the bounds.

CP structure

The CP-even structure of the couplings to SM gauge bosons for dilaton vs. CP-odd for A_5/PNGB's (discussed above: see Eqs. (3.41) and (3.14)) is an important issue. It can be discriminated by (for example) decays to $ZZ \to$ four leptons, using the additional observables therein, i.e., corresponding to polarization of Z (as compared to using just angular distribution of spin-summed SM gauge boson taken as "final" state, which is the same for both cases) [111].

3.3.2 Spin-1 composite

Here, we have more than one type, each with several competing decay channels. So, we need more detailed analysis for obtaining bounds/signals. We give

some general arguments first. In the *unified* case, based on same mass and composite coupling as in Eq. (3.24), we should find for $SU(5)$ unification as an example (similarly to the radion above)

$$\frac{\sigma_{q\bar{q}\to\rho_\gamma}}{g_\gamma^4} : \frac{\sigma_{q\bar{q}\to\rho_Z}}{g_Z^4} : \frac{\sigma_{q\bar{q}\to\rho_W}}{g_W^4} : \frac{\sigma_{q\bar{q}\to\rho_g}}{g_{QCD}^4} = \frac{8}{3} : \frac{5}{8} : 1 : 1 \tag{3.43}$$

where $\sigma_{q\bar{q}\to\rho_V}$ denotes the production cross section of the composite spin-1 resonance which mixes with external gauge boson V and g_V's are corresponding SM gauge couplings renormalized at a relevant energy scale (roughly at $\mu \sim M_{\rm KKgauge}$). In the *non*-unified case, while the above relations do not apply, the following *correlation* between radion decays and spin-1 production cross-section can nonetheless be tested: as seen from Eqs. (3.14) and (3.24), we expect

$$\begin{aligned} \frac{\left(\begin{smallmatrix}\text{coupling of dilaton}\\ \text{to SM gauge boson}\end{smallmatrix}\right) \times (\text{gauge coupling})^2}{(\text{corresponding})\ \text{composite spin-1}\ \textit{cross-section}} &\approx \begin{pmatrix}\text{same for } \textit{all}\\ \text{SM gauge groups}\end{pmatrix} \\ &\propto g_\star^{\rm grav}. \end{aligned} \tag{3.44}$$

Remarkably, in spite of apparent lack of unification (i.e., $b_{\rm strong}$ is different for different gauge groups), we find that the above ratio *is* universal! Moreover, it applies only for the case of composite scalar being dilaton, i.e., the above relation is *not* valid for a generic scalar composite. In contrast, in the unified case, the above correlation is *not* independent of the two separate relations discussed earlier, i.e., Eqs. (3.42) and (3.43).

Note that the universal constant on RHS of Eq. (3.44) involves $g_\star^{\rm grav}$ [apart from

other known factors: see Eq. (3.14) and last term of Eq. (3.24)]. Thus, independent determination of $g_\star^{\rm grav}$, for example, from KK graviton measurements could provide an interesting test of this framework using Eq. (3.44). This would apply to *both* unified and non-unified cases discussed above.

3.3.2.1 Current bounds in flavor-universal limit

Based on the suppressed (as compared to the SM, but still non-negligible) and flavor-universal coupling in the last term of Eq. (3.24), we find that spin-1 masses of a *few* TeV are still consistent with the LHC searches performed so far in *multiple* channels . We now move onto more details, discussing bounds on KK Z first, followed by KK gluon.

KK Z

(i) Di-lepton:

Note that composite/KK Z in this case is (approximately) like sequential SM Z', but with coupling to light quarks inside proton (the dominant production mechanism) being *reduced* by $\sim g_{\rm EW}/g_\star^{\rm EW}$. We find that predicted cross-section of sequential SM Z' exceeds the bound [112, 113] by ~ 70 (25) for $M_{Z'} \sim 2$ (2.5) TeV. Translating this bound to our case, we get (setting $g_{\rm EW} \sim 0.6$):

$$\Lambda_{\rm IR} \gtrsim 2 \text{ TeV for } g_\star^{\rm EW} \sim 5 \tag{3.45}$$

$$\gtrsim 2.5 \text{ TeV for } g_\star^{\rm EW} \sim 3 \tag{3.46}$$

Of course, only the smaller values of $g_\star^{\rm gauge}(\sim 3)$ are compatible with a controlled

5D description, but the somewhat larger values (~ 5) are still reasonable from the viewpoint of (purely) 4D strong dynamics, for example, $\rho\pi\pi$ coupling in real-world QCD is roughly of this size. We can of course interpolate for other composite spin-1 masses. To be more precise, we will have to add bound from composite photon (above was just composite Z) but as an estimate what we did should suffice. Similarly, we can obtain a bound on KK W in our model based on the searches for W''s (via their leptonic decays) at the LHC [114, 115]: we find that it is (roughly) comparable to that on the KK Z and KK gluon (as we discuss below).

(ii) Di-boson:

Even in the flavor-universal limit ($\Lambda_{\rm Higgs} \to \infty$) KK Z/W couples also to Higgs (including longitudinal W/Z, i.e., "di-bosons"). So, we can rescale from bound for heavy vector triplet (HVT) model [116], which is (roughly) similar to standard warped/composite case of Fig. 2.1 (i.e., couplings to Higgs/top dominate): The current bound [117, 118] on the mass is 2.8 TeV for $g_\star^{\rm EW} = 3$. However, composite W/Z's for the above HVT model decay to dibosons with a BR of $\approx 100\%$, since couplings to dibosons are (much) *larger* than to the SM fermions, latter being assumed to be flavor-universal. On the other hand, in the (fully) flavor-universal limit that we are considering here, we can readily estimate that the BR to dibosons is reduced to (roughly) 4%, in which case, bound is weaker than 2 TeV (rescaling from the experimental plots).

So, we conclude that di-lepton bound for our KK Z case is a bit stronger than di-boson.

Just for completeness' sake, we mention that there is also a Z' bound of 2-2.5

TeV from the di-jet search [110]. However, this assumes coupling to light quarks inside proton is same as SM Z, vs. smaller here. Similarly, Z' bound from di-top is ~ 2.5 TeV [119, 120] , but that is for a model with *enhanced* (even with respect to the SM) coupling to first *and* third generations [121]; hence for our case, bound should be weaker. Overall, then di-jet and d-top bounds for KK Z are sub-dominant to that from di-lepton discussed earlier.

KK gluon

(i) Di-top:

Similarly to KK Z/W above, we can rescale from the KK gluon bounds [119]: the predicted cross-section [all for $g_\star^{\rm QCD} \sim 5$, as assumed in [122], which is quoted in [119]] is larger than bound by ~ 6 (2) for mass of KK gluon of 2 (2.5) TeV. The above bounds are assuming BR to top quarks ≈ 1 (as in the standard scenario) so that for our case (i.e., with BR to top quarks of $\approx 1/6$ instead), we get

$$\Lambda_{\rm IR} \gtrsim 2.0 \text{ TeV for } g_\star^{\rm QCD} \sim 5 \tag{3.47}$$

$$\gtrsim 2.5 \text{ TeV for } g_\star^{\rm QCD} \sim 3 \tag{3.48}$$

As usual, we can interpolate for other composite spin-1 masses.

(ii) Di-jet:

Here, we can re-scale from axigluon bounds [110], i.e., coupling to our composite gluon is smaller by a factor of $\sim g_{\rm QCD}/\left(g_\star^{\rm QCD} \times \sqrt{2}\right)$, since coupling of axigluon [see discussion in [123] referred to by [110]] is larger than QCD by $\sqrt{2}$. The cross-section is constrained to be smaller than the prediction for axigluon by ~ 50 (30)

for axigluon mass of 2 (2.5) TeV. So, using the above couplings, we get for our case:

$$\Lambda_{\rm IR} \gtrsim 2.0 \text{ TeV for } g_\star^{\rm QCD} \sim 5 \tag{3.49}$$

$$\gtrsim 2.5 \text{ TeV for } g_\star^{\rm QCD} \sim 4 \tag{3.50}$$

Similarly, we can find the bound for other values of $\Lambda_{\rm IR}$.

So, di-top and di-jet bound are (roughly) *comparable* in the case of KK gluon.

3.3.2.2 Probing top/Higgs compositeness

Next, we discuss the possibility of being able to see some remnants of top/Higgs compositeness in the properties of composite resonances at $\Lambda_{\rm IR}$.

Summary

As seen from Eqs. (4.10), (3.38) and (4.5), spin-1 couplings (cf. dilaton and spin-2) at the LHC are most sensitive to flavor *non*-universal corrections. In particular, for spin-1 composite, the net coupling [combining Eqs. (3.24) and (4.10)] to SM fermions is then given (schematically) by:

$$\delta\mathcal{L} \sim \Big[-\frac{g_{\rm SM}^2}{g_{\star\,\rm IR}^{\rm gauge}} + h\frac{g_{\star\,\rm UV}^{\rm gauge\ 2}}{g_{\star\,\rm IR}^{\rm gauge}} \left(\frac{\Lambda_{\rm IR}}{\Lambda_{\rm Higgs}}\right)^2 \Big] \bar{q}\gamma^\mu \rho_\mu q \tag{3.51}$$

Here, h is an $O(1)$ factor which depends on details of the model (whether a 4D composite theory or 5D dual). Note that the 5D model gives *opposite* sign for the flavor *non*-universal coupling (to top/Higgs) of spin-1 vs. flavor universal one, i.e., $h > 0$, whereas from purely 4D CFT viewpoint, $h < 0$ cannot be ruled out.

Eq. (3.51) shows that the non-universal contributions (second term above) start becoming relevant (i.e., *comparable* to the universal first term) for:

$$\frac{\Lambda_{\rm Higgs}}{\Lambda_{\rm IR}} \sim \frac{g_{\star\,\rm UV}^{\rm gauge}}{g_{\rm SM}} \tag{3.52}$$

Setting $\Lambda_{\rm IR} \sim 3$ TeV; a universal $g_{\star\,\rm UV}^{\rm gauge} \sim 3$; $g_{\rm EW} \sim 0.6$ and $g_{\rm QCD} \sim 1$, we see that above equality occurs (roughly) for

$$\Lambda_{\rm Higgs} \sim 10\ (15)\ \text{TeV for KK gluon } (Z) \tag{3.53}$$

which is (roughly) the flavor bound, i.e., (in general) we *do* expect sensitivity to top/Higgs compositeness! Again, note that in the standard scenario, i.e., $\Lambda_{\rm Higgs} \sim \Lambda_{\rm IR}$, the non-universal contribution actually *dominates*: see Eq. (3.51).

KK gluon vs. KK Z

In particular, KK gluon might be especially promising in this regard, since for the flavor-universal case, di-jet bounds on KK gluon seem comparable to di-top as indicated above, which suggests that there should be significant sensitivity to above perturbations, for example, non-universal coupling to top being *comparable* to universal might then show up even at *discovery* stage! Whereas, in flavor-universal limit, it seems bounds from di-boson/di-top are somewhat weaker than from di-lepton final state for KK Z, thus suggesting that probe of top/Higgs compositeness (again, for the case when flavor non-universal couplings are comparable to flavor universal ones) might have to wait for *post*-discovery precision-level studies. On the

other hand, as discussed above, for the *same* top/Higgs compositeness scale, flavor non-universal effects are actually a bit *larger* for KK Z than for KK gluon. So, overall, the two modes might be complementary in this regard.

Details of analysis

Estimates of various BR's illustrating the above ideas are given in table 3.1: these were already mentioned in the introduction, including the tables. We now present more details. First, as a reminder, in this table 3.1, we fix KK Z/gluon mass to be 3 TeV and the composite gauge coupling ($g_{\star\,\mathrm{UV}}^{\mathrm{gauge}}$) to be 3. Hence, the production cross-section is the same throughout the tables, but we vary Higgs compositeness scale.

These numbers are obtained simply using the net coupling given in Eq. (3.51). Just for the sake of concreteness, we choose a "central" value for the $O(1)$ coefficient h in Eq. (3.51) so that $\Lambda_{\mathrm{Higgs}} = 10$ and 15 TeV gives *exact* equality between the two terms there for KK gluon and KK Z, respectively. Then, for each Λ_{Higgs}, we vary h between a factor of 2 and 1/2 around this central value. Thus, we obtain a *range* of BR's even for *fixed* Λ_{Higgs}. Mostly for simplicity, we assume only t_R (and Higgs) is (fully) composite, i.e., $(t, b)_L$'s compositeness is smaller. Also, we will assume of $h > 0$ (based on 5D model, as mentioned above). We then see that for values of $\Lambda_{\mathrm{Higgs}}/\Lambda_{\mathrm{IR}}$ around Eq. (3.52), there is actually a possibility of "cancellation" between the two terms in Eq. (3.51); this feature is reflected in these tables in BR's to top/dibosons becoming *smaller* than flavor-universal limit as we start lowering the Higgs compositeness scale from a high value. Note that, as reflected by our $O(1)$ variation of h factor, we are not really contemplating a fine-tuning here, rather only

pointing out that a mild suppression is possible in this way. Eventually, i.e., for even lower $\Lambda_{\rm Higgs}$, of course the non-universal part of couplings to top/Higgs dominates over universal one so that BR's to top/Higgs become larger, as they asymptote to the values of the minimal model of Fig. 2.1.

Finally, we have to consider the decay of (composite) spin-1 to a dilaton and a SM gauge boson. Based on Eqs. (3.14) and (4.11), it is straightforward to show that there exists choices of the relevant parameters such that this decay is (much) smaller than to the SM fermions. For simplicity, here we assume that is the case in tables shown above. Having said this, a dilaton and a SM gauge boson is an interesting final state (followed by dilation $\to$ two SM gauge bosons), which (to the best of our knowledge) has not been studied before. In fact, in Chap. 4, we determine (other) regions of parameter space where this new decay channel actually *dominates* over the SM fermion pair mode and analyzing the corresponding LHC signals. Also, in this case, the BR to SM fermion pairs is suppressed, thereby relaxing the bound on gauge KK particles that were discussed earlier.

As anticipated earlier (but now seen more explicitly in the tables), as we lower Higgs compositeness scale from decoupling limit, at $\sim O(10)$ TeV, we start seeing $\sim O(1)$ deviations from flavor-blindness (middle vs. rightmost columns), that too "earlier" for KK Z than for KK gluon. At the same time, these BR's significantly different than standard Higgs compositeness case (leftmost column). So, the moral here is that composite Z/gluon can provide "glimpse" into Higgs/top compositeness, provided that this scale is not too far from the lower limit from flavor/CP violation, i.e., $\sim O(10)$ TeV.

Other values of KK masses

For the sake of completeness, we mention that the (total) cross-sections for 2 and 4 TeV composite/KK Z and gluon for $g_{\star\,\mathrm{IR}}^{\mathrm{gauge}} = 3$ (at $\sqrt{s} = 13$ TeV LHC) are ~ 28, 0.3 fb (Z) and ~ 1834, 17 fb (gluon), respectively (of course, the 2 TeV case might be ruled out as per above discussion, unless we invoke extra decay modes, for example to light A_5's). From Eq. (3.52), it is clear that as we vary composite spin-1 masses in this way, one could then be sensitive to lower/higher top/Higgs compositeness scale.

Comparison to other probes of top/Higgs compositeness

Let us summarize by comparing the above signals of top/Higgs compositeness scale of $O(10)$ TeV to other approaches. One of the standard probes would be existing/upcoming low-energy flavor experiments, which will be sensitive to $\Lambda_{\mathrm{Higgs}} \sim O(10)$ almost by construction, since $O(10)$ TeV was chosen to barely satisfy the *current* flavor/CP violation bounds. Of course, this would provide the most indirect view, for example, even if we see a signal, we cannot be sure about which underlying new physics it corresponds to, i.e., whether it is $\Lambda_{\mathrm{Higgs}} \sim O(10)$ TeV of the warped/composite Higgs framework or some thing else. On the other hand, the most direct signal is possible at a *future* 100 TeV hadron collider, where the associated, i.e., $O(10)$ TeV, physics of compositeness can be produced without any suppression. In fact, this could serve as a motivation to build such a machine.

Here, we showed how extending the usual, minimal framework to include a intermediate brane (Fig. 3.2) results in novel probe of the general framework. Namely, it creates a *new* threshold, i.e., a few TeV resonances intermediate in mass between

$O(10)$ flavor scale and the SM/weak scale itself, whose leading couplings are flavor-universal, rendering such a mass scale safe from flavor bounds. This angle actually combines some of the virtues of both the above approaches, for example, we can *directly* produce the relevant particles at the *ongoing* LHC. Of course, simply discovering these few-TeV particles in flavor-blind channels – even if very exciting! – would not quite constitute a smoking-gun of top/Higgs compositeness which lies at the core of this framework. Remarkably, we have seen above that the *non*-universal contributions to the couplings of these few TeV particles – stemming from top/Higgs compositeness – are not far behind. Hence, precision studies of these new states can indeed unravel these effects. Clearly, this sensitivity to $O(10)$ TeV compositeness scale is intermediate between explicit production of compositeness physics by a 100 TeV collider and indirect low energy flavor tests.

Finally, we mention (other) *virtual* effects of this $\Lambda_{\rm Higgs}$ physics at the LHC such as on precision Higgs or top couplings measurements or analysis of *continuum* top/Higgs production. However, given $\Lambda_{\rm Higgs} \sim O(10)$ TeV, even the high-luminosity LHC will not be sensitive to the effects in these searches. The point is that such probes lack the resonance-enhancement[12] that the above *lighter* spin-1 studies afford: again, both these effects do have a (common) $(\text{few TeV}/\Lambda_{\rm Higgs})^2$ suppression.

[12] In fact, these states are quite *narrow*. For example, with the assumptions made above and for $\Lambda_{\rm Higgs} \sim 15$ TeV, we estimate that Γ/M for KK Z is $O(0.1\%)$.

3.3.3 Spin-2 composite

The (total) cross-sections (again, from gluon fusion, at $\sqrt{s} = 13$ TeV LHC) are ~ 40 (1.8) fb for $\Lambda_{\rm IR} = 2(3)$ TeV for $g^{\rm grav}_{\star\,\rm IR} = 1$ and $g^{\rm QCD}_{\star} = 3$. Just like for dilaton mentioned above, decays are dominated by two SM gauge bosons, unless $m_\varphi < \frac{1}{2} M_{\rm KKgrav}$, in which case, decay to the dilatons dominates (due to stronger coupling). Furthermore, in the *unified* case, we get coupling of spin-2 to two SM gauge bosons $\propto$ corresponding (SM gauge coupling)^2. Thus, (neglecting decays to dilaton, for example, assuming $m_\varphi > \frac{1}{2} M_{\rm KKgrav}$) BR's to $\gamma\gamma$, ZZ, WW, and gg are ≈ 0.7 %, 1%, 3% and 95%, respectively (like for radion). It is also clear that current bounds on cross-section from resonant di-photon search are satisfied for above choice of parameters, since there is not much difference between spin-0 and spin-2 here in so far as *experimental* bounds are concerned.

Significance of spin 2

Even though the final state for composite/KK graviton might be similar to dilaton (i.e., two SM gauge bosons), obviously, spin-2 vs. spin-0 can be distinguished using angular distributions. In fact, as already mentioned earlier, a random spin-2 has three different angular amplitudes [104] vs. KK graviton having only one (i.e., coupling to $T_{\mu\nu}$ only), hence providing disambiguation between generic strong dynamics and extra-dimensional frameworks (i.e., dual to a *special* structure of strong dynamics). Finally, it is interesting that mere discovery of spin-2 implies that there is an infinite tower of heavier states (whether composite or KK) because the theory of (massive) spin-2 is *non*-renormalizable (vs. spin-0 or 1), thus guaranteeing more

and rich discoveries in the future!

3.4 Model with *two* intermediate branes

Our work opens up other possibilities also: most significantly, we can have the gauge brane split (at $\Lambda_{\rm meson}$) from gravity ($\Lambda_{\rm glueball}$) as in Fig. 3.2. In this case, KK graviton/radion will be the lightest; in particular, radion can be lighter than KK graviton, as seen from Eq. (4.1)[13]. So, we have (parametrically speaking) $m_\varphi \lesssim \Lambda_{\rm glueball} \ll \Lambda_{\rm meson} \ll \Lambda_{\rm Higgs}$. Also, stabilization of the inter-brane separations (in this case, we have *three* of them) can be done via a generalization of what was done for the model with one intermediate brane above.

In more detail, the couplings of KK graviton and radion to SM *gauge* bosons will be suppressed by $(\Lambda_{\rm meson}/\Lambda_{\rm glueball})^4$ in this model, similarly to the case of their couplings to top/Higgs in the model of Fig. 3.4 studied here. As discussed in sections 3.2.3.1 and 3.2.3.2, these couplings result from exchange of (heavy) physics at $\Lambda_{\rm meson}$. Essentially, we perform the replacements $T^{(t/H)}_{\mu\nu} \to T^{(\rm gauge)}_{\mu\nu}$ in Eq. (3.38) and Higgs kinetic term $\to F_{\mu\nu}F^{\mu\nu}$ in Eq. (4.5), along with $\Lambda_{\rm Higgs} \to \Lambda_{\rm meson}$ in both equations. On the other hand, couplings of dilaton/spin-2 to *top/Higgs* and those of spin-1 to *all* SM matter remain the same. Here, we simply summarize all these couplings in table 3.4 (cf. table 3.2.4).

Note that for fixed mass of the spin-1 composites ($\Lambda_{\rm meson}$), the couplings of the lightest states in this model (i.e., KK graviton/radion) relevant for their production

[13] In fact, (very) recently [124] studied a 4D model (with new – pure glue – strong dynamics) which is sort of dual of the above gauge-gravity split case (with the lightest scalar glueball being roughly the radion/dilaton).

(i.e., to gluons) become weaker as we lower $\Lambda_{\text{glueball}}$, i.e., their mass. On the other hand, PDF's relevant for production are enhanced in this process, providing some compensation. Remarkably, it turns out that within the range of interest the former effect (i.e., weaker couplings) tends to dominate so that the cross-sections actually reduce (i.e., bounds and visibility get weaker) as we lower the KK graviton/radion mass.

A sample point is as follows: $\Lambda_{\text{meson}} = 3$ TeV, $m_\varphi = \Lambda_{\text{glueball}} = 1$ TeV, $g_\star^{\text{QCD}} = 3$ and $g_{\star\,\text{IR}}^{\text{grav}} = 3$ gives (total) cross-section of ~ 3.9 fb and ~ 1 fb, respectively, for KK graviton and dilaton (former being larger mostly due to multiple polarizations). The decay BR's are similar to the model with one intermediate brane case. Note that gauge KK/spin-1 composite cross-section at this point are comparable to/larger than that of graviton/dilaton; in fact, the gauge KK would be strongly constrained (if not ruled out), *assuming* decays directly to SM particles (as discussed above). However, the spin-1 states can decay directly into non-SM particles such that they are effectively "hidden" from SM pair-resonance searches such as dileptons or dijets. For example, light A_5's (dual to PNGB's) can provide such channels.[14]

In this way, KK graviton/dilaton can actually be the most visible channel. Table 3.1 in the introduction had already displayed this interesting possibility.

Based on the discussion in section 3.2.3.3 of KK graviton contributions to precision tests, it is clear that the only relevant constraint on the KK graviton mass scale, i.e., $\Lambda_{\text{glueball}}$, in this model comes from direct LHC searches.

[14] For a recent application of this idea in the context of the 750 GeV diphoton excess at the LHC, see [90].

Resonance \ Type of coupling	Higgs compositeness-sensitive	flavor-blind
dilaton	$\frac{g_\star^{\rm grav}}{\Lambda_{\rm glueball}}\left(\frac{\Lambda_{\rm glueball}}{\Lambda_{\rm Higgs}}\right)^4\left[m_t\bar{t}t+(\partial H)^2\right]$	$\frac{g_\star^{\rm grav}}{\Lambda_{\rm glueball}}\left(\frac{g_{\rm SM}}{g_\star^{\rm gauge}}\right)^2\left(\frac{\Lambda_{\rm glueball}}{\Lambda_{\rm meson}}\right)^4 F^{\mu\nu}F_{\mu\nu}$
KK Z	$g_\star^{\rm gauge}\left(\frac{\Lambda_{\rm glueball}}{\Lambda_{\rm Higgs}}\right)^2\left(\bar{t}\gamma^\mu t+H^\dagger\partial^\mu H\right)$	$\frac{g_{\rm EW}^2}{g_\star^{\rm gauge}}\left(\bar{q}\gamma^\mu q+\bar{l}\gamma^\mu l\right)$ (all generations)
KK gluon	$g_\star^{\rm gauge}\left(\frac{\Lambda_{\rm glueball}}{\Lambda_{\rm Higgs}}\right)^2\bar{t}\gamma^\mu t$	$\frac{g_{\rm QCD}^2}{g_\star^{\rm gauge}}\bar{q}\gamma^\mu q$ (all generations)
KK graviton	$\frac{g_\star^{\rm grav}}{\Lambda_{\rm glueball}}\left(\frac{\Lambda_{\rm glueball}}{\Lambda_{\rm Higgs}}\right)^4 T_{\mu\nu}^{(t/H)}$	$\frac{g_\star^{\rm grav}}{\Lambda_{\rm glueball}}\left(\frac{g_{\rm SM}}{g_\star^{\rm gauge}}\right)^2\left(\frac{\Lambda_{\rm glueball}}{\Lambda_{\rm meson}}\right)^4 T_{\mu\nu}^{(\rm gauge)}$

Table 3.4: Summary of universal and non-universal couplings of various composites in the model with two intermediate branes.

In particular, using the cross-sections given above and bounds given earlier, we see that $\Lambda_{\text{glueball}}$ is then allowed to be as low as ~ 1 TeV (or even smaller).

Chapter 4: LHC Signals from Cascade Decays of Warped Vector Resonances

In Chap. 3 we presented a possible generalization of the minimal warped extra dimensional framework of Randall-Sundrum type. There, we derived all relevant couplings and show that low energy constraints from electroweak precision, flavor and CP violation tests are readily satisfied. As a striking collder signal for the Higgs/top compositeness as the solution to the hierarchy problem, we argued that our extension can lead to a significant deviation of the decay branching fractions of KK gauge bosons, e.g. KK Z and KK gluon, to pairs of the SM particles compared to the minimal/standard framework (where the Higgs compositeness arises around TeV). Moreover, we showed that if the Higgs/top compositeness physics is realized around $\mathcal{O}(10)$ TeV as suggested by the flavor bound, then the decay branching ratios of KK Z and KK gluon into pairs of the SM particles will display $\mathcal{O}(1)$, still noticeable, deviation relative to the flavor universal limit (where the Higgs compositeness scale is decoupled to infinity).

In this chapter, we focus on another part of parameter space and show that new exciting collider signals exists: cascade decay (as opposed to the two-body decays discussed above) of KK gauge bosons into a radion and the corresponding SM gauge

boson, followed by the decay of the radion into a pair of SM gauge bosons.[1] Such a new possibility was already mentioned in Chap. 3 and here we actually conduct detailed analysis.

As was already indicated in Chap. 1, for the sake of completeness, below we give a review on the extended framework we developed in Chap. 3, gathering necessary formulae for the phenomenological study.

4.1 Introduction

The usual framework of warped higher-dimensional compactifications involves fields corresponding to *all* SM particles (including graviton) propagating in the bulk of a warped extra dimension, which is terminated on the two ends by the UV and IR branes (see Fig. 2.1).

However, it is well known that stringent constraints from flavor and CP tests on effects of (lightest) gauge *and* fermion KK modes require their masses to be $\gtrsim$ $\mathcal{O}(10)$ TeV [59], unless some additional flavor structure is imposed (see Refs. [65–68] for recent work in the context of a "simplified" version of the 5D model). This equivalently means that the IR brane scale should be $\gtrsim$ $\mathcal{O}(10)$ TeV. [2] We will refer to this setup as "standard" from here on. This creates a "meso"-tuning to be imposed on the theory (see for example [131]), since a fully natural solution would

[1] Throughout this chapter, when we refer to Chap. 3, we will actually refer to our published work [131].

[2] Electroweak Precision Measurements also impose strong constraints on the IR brane scale. For example, with only SM gauge group in the bulk, the consistency with the electroweak precision measurements requires KK scale $\gtrsim \mathcal{O}(10)$ TeV [132–135]. However, it was shown in Ref. [50] that extension of the bulk gauge group to $SU(2)_{\rm L} \times SU(2)_{\rm R} \times U(1)_{\rm B-L}$, which contains the built-in custodial symmetry of the electroweak sector, can relax this bound and KK scale $\gtrsim 3$ TeV is still allowed.

require the IR brane scale to be $\sim \mathcal{O}(1)$ TeV. Of more concern to us is, however, the possible lack of LHC signals resulting from direct production of the associated new physics, namely, the KK modes, simply based on the kinematic reach of the LHC.

With the above situation in mind, the new idea in [131] involves, broadly speaking, the introduction of extra branes in-between the UV and IR ones. Various bulk fields are allowed to propagate different amounts in the bulk, consistent with general principles and symmetries. In particular, gravity must propagate in the entire spacetime due to its dynamical nature, while the gauge fields must propagate at least equal or more than the matter fields in the extra dimension. This is because the matter currents need a gauge field to couple to, while the gauge fields can exist on their own. In the simplest incarnation of this proposal the basic setup is modified by the inclusion of one such extra brane, chosen to be located very close to the IR brane. The SM matter and Higgs fields are allowed to propagate only in the subspace from UV to this "intermediate" brane, whereas gauge and gravity occupy the entire bulk (see Fig. 3.5). We will henceforth refer to this framework as the "extended" framework, and the intermediate brane as the "Higgs" brane. We choose the Higgs brane scale to be $\gtrsim \mathcal{O}(10)$ TeV, i.e., same as the IR brane scale of the standard scenario. We then see that in this extended setup, we retain solutions to both the Planck-weak and flavor hierarchy problems. This is of course modulo the meso-tuning mentioned earlier. It is useful to keep in mind that the standard framework described above is a special case of this extended framework, if the Higgs brane and the IR brane are identified as one.

In order to determine how the bound from flavor and CP tests on the lightest

gauge KK mass scale is modified,[3] we need to, in turn, figure out the couplings of gauge KK modes to the light SM fermions. To this end, we make use of the usual conceptual approach that couplings between 4D particles are dictated by the overlap of their respective profiles in the extra dimension. The point is that flavor *dependence* of these couplings of the gauge KK modes arises *primarily* from the part of the overlap in the infra-red region, where the KK modes are localized. Because of the splitting of IR brane (where gauge KK are peaked) from the brane where matter fields end, we see that the flavor *non*-universal component of gauge KK couplings to SM fermions is *reduced*. Thus, bounds on gauge KK mass from flavor and CP violation are relaxed in the extended case. It is noteworthy that gauge KK couplings to SM fermions/Higgs also have a contribution from overlap near the UV brane: this is, however, universal, given the constant profile of the gauge KK in that region. To summarize then, this setup has an important feature: the lightest gauge KK particle mass of *a few* TeV (related to the location of the IR brane) can be consistent with the flavor and CP bounds. This makes the gauge KK modes lie within the kinematic reach of the LHC. But in order to complete this story, we need to check the fate of the *couplings* involved in their *production*. In the standard scenario, the gauge KK production at the LHC occurs dominantly via the coupling to the light quarks (inside protons). This coupling is the flavor-universal UV-region-dominated coupling, as mentioned above. It is therefore clear that the size of this coupling is not modified in the extended setup. Combining the above couplings and

[3] By the above construction, the KK fermions satisfy these bounds even in the extended framework.

masses, the stated goal of the gauge KK particles being within the LHC reach is thus achieved.

Having ensured significant production at the LHC, we next move onto the *decays* of the gauge KK modes. As already indicated above, the coupling between modes near the IR brane is the largest. In the standard scenario, examples of such couplings would be those between gauge KK modes and top quark/Higgs. Note that here by "Higgs" we mean the Higgs doublet, which includes the longitudinal W/Z as well as the physical Higgs. We will use this in the rest of the chapter, and clarify where needed. Concomitant to what happens to flavor-violation, these top/Higgs-philic couplings of gauge KK modes – hence their decays to top/Higgs (which are usually the dominant channels) – are then also suppressed. This is because top/Higgs are localized on the intermediate brane in the new framework, while the KK gauge bosons are localized on the IR brane. Such a twist then opens the door for *other* couplings (i.e., involving profiles not necessarily peaked near IR brane) to become relevant for the gauge KK boson decays. For example, there is a coupling among KK gauge boson, radion and SM gauge boson, which involves two profiles which are IR-localized and one flat profile (of the SM gauge boson). Due to the suppression of the gauge KK modes coupling to the top/Higgs, this coupling becomes important. As already mentioned, the radion can be lighter than the gauge KK modes by a factor of a few so that the above coupling can mediate the decay of a KK gauge boson into a radion and the corresponding SM gauge boson. Note that in the standard setup, radion subsequently decays dominantly into top/Higgs, because its profile is peaked near IR brane, where the top/Higgs are localized. Remarkably,

in the extended framework, radion instead decays mostly into a pair of SM gauge bosons. This is because the other dominant channels are suppressed for the same reason as for gauge KK – top/Higgs profiles have now moved away from the radion.[4]

Similarly, we have a flavor-universal decay of KK gauge boson into two SM fermions (again, from overlap near UV brane) which might come into play here. Note that this is the same coupling which is involved in the production of gauge KK modes at the LHC, as mentioned earlier. We would like to emphasize here that both of these couplings are present, with similar strength, in the standard framework as well, but it is just that the associated decays are swamped by top/Higgs final states. After this motivation, we summarize the important aspects of this extended setup in Table 4.1, contrasting them with those in the standard setup. Motivated by these characteristics of the production and decay of gauge KK modes, in this chapter, we perform a detailed study of the potential LHC signals resulting from the above-mentioned new, cascade decay process into a SM gauge boson and a radion. As indicated above, this interesting mode competes mainly with decays to a pair of SM fermions (via universal coupling). As the first step, we therefore determine the region of parameter space where the decay channel of a KK gauge boson into a radion and a corresponding SM gauge boson (with the radion decaying into two SM gauge bosons) dominates.

We also map out the parameter region which respects bounds on gauge KK modes, from dilepton, dijet, and ditop (i.e., the other competing channels) *and* direct

[4]Note that decays of spin-1 gauge KK into a pair of SM/massless gauge bosons are not allowed by the Landau-Yang theorem.

		Standard	Extended
KK fermion	Mass	$\gtrsim \mathcal{O}(10)$ TeV	$\gtrsim \mathcal{O}(10)$ TeV
KK gauge	Mass	$\gtrsim \mathcal{O}(10)$ TeV	a few TeV
	Production	$q\bar{q}$	$q\bar{q}$
	Decay	$t\bar{t}$, hV_L, V_LV_L	$f\bar{f}$ (universally), radion $+\gamma/W/Z/g$
Radion	Mass	$\gtrsim \mathcal{O}(10)$ TeV/(a few)	$\mathcal{O}(1)$ TeV
	Production	gg	gg
	Decay	$t\bar{t}$, hh, V_LV_L	$gg \gg WW/ZZ \gg \gamma\gamma$

Table 4.1: Summary of properties (masses, dominant production and decay channels) of relevant new particles in the extended warped model (fourth column). The corresponding properties in the standard warped model (third column) are listed for comparison. Here q represents a light SM quark, f represents any SM fermion, h is the physical Higgs, and V_L represents a longitudinal W/Z.

(or via above gauge KK decay) production of the radion, where the dominant bound arises from the decay into a photon pair. We then analyze production of KK photon, KK gluon and KK W/Z and their decay into the corresponding SM gauge boson and the radion in this viable and relevant part of parameter space, with all allowed subsequent radion decays. Among all these possible final states, we focus on a few which can make discovery feasible at the LHC. Overall, we show that the prospects are quite promising. In particular, an integrated luminosity of $\mathcal{O}(100)$ fb^{-1} suffices for discovery via the new channel of KK gluon, whereas $\mathcal{O}(1000)$ fb^{-1} is required for KK W/Z and KK photon due to their small production cross sections.

We also would like to emphasize here that, although our study is rather specific to the warped/composite Higgs model, the event topology of interest might actually arise in other situations as well. In fact, we would like to mention that our modeling of this decay channel has enough number of independent parameters (for example, roughly one per coupling) so that it can be readily adapted to a more general case. More importantly, we think that such a channel (i.e., of a heavy particle decaying into SM gauge boson plus another – possibly different - pair of SM gauge bosons from the decay of an intermediary, *on*-shell particle) has not received much attention (phenomenologically or experimentally) in the past.[5]

Nevertheless, some related analysis of experimental data has been performed, which is worth mentioning here. First one is the resonant channel search such as a single jet plus a photon (from an excited quark, for example, Ref. [138]): this

[5]See, however, Ref. [136] for an analysis of a photo-cascade decay of KK *graviton* and Ref. [137] for KK gluon in the standard warped model.

does apply to our case, but only when the radion is very light, thus highly boosted so that the two jets from its decay merge. On the other hand, searches for dijet resonances produced in association with photon/jet (mostly originating from ISR) have been performed [139], where the ISR jet/photon is used for the purpose of tagging to reduce background, especially in the context of looking for low mass dijet resonances. In this case, there was clearly no reason to simultaneously study the three-particle invariant mass (i.e., dijet + photon/jet). However in our case, it is crucial in reducing background. Finally, there is a "general" search performed by the ATLAS Collaboration [140], where invariant mass distributions of various final states (involving combinations of SM objects such as photons, jets and leptons) were studied for possible excesses relative to the SM predictions. The channels studied by the ATLAS Collaboration include some of the three-particle ones found in the new decay channel in our extended warped/composite Higgs model such as dijet + photon. However, the invariant masses of a subset of two particles therein were not considered at the same time, presumably for simplicity. Crucially, the striking feature about the new channel that we study here is that the final state features *both* three-particle (i.e., KK/composite gauge boson) and two-particle (i.e., radion/dilaton) resonances.

The rest of the chapter is organized as follows. We begin with a rather detailed review on the new framework in Sec. 4.2. In particular, we review the mass spectrum of relevant particles and their couplings in terms of model parameters. In Sec. 4.3, we take the simplified model for our phenomenological study and provide the allowed parameter space consistent with the existing bounds. An overview of the various

signal channels that we shall study follows, especially in the sense of their production and decay rates, guiding us to establishing our benchmark points. In Sec. 4.4, we then discuss general details of our event simulation and key mass variables for our collider study. Sec. 4.5 is reserved for presenting our main results from the data analyses in various signal channels.

4.2 Review on the Model

In this section, we review a natural extension of the "standard" Randall-Sundrum framework introduced in Ref. [131]. We begin with a brief discussion on the motivation for such an extension and 4D dual description. We then move our focus onto the mass spectrum of relevant particles and their interactions in detail, providing the corresponding explicit formulae.

4.2.1 Motivation for a natural extension: 5D and 4D-dual pictures

As discussed in the introductory section, the stringent constraints from flavor/CP experiments push the IR-brane scale of the "standard" RS framework to $\gtrsim \mathcal{O}(10)$ TeV. This bound implies that the new particles in this framework, i.e., the KK excitations of the SM, might be beyond LHC reach. This situation suggests we should speculate about other logical possibilities within this broad framework and study its phenomenological consequences thoroughly, in particular, in order to see if LHC signals are possible therein. Indeed, Ref. [131] has pointed out a simple but robust observation along this line: different fields in 5D can propagate different

amounts into the IR along the extra dimensions.

- The gravity itself is the dynamics of the spacetime, and therefore, the 5D gravity field should be present in the entire 5D spacetime in the form of 5D general relativity.

- Gravity may stand alone without gauge fields, since graviton does not have any gauge charge. However, the opposite option is not possible (as is clear from above, i.e., gauge fields will always radiate gravitons). Combining these two points, we see that the gauge fields can propagate a lesser extent into the bulk than gravity.

- Wherever matter fields exist, the gauge fields under which that matter is charged must be present also. The reason is that the matter field can emit the associated gauge field. [6]

- Analogous to the second point above, there can be a region with gauge fields, but with no matter charged under it, i.e., the matter fields can exist in an even smaller amount of 5D than the gauge fields. Therefore, the ordering between the gravity and the gauge fields (and similarly gauge and matter) is not random but fixed as described here.

Based on the above-listed observation, the possibility of letting different fields propagate modestly different degrees into the IR of the warped dimension is not only *robust* but *natural*. A concrete realization of the idea is to introduce extra branes

[6] Of course, for any gauge fields under which the SM matter fields are not charged (if existed), this argument does not directly apply and the fraction in the extra dimensions that they occupy is rather free of constraint.

relative to the set-up in Fig. 2.1. As an example of minimal extensions, Fig. 3.5 schematically displays the configuration in which gravity and gauge fields propagate the same amount along the fifth direction while matter fields are present in a smaller amount. It is straightforward to see that within this generalized framework, the "standard" RS setup is merely a special case with the last two branes (i.e., the Higgs and IR branes) in Fig. 3.5 identified. From now on, we shall focus on this setup for concreteness of our discussion.

In the language of the 4D-dual picture, the above extension can be understood as follows. In the far UV, the physics is strongly coupled dynamics of preons with conformal invariance. This conformally invariant "UV strong dynamics" is deformed by some explicit breaking term(s), and as a result the theory runs until it undergoes a confinement at, say, $\Lambda_{\rm Higgs}$. Composite hadrons and mesons are "born" at this stage and SM top quark and Higgs are part of such massless composite states, whereas the massive states correspond to KK fermions of the 5D model. This confinement scale is dual to the position of brane in the warped fifth dimension where top and Higgs are localized (i.e., the Higgs brane in Fig. 3.5). Unlike QCD-like strong dynamics, however, this confinement can also produce composite preons; the resulting theory flows to a new fixed point in the farther IR. In addition, the physics at $\Lambda_{\rm Higgs}$ may also produce deformation terms to the CFT of the composite preons, including couplings between composite preons and composite hadrons. Thus, this "IR strong dynamics" runs as before until it confronts the second confinement at $\Lambda_{\rm IR}$ which is dual to the position of the IR brane. This second confinement then creates its own composite mesons and glueballs. However, these composite states do not possess the

quantum numbers of the SM matter, although they might have SM gauge charges. Composite vector mesons resulting from this second confinement are dual to KK-excited gauge bosons, and the dilaton, a pseudo Nambu-Goldstone boson of the spontaneously broken scale invariance, is dual to the radion. Due to this duality, we refer to these particles as dilaton/radion and composite mesons/KK gauge bosons interchangeably throughout this section.

4.2.2 Mass spectrum and couplings

With the model setup delineated in the preceding section in mind, we now consider the mass spectrum of the radion and the lightest KK gauge bosons in terms of model parameters.[7] The discussion on the couplings relevant to our study follows. In particular, we shall demonstrate that light states below $\Lambda_{\rm Higgs}$, e.g., spin-0 glueball (dual to radion) and spin-1 mesons (dual to KK gauge bosons), interact with SM matter fields dominantly via flavor-blind couplings, from which we find interesting and important phenomenology.

4.2.2.1 Radion

First of all, the mass of the dilaton m_φ [96–99] is given by

$$m_\varphi^2 \sim \epsilon\, \lambda\, \Lambda_{\rm IR}^2\,, \tag{4.1}$$

[7] See also Ref. [131] for more detailed derivations and dedicated discussions.

where λ is dual to the amount of detuning of the IR brane tension in 5D and ϵ denotes the parameter encoding the ratio between the first and the second confinement scales [131]. Their typical sizes are

$$\lambda < 1\,, \quad \epsilon \sim \frac{1}{\log(\Lambda_{\rm Higgs}/\Lambda_{\rm IR})} < 1\,, \tag{4.2}$$

from which we find that the mass of the dilaton is generally lighter than that of spin-1 resonances ($\sim \Lambda_{\rm IR}$) which opens up the decay mode of a spin-1 resonance into a dilaton along with an associated SM gauge boson.

Coupling to SM gauge bosons (flavor-blind): One can derive the coupling of the dilaton to a pair of SM gauge bosons, considering the running of the SM gauge coupling and using the fact that dilaton is the Goldstone boson that parameterizes the fluctuation of $\Lambda_{\rm IR}$. The final form of the coupling [99, 101, 102] is

$$\delta\mathcal{L} \;\sim\; \left(\frac{g_{\rm SM}}{g_{\star\,\rm IR}^{\rm gauge}}\right)^2 \frac{g_\star^{\rm grav}}{\Lambda_{\rm IR}} \varphi A_{\mu\nu} A^{\mu\nu} \tag{4.3}$$

where $g_{\rm SM}$ is the usual SM gauge coupling associated with the gauge field strength tensor $A_{\mu\nu}$ for which the gauge indices are suppressed for notational brevity. The stared quantities $g_\star^{\rm grav}$ and $g_{\star\,\rm IR}^{\rm gauge}$ parameterize the cubic couplings of the IR strong dynamics with at least one composite state being of spin-2 and spin-1, correspondingly. Denoting $N_{\rm strong}$ as the number of "color" charges of strong dynamics, we remark that in the large-$N_{\rm strong}$ limit, these composite cubic couplings generically

have the size of

$$g_\star \sim \frac{4\pi}{\sqrt{N_{\rm strong}}}. \tag{4.4}$$

Coupling to top/Higgs (flavor non-universal): Since the radion is localized near the IR brane in the minimal RS setup, it predominantly decays into the pairs of top quark, Higgs, and longitudinal modes of W/Z gauge bosons (through the Goldstone equivalence theorem). In particular, the decay rate of the radion in a pair of SM gauge bosons via the coupling in (4.3) is negligible. However, in the extended framework, the Higgs brane is *de*localized from the IR brane, and as a consequence, the radion has a small overlap with top quark or Higgs in their 5D profiles, yielding a reduced coupling to top quark or Higgs as follows [131]:

$$\delta\mathcal{L}\left(\Lambda_{\rm IR}\right) \sim \left(\frac{\Lambda_{\rm IR}}{\Lambda_{\rm Higgs}}\right)^{4-\epsilon} \frac{g^{\rm grav}_{\star\,\rm IR}}{\Lambda_{\rm IR}} \varphi \Big[m_t \bar{t} t + \left(\partial_\mu H\right)^\dagger \partial^\mu H \Big] . \tag{4.5}$$

As we will discuss in more detail later, we will (roughly) choose $\Lambda_{\rm IR}$ a couple of TeV, whereas $\Lambda_{\rm Higgs} \gtrsim \mathcal{O}(10)$ TeV and $g^{\rm gauge}_{\star\,\rm IR}$ of a few. With these parameters, we see that the couplings of the radion to top quark (first term) and Higgs (second term) in (4.5) are (highly) suppressed as compared to the coupling of radion to SM gauge bosons in (4.3). Thus, an interesting phenomenological implication is that the branching fractions of the radion into SM gauge boson pairs become sizable, playing an important role in our collider study.

4.2.2.2 KK gauge boson

As mentioned before, the mass scale of the spin-1 resonance (henceforth represented by ρ), which is dual to the KK gauge boson, is simply given by

$$m_{\rm KK} \sim \Lambda_{\rm IR}. \tag{4.6}$$

Coupling to SM matter (flavor-universal): The flavor universal couplings of ρ to SM fermions and Higgs are given by the famous $\gamma - \rho$ mixing mechanism observed in QCD + QED system, which we summarize as follows. When the strong sector (QCD) is confined and produces hadrons, there exists a vector meson which has the same quantum number as the elementary gauge boson in QED due to the fact that the external or elementary gauge symmetry gauges subgroups of its global symmetries. Therefore, there arises a mixing between the vector meson ρ and the corresponding elementary gauge boson γ. This mixing induces the breakdown of the elementary gauge symmetry in such a way that a certain linear combination between ρ and γ remains massless and the associated unbroken symmetry is interpreted as the SM gauge symmetry. Physical mass eigenstates are admixture of composite and elementary states and their mixing angle θ [131] is simply given by

$$\sin\theta = \frac{g_{\rm elem}}{\sqrt{g_{\rm elem}^2 + (g_\star^{\rm gauge})^2}} \sim \frac{g_{\rm elem}}{g_\star^{\rm gauge}}\,, \tag{4.7}$$

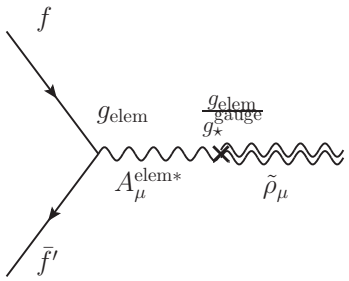

Figure 4.1: Flavor-universal coupling of spin-1 composite states to (light) SM fermions via an elementary-composite mixing. $A_\mu^{\rm elem\star}$ and $\tilde{\rho}_\mu$ denote the (virtual) elementary and composite states before the mixing. f and f' denote SM fermions.

where $g_{\rm elem}$ and $g_\star^{\rm gauge}$ are gauge couplings of elementary and strong sectors, respectively. The interaction between the composite state and *all* SM fermions via the mixing is shown in Fig. 4.1, wherein $A_\mu^{\rm elem}$ and $\tilde{\rho}_\mu$ denote the elementary and composite states before the mixing. Using the mixing angle given above, we write the coupling between them [131] as

$$\delta\mathcal{L} \sim \frac{g_{\rm SM}^2}{g_\star^{\rm gauge}} \rho^\mu \bar{f}\gamma_\mu f \tag{4.8}$$

where f represents the SM fermions and we used the relation

$$g_{\rm SM} = \frac{g_\star^{\rm gauge} g_{\rm elem}}{\sqrt{g_{\rm elem}^2 + g_\star^{\rm gauge\ 2}}} \approx g_{\rm elem}. \tag{4.9}$$

In addition to the above flavor-*universal* coupling, there is a non-universal part which is significant only for top/Higgs: we discuss this effect next.

Coupling to top/Higgs (flavor-non-universal): The profile of KK gauge bosons is localized near the IR brane, implying that its value at the Higgs brane is sup-

pressed, accordingly. An explicit calculation shows (either a 5D or 4D analysis) that the flavor *non*-universal part of the coupling of gauge KK to top/Higgs can be expressed as follows [131]:

$$\delta\mathcal{L}\left(\Lambda_{\rm IR}\right) \;\sim\; \frac{\left(g^{\rm gauge}_{\star\,\rm UV}\right)^2}{g^{\rm gauge}_{\star\,\rm IR}} \left(\frac{\Lambda_{\rm IR}}{\Lambda_{\rm Higgs}}\right)^2 \rho^\mu \left(\bar{t}\gamma_\mu t + H^\dagger D_\mu H\right) \,, \tag{4.10}$$

where $g^{\rm gauge}_{\star\,\rm UV}$ and $g^{\rm gauge}_{\star\,\rm IR}$ are the composite gauge couplings of UV and IR strong dynamics, correspondingly. Again ρ^μ represents a composite state obtained by the confinement of IR strong dynamics. The size of this coupling depends on the position of the Higgs brane relative to the IR brane as encoded in the factor $(\Lambda_{\rm IR}/\Lambda_{\rm Higgs})^2$.

Ref. [131] has extensively discussed the significance of this coupling and the resultant, (potentially) striking phenomenology. An interesting possibility is that this flavor-non-universal coupling is comparable to the flavor-universal in (4.8). This happens in the case of KK gluon (KK Z) for $\Lambda_{\rm Higgs} \sim 10$ (15) TeV; remarkably this value of the top/Higgs compositeness scale is (roughly) the flavor/CP bound on the KK scale! If KK gauge bosons (e.g., KK gluon and KK Z) are discovered at the LHC, their decay branching fractions would show $\mathcal{O}(1)$ deviation from those in the flavor-blind limit ($\Lambda_{\rm Higgs} \to \infty$), i.e., when we only have the couplings in (4.8). At the same time, these are significantly different than the standard warped model, which corresponds to the limit $\Lambda_{\rm Higgs} \to \Lambda_{\rm IR}$, i.e., (4.10) dominates over (4.8), so that gauge KK modes decay mostly into top/Higgs final state. In other words, the LHC may be sensitive to the top/Higgs compositeness scale, a striking signature for composite physics as a solution to the gauge hierarchy problem. In our current

study, we shall demonstrate another possibility, namely, a cascade decay of KK gauge bosons: while this will not *per se* be a probe of top/Higgs compositeness (cf. above idea), it nevertheless is very exciting since it is quite different from the "vanilla" decay of gauge KK modes into pairs of SM fermions/Higgs. Furthermore, we will see that these two signals are interestingly independent, i.e., this new channel exists no matter $\Lambda_{\rm Higgs} \sim \mathcal{O}(10)$ TeV or much higher (in the latter case, the above probe of top/Higgs compositeness obviously fades away).

Coupling to radion and SM gauge bosons (flavor-blind): The interaction among KK gauge boson-radion-SM gauge boson arising as a consequence of radius stabilization was discussed in Ref. [131]. The relevant coupling is given by

$$\delta\mathcal{L}\left(\Lambda_{\rm IR}\right) \;\sim\; \epsilon\,\lambda\, g_{\star\,\rm IR}^{\rm grav}\left(\frac{\Lambda_{\rm IR}}{\Lambda_{\rm Higgs}}\right)^{-\epsilon}\frac{g_{\rm elem}}{g_{\star\,\rm IR}^{\rm gauge}}\frac{\varphi}{\Lambda_{\rm IR}}\rho_{\mu\nu}A^{\mu\nu}\,, \tag{4.11}$$

where $\rho^{\mu\nu}$ is the field strength tensor for the spin-1 composite field ρ^{μ}. As mentioned earlier, $\epsilon \sim 1/\log\left(\Lambda_{\rm Higgs}/\Lambda_{\rm IR}\right) \sim 1/(\text{a few})$, thus we find that $\left(\Lambda_{\rm IR}/\Lambda_{\rm Higgs}\right)^{-\epsilon}$ is an $\mathcal{O}(1)$ factor. This implies that the KK gauge boson-radion-SM gauge boson coupling can be (roughly) comparable to the flavor-universal coupling of the KK gauge boson to SM fermions in (4.8) (in turn, the latter is comparable to/larger than the non-universal one for $\Lambda_{\rm Higgs} \gtrsim \mathcal{O}(10)$ TeV). In Ref. [131], as mentioned above, the focus was on probing top/Higgs compositeness so that, for simplicity, in the analysis there it was assumed that we live in the part of parameter space where the new decay channel is smaller (and hence was neglected in the BR's shown), for example, small

$g^{\rm grav}_{\star\,\rm IR}$ and/or ϵ in eq. (4.11). While here, we choose the *another* part of parameter space where the branching ratio of the KK gauge boson decay into a radion and the corresponding SM gauge boson can be substantial, even dominating over pair of SM fermions. Furthermore, as we discussed earlier, the radion, in turn, decays predominantly into a pair of SM gauge bosons. We emphasize that in the standard warped model, although both the interaction vertices involved in the above new decay channel are present, both KK gauge bosons and radion have overwhelming decay rates into top/Higgs final states, leaving a little chance for the above novel channels to be probable at the LHC.

4.3 Overview of LHC Signals

As we reviewed in Sec. 4.2, the extended warped extra-dimensional framework proposed in Ref. [131] renders significant branching ratios for (i) the decay of KK gauge bosons to radion and the corresponding SM gauge boson and (ii) the decay of radion to a pair of SM gauge bosons. The *combination* of these two features creates a very novel search channel for KK gauge bosons and radion. Namely, the LHC can produce on-shell KK gauge bosons via the same, i.e., flavor-universal, coupling to light quarks as in the standard RS model. These heavy particles subsequently decay into a radion and a corresponding SM gauge boson, followed by the radion decay into a pair of SM gauge bosons. This offers final states containing various combinations of three SM gauge bosons from decays of *two resonances*: KK gauge boson and radion. Fig. 4.2 displays the decay topology associated with various signal

channels. When it comes to the study on collider signatures, instead of working with a full 5D warped extra-dimensional model or its 4D dual theory, it is much more convenient to conduct the study with a simplified model containing only relevant particles and parameters. Therefore, we first construct the simplified model for our phenomenological study in the next section, and then discuss the production and decays of all types of KK gauge bosons and radion together with current bounds. We finally close this section by identifying relevant parameter space for our study and choosing the benchmark points for various channels.

4.3.1 Simplified model and allowed parameter space

We now describe a simplified model on which our collider analyses in Sec. 4.5 are based, presenting the relevant particles and their interactions. The notation for the particles (and their masses and couplings) that we will set-up in this section (and which is to be used for rest of the chapter) is somewhat *different* than in the earlier section. However, (as much as is possible) we will try to provide a correspondence between the two sets: the one we develop in this section is more convenient for phenomenological studies, whereas the previous might be better suited for a more theoretical discussion. The simplified-model approach also allows enough generality to encompass a broad class of models which could accommodate the same signatures.

Relevant particles in our study include four types of (lightest) KK gauge bosons $A_{\rm KK} = \{\gamma_{\rm KK}, W_{\rm KK}, Z_{\rm KK}, g_{\rm KK}\}$,[8] their zero-mode SM gauge bosons $A = \{\gamma, W, Z, g\}$, radion φ, and (light) SM fermions ψ. For convenience, we tabulate the symbols for

[8]Here we assume the masses of electroweak KK gauge bosons are degenerate.

	Name	Mass
KK gauge bosons	$A_{\rm KK}$	$m_{\rm KK}$
KK photon	$\gamma_{\rm KK}$	$m_{\gamma_{\rm KK}}$
KK W gauge boson	$W_{\rm KK}$	$m_{W_{\rm KK}}$
KK Z gauge boson	$Z_{\rm KK}$	$m_{Z_{\rm KK}}$
KK gluon	$g_{\rm KK}$	$m_{g_{\rm KK}}$
Radion	φ	m_{φ}

Table 4.2: Notation of names and mass parameters for new physics particles.

new physics particles together with their respective mass parameters in Table 4.2.

We now comment on the choice of $\Lambda_{\rm Higgs}$ that we will make in our subsequent analysis. As mentioned just above, the motivation in this chapter is different from that in Ref. [131], where the idea was to obtain signals for top/Higgs compositeness, thus the cascade decay channel was neglected. Namely, we are *now* precisely interested in the new decay channel. So, for simplicity, here we will instead neglect the top/Higgs *non*-universal coupling (which drove sensitivity to top/Higgs compositeness) by (formally) setting $\Lambda_{\rm Higgs} \to \infty$; we are then left with only the flavor-universal coupling of gauge KK modes to pair of SM fermions/Higgs. Note that, as discussed above, the non-universal coupling can at most be as large as universal one, as long as $\gtrsim \mathcal{O}(10)$ TeV (flavor bound) so that, in reality (i.e., if we assume $\Lambda_{\rm Higgs}$ finite), it will be at most $\mathcal{O}(1)$ effect on our signal. We re-iterate that the decay rates of KK gauge bosons into top/Higgs pairs are much smaller than those in the standard warped model (where the non-universal coupling to top/Higgs dominates over all others).

Three types of (new) couplings are relevant in the signal processes as clear

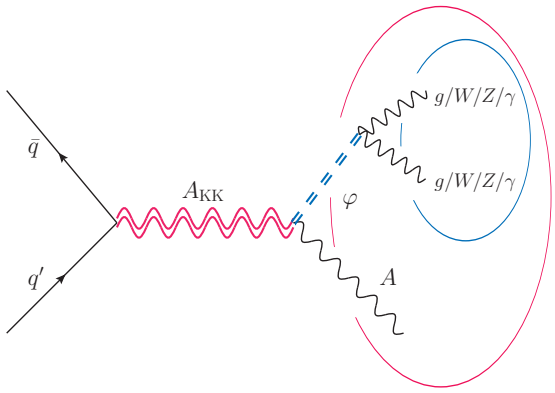

Figure 4.2: Feynman diagram for the signal process. Double (single) lines represent composite (SM elementary) particles and q/q' denote light quarks inside the proton. The signal process is characterized by two resonance bumps illustrated by blue and red circles.

from Fig. 4.2: (1) KK gauge bosons coupling to SM quarks, (2) KK gauge boson-radion-SM gauge boson coupling, and (3) radion coupling to a pair of SM gauge bosons. First of all, KK gauge boson coupling to SM quarks has the form:

$$\delta\mathcal{L}_{(1)} = Q_A \frac{g_A^2}{g_{A_{\rm KK}}} A^\mu_{\rm KK} \bar{\psi}\gamma_\mu\psi \tag{4.12}$$

where g_A and $g_{A_{\rm KK}}$ are SM and KK gauge couplings for respective gauge bosons A and $A_{\rm KK}$. Here Q_A denotes SM A-gauge charge of the SM fermion ψ. One can easily notice that this coupling is nothing but the expression in (4.8), but with change of notation from $g_\star^{\rm gauge}$ to $g_{A_{\rm KK}}$. Second, KK gauge boson-radion-SM gauge boson coupling is of the form:

$$\delta\mathcal{L}_{(2)} = \epsilon g_{\rm grav} \frac{g_A}{g_{A_{\rm KK}}} \frac{\varphi}{m_{\rm KK}} A_{\mu\nu} A^{\mu\nu}_{\rm KK}, \tag{4.13}$$

where $g_{\rm grav}$ is the KK gravity coupling and $m_{\rm KK}$ is the mass of KK gauge boson (or

equivalently, KK scale). $A^{\mu\nu}_{\rm KK}$ is the field strength tensor for the KK gauge boson $A_{\rm KK}$. This coupling is just a rewriting of (4.11), but with $\Lambda_{\rm IR}$ identified as $m_{\rm KK}$ and $\mathcal{O}(1)$ factors like λ and $(\Lambda_{\rm IR}/\Lambda_{\rm Higgs})^{-\epsilon}$ dropped from it. One can interpret that other parameters like ϵ and $g_{\rm grav}$ absorb those $\mathcal{O}(1)$ factors and get redefined. Finally, the radion coupling to a pair of SM gauge bosons has the structure of

$$\delta\mathcal{L}_{(3)} = -\frac{1}{4}\left(\frac{g_A}{g_{A_{\rm KK}}}\right)^2 \frac{g_{\rm grav}}{m_{\rm KK}}\varphi A_{\mu\nu}A^{\mu\nu}\,, \tag{4.14}$$

where again $m_{\rm KK}$ corresponds to $\Lambda_{\rm IR}$. This coupling structure obviously originates from (4.3), while the prefactor $-1/4$ comes from the normalization of gauge kinetic terms. We will simply neglect the coupling of radion to top/Higgs in (4.5), just like we did above for gauge KK couplings. We are now about to detail the scheme of scanning the above parameter space in order to obtain the allowed region therein.

KK gauge and KK gravity couplings: Although there are four KK gauge couplings ($g_{\gamma_{\rm KK}}$, $g_{W_{\rm KK}}$, $g_{Z_{\rm KK}}$, and $g_{g_{\rm KK}}$) under consideration, just like in the SM, only three of them are independent, which are $g_{g_{\rm KK}}$, $g_{W_{\rm KK}}$, and $g_{B_{\rm KK}}$. The KK gauge couplings of $\gamma_{\rm KK}$ and $Z_{\rm KK}$ are obtained via well-known relations

$$g_{\gamma_{\rm KK}} = \frac{g_{W_{\rm KK}} g_{B_{\rm KK}}}{\sqrt{g^2_{W_{\rm KK}} + g^2_{B_{\rm KK}}}}\,, \qquad g_{Z_{\rm KK}} = \sqrt{g^2_{W_{\rm KK}} + g^2_{B_{\rm KK}}}. \tag{4.15}$$

Although perturbativity in 5D warped models demands $g_{g/W/B_{\rm KK}} \lesssim 3$ [131], in this simplified model approach, we allow those KK couplings to be larger. This way, we can explore broader parameter space, even covering the possibility that some

strongly-coupled 4D theories might be realized in some parameter space without obvious 5D dual. However, reasonably requiring $N \gtrsim$ (a few) in the relation $g_{A_{\rm KK}} \sim 4\pi/\sqrt{N_{\rm strong}}$ does set a rough upper limit on $g_{g/W/B_{\rm KK}}$ to be around 6.[9] On the other hand, a lower limit for gauge KK coupling arises from requiring that the Landau pole scale is higher than GUT scale and comes out to be 3. Therefore, the allowed ranges for KK gauge couplings are

$$3 \lesssim g_{g_{\rm KK}}\,, g_{W_{\rm KK}}\,, g_{B_{\rm KK}} \lesssim 6, \tag{4.16}$$

from which we deduce the constraints for $g_{\gamma_{\rm KK}}$ and $g_{Z_{\rm KK}}$ in conjunction with the relation (4.15).

Similarly to the case of KK gauge couplings, the KK gravity coupling has the upper limit around 6. However, since there is no Landau pole issue in gravity sector, KK gravity coupling is unbounded below although too small $g_{\rm grav}$, which implies too large $N_{\rm strong}$, may not be reasonable. Hence, the allowed KK gravity coupling is given by $\mathcal{O}(1) \lesssim g_{\rm grav} \lesssim 6$.

KK gauge boson and radion masses: Ongoing experimental effort on various resonance searches constrain the masses for KK gauge bosons. We shall discuss the associated bounds in Sec. 4.3.3 in detail. We choose $m_{\rm KK}$ to be somewhat heavier than the current bound: in most channels $m_{\rm KK} = 3$ TeV. When it comes to the radion mass, the diphoton resonance search mainly constrains it: we consider both $m_\varphi = 1$ TeV and 1.5 TeV.

[9] Note that this is also roughly the size of $\rho\,\pi\,\pi$ coupling in QCD.

Parameter ϵ: The ϵ parameter appears in the radion mass, where its effect can be "compensated" by the detuning parameter λ. Its only other appearance is in the KK gauge-radion-SM gauge coupling (see (4.13)), i.e., our signal channel; in particular, this means that this parameter is not constrained by experimental bounds. Generically, ϵ needs to be $\mathcal{O}(1/$ a few) in order for the hierarchy $\Lambda_{\rm Higgs}/\Lambda_{\rm IR}$ to be stabilized. As is evident from eq. (4.13), taking larger value of ϵ enhances the signal cross section, so for our benchmark points, we set ϵ to be 0.5 in this study.

4.3.2 Radion direct production, decay, and current bounds

Radion is produced at the LHC via gluon fusion using flavor-universal coupling in (4.14). The same interaction vertices are responsible for its dominant decays to a pair of SM gauge bosons gg, WW, ZZ, and $\gamma\gamma$. To leading order, the radion decay width is given by

$$\Gamma(\varphi \to AA) = N_A g_{\rm grav}^2 \left(\frac{g_A}{g_{A_{\rm KK}}}\right)^4 \left(\frac{m_\varphi}{m_{\rm KK}}\right)^2 \frac{m_\varphi}{64\pi} \tag{4.17}$$

where N_A is the degrees of freedom of SM gauge boson: 8 for gluon, 2 for W, and 1 for γ and Z. From this we see that radion decay branching ratios are determined by the relative size of KK gauge couplings. Numerically, we find that BRs to $\gamma\gamma$, ZZ, WW, and gg are roughly $\mathcal{O}(0.1)\%$, $\mathcal{O}(1)\%$, $\mathcal{O}(1)\%$, and $\mathcal{O}(95)\%$, respectively: here, we have used the numerical values $g_\gamma \approx 0.3$, $g_W \approx 0.65$, $g_Z \approx 0.74$, and $g_g \approx 1$. We display the branching ratios of various radion decay modes as a function of $g_{\gamma_{\rm KK}}$ ($g_{W_{\rm KK}}$) with $g_{g_{\rm KK}} = 6$ and $g_{W_{\rm KK}} = 6$ ($g_{\gamma_{\rm KK}} = 2.5$) in the left (right) panel of Fig. 4.3.

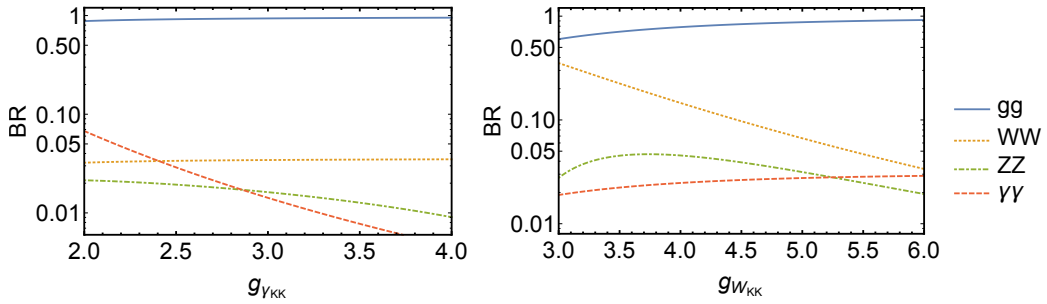

Figure 4.3: The left panel shows BR of radion as a function of $g_{\gamma_{\rm KK}}$, keeping $g_{W_{\rm KK}} = 6$. The right panel shows BR as a function of $g_{W_{\rm KK}}$, keeping $g_{\gamma_{\rm KK}} = 2.5$. In both cases we choose $g_{g_{\rm KK}} = 6$.

Although the diphoton channel has the smallest branching ratio in most of parameter space of interest, the cleaner nature of photonic final states than diboson or dijet ones leads to the most stringent bound for radion. The current diphoton searches performed by the ATLAS and CMS Collaborations [70, 108] suggest 0.7 (0.4) fb for 1 (1.5) TeV radion. Since all our signal channels contain a radion as an intermediary on-shell state, this bound is relevant so that we take this into account in our study. As stated before, we choose 1 TeV and 1.5 TeV as benchmark values for the radion mass. Even though heavier radions could be safe from the bounds, they would result in smaller signal cross sections because of the phase space suppression in decay width $\Gamma(A_{\rm KK} \to \varphi A)$. On the other hand, lower radion masses would be more constrained by the current diphoton bounds and also develop narrower possible parameter space. We shall discuss the bounds again more explicitly in the context of benchmark points for our collider study (see Fig. 4.5).

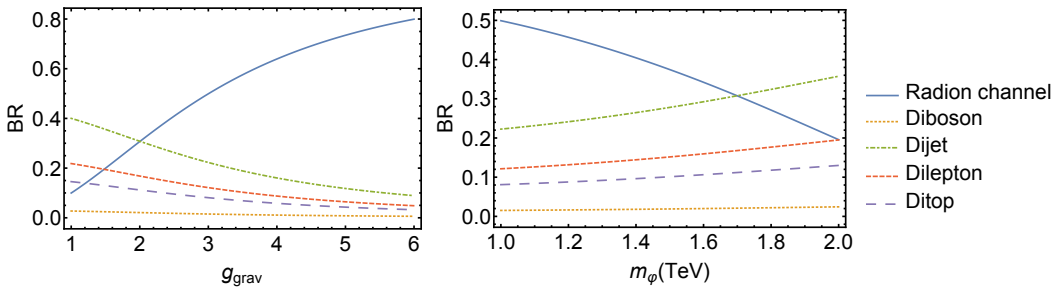

Figure 4.4: The left panel shows BR of KK photon as a function of $g_{\rm grav}$, keeping $m_\varphi = 1$ TeV. The right panel shows BR as a function of m_φ, keeping $g_{\rm grav} = 3$. In both cases we choose $m_{\rm KK} = 3$ TeV and $\epsilon = 0.5$.

4.3.3 Gauge KK production, decay, and current bounds

KK gauge bosons are produced via pair-annihilation of light quarks inside the proton, whose coupling structures are encoded in (4.12). They can then decay directly into a pair of SM fermions via the same interaction vertices. Another decay mode of them is to a radion and a corresponding SM gauge boson, whose coupling is governed by (4.13). Let us call this "radion channel" for short. As we explained earlier, decays to tops/Higgs via flavor-non-universal couplings are usually very suppressed, and hence neglected. However, we remark that decays to top/Higgs would still occur via the flavor-universal coupling in (4.12). We first summarize decay widths for all KK gauge bosons and move onto their current bounds.

4.3.3.1 Decay widths of KK gauge bosons

KK photon: Decay channels for the KK photon are radion channel, WW, dilepton, dijet, and ditop channels:

$$\Gamma \quad (\gamma_{KK} \to \varphi\gamma) = \left(\epsilon g_{\rm grav} \frac{g_\gamma}{g_{\gamma_{\rm KK}}}\right)^2 \left(1 - \left(\frac{m_\varphi}{m_{\rm KK}}\right)^2\right)^3 \frac{m_{\rm KK}}{24\pi}\,, \tag{4.18}$$

$$\Gamma \quad (\gamma_{KK} \to WW) \approx \left(\frac{g_\gamma^2}{g_{\gamma_{\rm KK}}}\right)^2 \frac{m_{\rm KK}}{48\pi}\,, \tag{4.19}$$

$$\Gamma \quad (\gamma_{KK} \to \psi\psi) \approx N_\psi Q_\gamma^2 \left(\frac{g_\gamma^2}{g_{\gamma_{\rm KK}}}\right)^2 \frac{m_{\rm KK}}{12\pi}\,, \tag{4.20}$$

where $\gamma_{KK} \to \psi\psi$ represents the KK photon decay into a pair of SM fermions. N_ψ denotes the degrees of freedom of SM fermions (e.g., 3 for quarks and 1 for leptons), while Q_γ denotes the electric charge of the associated fermions. The approximation signs in some of the partial decay width formulae in this section originate from taking the massless limit of SM particles. Based on the formulae listed above, we exhibit branching ratios of KK photon as a function of $g_{\rm grav}$ (left panel) and m_φ (right panel) in Fig. 4.4. For both panels, $m_{\rm KK}$ and ϵ are set to be 3 TeV and 0.5, respectively, whereas m_φ ($g_{\rm grav}$) is fixed to 1 TeV (3) for the left (right) panel. We clearly observe that the radion channel can be the dominant decay mode of KK photon in a wide range of the parameter region of interest. The BR of other KK gauge bosons will be roughly similar to that of KK photon, so we only show plots for BR of KK photon as a representative example.

KK gluon: Decay channels for the KK gluon are radion channel, dijet, and ditop channels:

$$\Gamma \quad (g_{KK} \to \varphi\ g) = \left(\epsilon g_{\rm grav} \frac{g_g}{g_{g_{\rm KK}}}\right)^2 \left(1 - \left(\frac{m_\varphi}{m_{\rm KK}}\right)^2\right)^3 \frac{m_{\rm KK}}{24\pi}\,, \tag{4.21}$$

$$\Gamma \quad (g_{KK} \to qq) \approx \left(\frac{g_g^2}{g_{g_{\rm KK}}}\right)^2 \frac{m_{\rm KK}}{24\pi}\,. \tag{4.22}$$

KK W: Decay channels for the KK W boson are radion channel, diboson, dijet, and dilepton channels:

$$\Gamma \quad (W_{KK} \to \varphi\ W) = \left(\epsilon g_{\rm grav} \frac{g_W}{g_{W_{\rm KK}}}\right)^2 \left(1 - \left(\frac{m_\varphi}{m_{\rm KK}}\right)^2\right)^3 \frac{m_{\rm KK}}{24\pi}\,, \tag{4.23}$$

$$\Gamma \quad (W_{KK} \to WZ/Wh) \approx \left(\frac{g_W^2}{g_{W_{\rm KK}}}\right)^2 \frac{m_{\rm KK}}{192\pi}\,, \tag{4.24}$$

$$\Gamma \quad (W_{KK} \to \psi\psi') \approx N_\psi \left(\frac{g_W^2}{g_{W_{\rm KK}}}\right)^2 \frac{m_{\rm KK}}{48\pi}\,, \tag{4.25}$$

where $W_{KK} \to \psi\psi'$ represents KK W decay into a pair of (different-flavored) SM fermions.

KK Z: Decay channels for the KK Z boson are radion channel, diboson, dijet, ditop, and dilepton channels:

$$\Gamma \quad (Z_{KK} \to \varphi\ Z) = \left(\epsilon g_{\rm grav} \frac{g_Z}{g_{Z_{\rm KK}}}\right)^2 \left(1 - \left(\frac{m_\varphi}{m_{\rm KK}}\right)^2\right)^3 \frac{m_{\rm KK}}{24\pi}\,, \tag{4.26}$$

$$\Gamma \quad (Z_{KK} \to WW/Zh) \approx Q_Z^2 \left(\frac{g_Z^2}{g_{Z_{\rm KK}}}\right)^2 \frac{m_{\rm KK}}{48\pi}\,, \tag{4.27}$$

$$\Gamma \quad (Z_{KK} \to \psi\psi) \approx N_\psi Q_Z^2 \left(\frac{g_Z^2}{g_{Z_{\rm KK}}}\right)^2 \frac{m_{\rm KK}}{24\pi}\,, \tag{4.28}$$

where $Q_Z = \frac{1}{2} - \sin^2\theta_W$ (θ_W being Weinberg angle) for WW channel and $Q_Z = \frac{1}{2}$ for Zh channel in (3.16). Besides, Q_Z in (3.17) denotes the SM Z charge of the associated fermion ψ.

4.3.3.2 Current bounds of KK gauge bosons

KK Z: As mentioned in Ref. [131], the strongest bound for KK Z comes from the dilepton resonance search. We can obtain it by simply using the experimental searches for sequential SM Z' [112], but taking into account the coupling to light quarks, which is involved in the dominant production mechanism, being *reduced* by $\sim g_Z/g_{Z_{\rm KK}}$. We expect that our cascade decay signal channel further relaxes the bounds since the original dilepton branching ratio is reduced by half for 50% branching ratio for the radion channel:[10] based on the discussion in the previous section, we see that such a suppression of BR for decay to pair of SM fermions/Higgs can be easily achieved. We find that the predicted cross section of sequential SM Z' exceeds the bound [112] by ~ 70 (25) for $m_{Z'} \sim 2$ (2.5) TeV. Translating this bound for our case, including radion channel, we obtain

$$m_{Z_{\rm KK}} \gtrsim 2.5 \text{ TeV for } g_{Z_{\rm KK}} \sim 5\,, \tag{4.29}$$

$$\gtrsim 3 \text{ TeV for } g_{Z_{\rm KK}} \sim 3\,, \tag{4.30}$$

with g_Z set to be around 0.75.

[10] Note that in Ref. [131], the new decay channel for KK Z was neglected so that the bounds quoted there are slightly stronger than here.

KK photon: Similarly to the KK Z boson, the mass of the KK photon is most severely constrained by the dilepton resonance search. Indeed, $\mathrm{BR}(\gamma_{\mathrm{KK}} \to \ell^+\ell^-) = (8/3) \cdot \mathrm{BR}(Z_{\mathrm{KK}} \to \ell^+\ell^-)$ with the assumption of the same branching ratio for the radion channel in both cases. However, $\sigma(pp \to \gamma_{\mathrm{KK}}) \cdot \mathrm{BR}(\gamma_{\mathrm{KK}} \to \ell^+\ell^-)$ is smaller than $\sigma(pp \to Z_{\mathrm{KK}}) \cdot \mathrm{BR}(Z_{\mathrm{KK}} \to \ell^+\ell^-)$, given that γ_{KK} and Z_{KK} have the same mass. This is because their production rates are proportional to $g_A^4/g_{A_{\mathrm{KK}}}^2$, and therefore, with $g_{Z_{\mathrm{KK}}} \sim g_{\gamma_{\mathrm{KK}}}$, $\sigma(pp \to \gamma_{\mathrm{KK}})/\sigma(pp \to Z_{\mathrm{KK}})$ is roughly $g_\gamma^4/g_Z^4 < 1$.[11] So, we expect that KK photon is less constrained than KK Z from dilepton bounds. Considering 50% branching ratio for the radion channel again, we find that the bound is roughly

$$m_{\gamma_{\mathrm{KK}}} \gtrsim 2 \text{ TeV for } g_{\gamma_{\mathrm{KK}}} \sim 3\,. \tag{4.31}$$

KK W: The dominant bound comes from the leptonic decay of KK W, i.e., $W_{KK} \to \ell v$ [131]. In our model, assuming that the radion channel comprises 50% of the branching ratio for KK W decays, we see that the leptonic decay of one generation (either $e\nu_e$ or $\mu\nu_\mu$) has the branching ratio of 4%. From the new resonance search in $\ell\nu$ channels conducted by the ATLAS Collaboration [114], we find that the bound therein can be interpreted as

$$m_{W_{\mathrm{KK}}} \gtrsim 2.5 \text{ TeV for } g_{W_{\mathrm{KK}}} \sim 3\,. \tag{4.32}$$

[11] This is just a rough estimate. For a more accurate analysis one needs to take into account the difference between electric charge and SM Z charge of quarks (i.e., Q_γ vs. Q_Z).

KK gluon: The constraints for the KK gluon come from both ditop and dijet searches. The ditop bound can be obtained by rescaling the KK gluon bound given in Ref. [119]. The predicted cross-section (all for $g_{g_{\rm KK}} \sim 5$, as assumed in Ref. [122], which is quoted in Ref. [119]) is larger than the bound by ~ 6 (2) for mass of KK gluon of 2 (2.5) TeV. The above bounds are assuming BR to top quarks ≈ 1 (as in the standard scenario) so that for our case, with the radion channel having 50% branching ratio and BR to top quarks is $\approx 1/12$, we get

$$m_{g_{\rm KK}} \gtrsim 2.0 \text{ TeV for } g_{g_{\rm KK}} \sim 3.5\,, \tag{4.33}$$

$$\gtrsim 2.5 \text{ TeV for } g_{g_{\rm KK}} \sim 2\,. \tag{4.34}$$

For the dijet bound, we may rescale from axigluon bounds in Ref. [110], i.e., coupling to our composite gluon is smaller by a factor of $\sim g_G/\left(\sqrt{2}g_{g_{\rm KK}}\right)$, since coupling of axigluon is larger than QCD by $\sqrt{2}$ (see also the discussion in Ref. [123] referred to by Ref. [110]). The cross-section is constrained to be smaller than the prediction for axigluon by ~ 50 (30) for axigluon mass of 2 (2.5) TeV. So, using the above couplings, and taking radion channel BR to be 50%, we get for our case:

$$m_{g_{\rm KK}} \gtrsim 2.0 \text{ TeV for } g_{g_{\rm KK}} \sim 3.5\,, \tag{4.35}$$

$$\gtrsim 2.5 \text{ TeV for } g_{g_{\rm KK}} \sim 3\,. \tag{4.36}$$

4.3.4 Benchmark points

In this section, we list the benchmark points (BPs) for all channels that we examine in Sec. 4.5. We carefully choose them to satisfy all experimental/theoretical bounds that we discussed in previous sections. We tabulate parameter values for each benchmark point in Table 4.3. The name of each BP obeys the following pattern.

the name of the KK gauge boson - final states - BP1 or BP2

For example, γ-γgg-BP1 means the first benchmark point (BP1) for KK photon (γ in the first placeholder) with final states photon + dijet (γgg).

We show the contour plots of estimated signal cross sections for all ten benchmark points in the plane of $g_{\gamma_{\rm KK}}$ (first six panels) or $g_{W_{\rm KK}}$ (last four panels) vs. $g_{\rm grav}$ in Fig. 4.5. All cross sections are reported in fb, and the input radion masses are either 1 TeV (BP1) or 1.5 TeV (BP2). The other parameters unspecified in each panel are chosen to be the same as those in the associated benchmark point of Table 4.3.

We remark that diphoton bounds constrain *any* radion decaying to a pair of photons. Two sources for radion production are affected by the diphoton constraint: one is direct production via gluon fusion, and the other is from KK gauge boson decays. All diphoton bounds displayed in Fig. 4.5 by blue regions result from taking these two sources into consideration.

	Process	Name	m_{KK}	m_φ	$g_{\gamma_{\text{KK}}}$	$g_{W_{\text{KK}}}$	$g_{g_{\text{KK}}}$	g_{grav}
γ_{KK}	$\gamma_{\text{KK}} \to \gamma\varphi \to \gamma gg$ (4.5.1)	γ-γgg-BP1 γ-γgg-BP2	3 3	1 1.5	3 2.7	6 6	3 3	3 4.1
g_{KK}	$g_{\text{KK}} \to g\varphi \to g\gamma\gamma$ (4.5.2.2)	g-$g\gamma\gamma$-BP1 g-$g\gamma\gamma$-BP2	3 3	1 1.5	2.7 2.7	6 6	6 6	2.25 3
	$g_{\text{KK}} \to g\varphi \to ggg$ (4.5.2.1)	g-ggg-BP1 g-ggg-BP2	3 3	1 1.5	2.7 2.7	6 6	3 3	2.45 4
	$g_{\text{KK}} \to g\varphi \to gV_hV_h$ (4.5.2.3)	g-gVV-BP1 g-gVV-BP2	3 3	1 1.5	2.65 2.65	3 3	6 6	3 5
W/Z_{KK}	$W_{\text{KK}} \to W_l\varphi \to W_lgg$ (4.5.3)	W-Wgg-BP1 W-Wgg-BP2	2.5 3	1 1.5	3.5 3	4.4 3.5	3 3	3.5 5.1

Table 4.3: A list of benchmark points defined by their associated process and chosen parameter values. For all of them, the ϵ parameter is set to be 0.5. We assign the name of the channels in the following pattern: *the name of the KK gauge boson - final states - BP1 or BP2*. The numbers in the parentheses of the second column refer to the section discussing the corresponding collider analysis. V refers to either W or Z and the subscript h (l) stands for hadronic (leptonic) decay. All mass quantities are in TeV.

For channels involving $W_{\rm KK}$, we also consider the bound from the leptonic decay of $W_{\rm KK}$ (red regions). There is another strong theoretical constraint applied to all channels, which demands $g_{B_{\rm KK}} \in [3, 6]$ as discussed near relation (4.16) (orange regions). We clearly see from the contour plots that all our benchmark points are not ruled out.

4.4 Collider Study

Armed with the benchmark points defined in the previous section, we now discuss our strategy for their collider studies. We begin by explaining how we conduct Monte Carlo simulation and reconstruct/identify objects out of the simulated data. As some of the signal channels include W/Z gauge boson-induced jets in addition to the quark/gluon jets, we briefly review the jet substructure technique that we employ here. Moving onto data analyses, we discuss key mass variables allowing us to suppress background events significantly, thus increase signal sensitivity.

4.4.1 Event simulation

Simulated event samples are used to model signal predictions in various channels discussed in the previous section and estimate SM background processes associated with each of the signal processes. For more realistic Monte Carlo simulation, we take into consideration various effects such as parton shower, hadronization/fragmentation, and detector responses. To this end, we employ a sequence of simulation tools. We begin with creating our model files with FeynRules [141] and

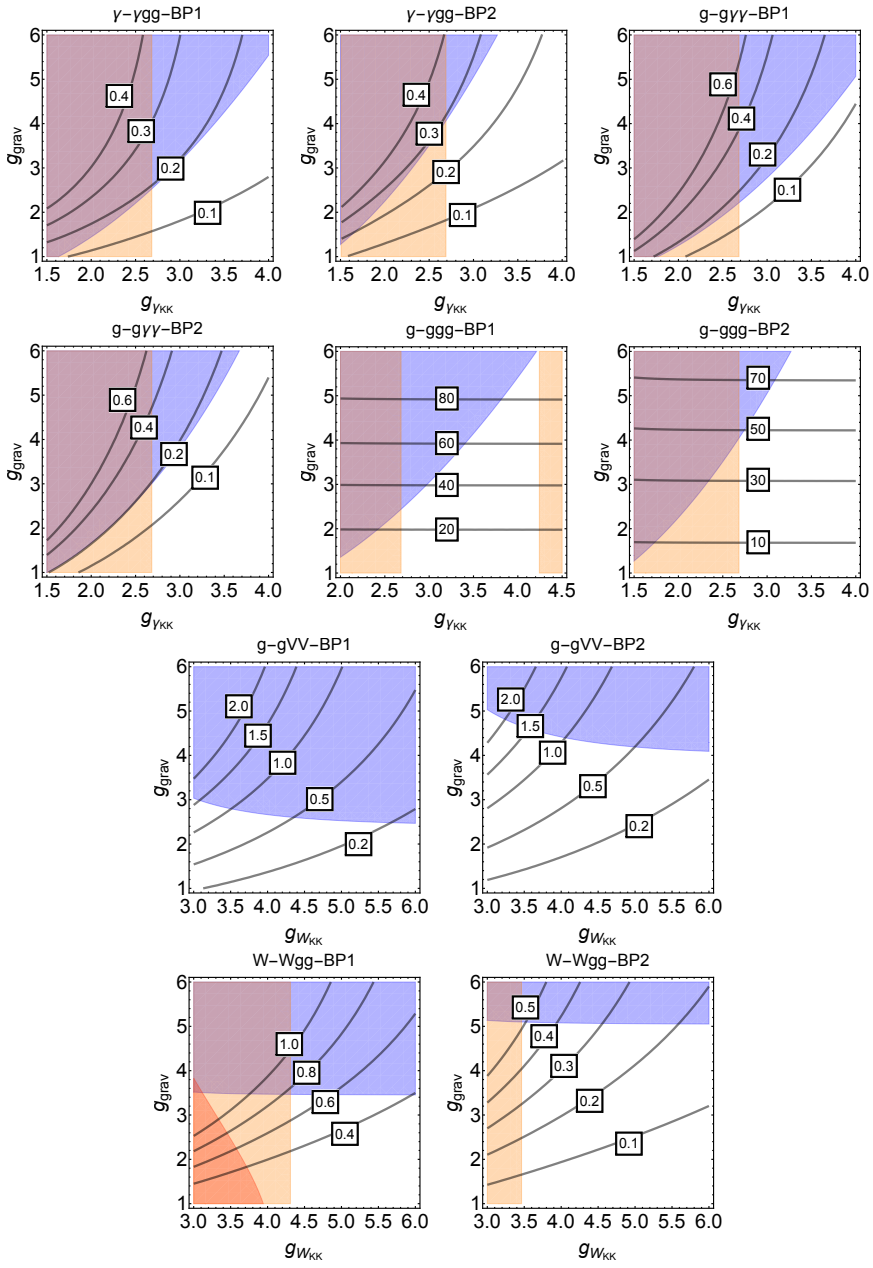

Figure 4.5: Contour plots of the cross sections for ten benchmark points in the plane of $g_{\gamma_{\rm KK}}$ (first six panels) or $g_{W_{\rm KK}}$ (last four panels) vs. $g_{\rm grav}$. All cross sections are in fb, and the input radion masses are either 1 TeV (BP1) or 1.5 TeV (BP2). The blue (red) regions are excluded by diphoton ($W_{\rm KK}$ leptonic decay) bounds. The orange regions are forbidden due to $g_{B_{\rm KK}} \notin [3, 6]$. Each plot is labelled by the associated benchmark point. The other parameters which are not specified in each contour plot are chosen to be the same as those in the associated benchmark point of Table 4.3.

	Regular jets	Merged jets
R	0.4 (anti-k_t jet)	0.8 (Cambridge-Achen jet)
μ_*	–	1.0
y_*	–	0.04
R_*	–	0.3

Table 4.4: Jet parameters for regular jets (second column) and merged jets (third column).

plug the outputs into a Monte Carlo event generator MG5@aMC [142] with parton distribution functions parameterized by NN23LO1 [143]. All the simulations are performed with a $\sqrt{s} = 14$ TeV pp collider at the leading order. The generated events are then streamlined to Pythia 6.4 [144] for taking care of showering and hadronization/fragmentation.

As some of our signal processes accompany boosted gauge bosons in the final state, our scheme to find jets depends whether or not we require merged jets. For the channels involving only regular jets, we feed the output from Pythia 6.4 into Delphes 3 [147] interfaced with FastJet [145, 146] for describing the detector effects and forming jets. The jets are constructed with the anti-k_t algorithm [146] with a radius parameter $R = 0.4$ (see also Table 4.4).

For merged jets, we begin with the Cambridge-Achen jet algorithm [148,149] to cluster particles from hadronically decaying W/Z bosons. Tagging W/Z-induced jets is done by a jet substructure technique. In our analysis, we employ the Mass Drop Tagger (MDT) [150]. The MDT essentially traces back the clustering sequences of a C/A jet and attempts to find subjets satisfying appropriate conditions. We briefly summarize an MDT procedure below.

(1) Clustering: We cluster energy deposits in the calorimeters using the C/A jet algorithm together with a jet radius parameter $R = 0.8$ in order to capture all decay products from a boosted gauge boson.

(2) Splitting: We rewind the last clustering sequence of a jet j, denoting two subjets as j_1 and j_2 by the order of decreasing mass.

(3) Checking symmetry conditions: We set an upper bound μ_* and a lower bound y_* on MDT parameters μ and y as follows:

$$\mu \equiv \frac{m_{j_1}}{m_j} < \mu_* \,, \quad y \equiv \frac{\min\left[p_{T,j_1}^2,\, p_{T,j_2}^2\right]}{m_j^2} \Delta R_{j_1 j_2}^2 > y_* \,. \tag{4.37}$$

If subjets fail in satisfying the above conditions, the MDT procedure redefines j_1 as j and repeats the step described in (2). Our choice of μ_* and y_* are tabulated in Table 4.4.[12]

Once the MDT finds a signal merged jet and identify two prongs in it, the MDT attempts to get rid of QCD contamination in subjets by reclustering energy deposits in the merged jet again employing the C/A jet algorithm of a smaller jet radius $R_{\rm filt}$.

(4) Filtering: We recluster the merged jet constituents with the C/A jet algorithm of radius,

$$R_{\rm filt} = \min\left(R_*,\, \frac{\Delta R_{j_1 j_2}}{2}\right) \tag{4.38}$$

[12]Detailed values for the C/A-jet radius R and μ_* do not affect the W/Z-jet tagging efficiency substantially, as it is mostly dictated by y_* [151].

to obtain n new subjets $\{s_1, \cdots, s_n\}$ sorted in decreasing p_T. R_* denotes the maximum allowed size for subjets to minimize the QCD contamination. The MDT considers an $\mathcal{O}(\alpha_s)$ correction from hard emission, by accepting at most three subjets in redefining a merged jet as

$$p^{\mu}_{\text{merged jet}} = \sum_{i=1}^{\min(n,3)} p^{\mu}_{s_i} \,. \tag{4.39}$$

(5) The sum of these $n \leq 3$ subjets is taken as a groomed merged jet for further analysis.

For candidate merged jets obtained by the MDT procedure, we retain the ones which satisfy a jet mass window requirement around the vector boson mass, and sort them by their hardness in p_T.

Vector boson jet candidates are required to satisfy two additional substructure requirements. First, we require a selection based on the $D_2^{(\beta=1)}$ energy correlation function calculated from the groomed jet [156,157] which is useful for discriminating two-pronged structures from QCD jets, with W-jets tending to have smaller values and Z-jets larger values. The $D_2^{(\beta=1)}$ distribution for W-jets is p_T dependent, requiring a cut which also varies with p_T. The D_2 cut required for 50% efficiency of selecting a true W-jet is very close to linear for 250 GeV $< p_T <$ 1500 GeV [155],

motivating a cut:[13]

$$D_2 < 1 + (p_T - 250\ \text{GeV}) \times 7.7 \times 10^{-4}\ \text{GeV}^{-1}. \tag{4.40}$$

The second jet tagging requirement is a cut on the number of tracks in the W-jet, which is typically smaller than in QCD quark or gluon jets with $p_T \sim 1$ TeV. We therefore require

$$N_{\text{trk}} \leq 30, \tag{4.41}$$

where this is counted from the constituents of the ungroomed merged jet.

Finally, if the signal channel of interest accompanies N boosted W/Z gauge bosons in the final state, we take N hardest merged jets as our W/Z-induced jets.

4.4.2 Mass variables

In this section, we discuss several key mass variables which enable us to separate signal events from relevant background ones. We remark that some of our signal channels contain W or/and Z gauge bosons in the final state and they are either boosted or semi-invisible. In the semi-invisible cases, we are interested in the signal processes where only one W decays leptonically, and thus, we can reconstruct the neutrino momentum, hence the W momentum. If we regard each the massive SM gauge bosons as a single object along this line, every signal process in our study can be understood as a two-step cascade decay of a KK gauge boson into three visible

[13]This cut is derived from a rough linear fit to Fig. (8c) of Ref. [155]. While their analysis used different jet clustering and grooming techniques, the analysis presented here should not be strongly affected by modest changes to this cut.

particles via an on-shell intermediary state, radion:

$$A_{\rm KK} \to v_a \varphi \to v_a v_b v_c \,, \tag{4.42}$$

where $v_{a/b/c}$ denote the visible particles which will be either γ, g, or W/Z in our collider analyses. Since the mass spectra for our benchmark points listed in the preceding section suggest that massive electroweak gauge bosons are highly boosted, we assume that $v_{a/b/c}$ are (at least, effectively) massless for convenience of the subsequent argument.

We here and henceforth denote any reconstructed mass quantity by the uppercase M. Two invariant mass variables are readily available, which are reconstructed masses M_{bc} $(= \sqrt{(p_b + p_c)^2})$ and M_{abc} $(= \sqrt{(p_a + p_b + p_c)^2})$ which are supposed to be the same as m_φ and $m_{\rm KK}$, respectively. Assuming that the decay widths for $A_{\rm KK}$ and φ are negligible, we see that they are very powerful in suppressing relevant SM backgrounds. Another set of mass variables are M_{ab} $(= \sqrt{(p_a + p_b)^2})$ and M_{ac} $(= \sqrt{(p_a + p_c)^2})$. Without considerable spin correlation, their differential distributions develop the famous triangular shape spanning from 0 to the kinematic endpoint

$$M_{ab}^{\rm max} = M_{ac}^{\rm max} = \sqrt{m_{\rm KK}^2 - m_\varphi^2} \,. \tag{4.43}$$

However, both M_{ab} and M_{ac} provide useful handles orthogonal to M_{bc} and M_{abc} because energy-momentum conservation $p_{A_{\rm KK}} = p_a + p_b + p_c$ implies the following

sum rule:

$$M_{abc}^2 = M_{ab}^2 + M_{bc}^2 + M_{ac}^2 \,, \tag{4.44}$$

where we again assume massless visible particles in the equality. Indeed, M_{abc} and M_{bc} enforce us to select "signal-like" background events in terms of both the mass spectrum and the underlying event topology. So, one may argue that they are sufficient to reduce background events and we do not benefit from additional mass variables. It turns out that still the extra invariant mass variables are beneficial in the sense that they enable us to access the remaining difference between the signal and the background processes, which is encoded in the shapes of their distributions. This point will be explicitly demonstrated in the context of concrete signal channels in the next section.

Finally, it is noteworthy that we have implicitly assumed that the three visible particles v_a, v_b, and v_c are perfectly distinguishable although combinatorial ambiguity often arises in more realistic situations. Unfortunately, all signal channels of ours summarized in Table 4.3 face this issue, motivating us to devise appropriate prescriptions. Two types of combinatorial ambiguity are possible.

- Type I: v_b and v_c are indistinguishable while v_a is distinguishable from the others,
- Type II: v_a, v_b, and v_c all are indistinguishable.

The channel of three-gluon final state falls into Type II, while the others are cate-

gorized to Type I.

For Type I, there is no ambiguity in M_{bc} and M_{abc}, whereas some recipe is needed for M_{ab} and M_{ac}. Denoting indistinguishable v_b and v_c by j, we consider two sets of experimental observables.

$$\text{Set I.1:} \quad M_{aj_h},\ M_{aj_s} \tag{4.45}$$

$$\text{Set I.2:} \quad M_{aj(\text{high})} \equiv \max[M_{ab}, M_{ac}],\ M_{aj(\text{low})} \equiv \min[M_{ab}, M_{ac}] \tag{4.46}$$

In Set I.1, we first rank v_b and v_c by their p_T-hardness (i.e., $j_{h(s)}$ = the harder (softer) of the two) and form the respective invariant mass variables, while in Set I.2, we rank the two possible invariant masses by their magnitude [158–162]. Which one is superior to the other is beyond the scope of this thesis, and their usefulness can be discussed in the context of specific signal channels.

On the other hand, for Type II, all two-body invariant mass variables, M_{ab}, M_{bc}, and M_{ac}, are *not* experimental observables. Again denoting indistinguishable v_a, v_b, and v_c by j, we propose two possible prescriptions.

$$\text{Set II.1:} \quad M_{\tilde{a}j_h},\ M_{\tilde{a}j_s} \tag{4.47}$$

$$\text{Set II.2:} \quad M_{jj(\text{high})} \equiv \max[M_{ab}, M_{bc}, M_{ac}],\ M_{jj(\text{mid})} \equiv \text{med}[M_{ab}, M_{bc}, M_{ac}],$$
$$M_{jj(\text{low})} \equiv \min[M_{ab}, M_{bc}, M_{ac}] \tag{4.48}$$

For Set II.1, we guess v_a among the three particles by, for example, their p_T-hardness and repeat the same procedure as in Set I.1 with $\tilde{a}$ symbolizing the conjectured

v_a. In Set II.2, we rank all three invariant masses by their magnitude followed by constructing invariant mass distributions in the maximum, the median, and the minimum [162]. Again the discussion on their actual performance will be available in the context of concrete signal processes.

4.5 Results for LHC Signals

In this section, we study the LHC signals for the model discussed in Sec. 4.3. We focus on the production and dominant decay channels of the lightest KK particles corresponding to the SM gauge bosons, employing the representative benchmark points presented in Table 4.3. For each channel, we take two benchmark points, which correspond to two values of the radion mass: 1.0 TeV and 1.5 TeV. We present our results in the order of KK photon, KK gluon, and KK W/Z channels.

4.5.1 KK photon: photon + dijet

We begin by considering the production and decay of KK photons in our model. As discussed before, the final state particles in the *dominant* decay channel are a SM photon and two jets. We will find that indeed a small rate in this signal process limits the associated discovery potential. As the other decay modes do not have a large enough rate, we simply focus on the photon + dijet channel via two benchmark points γ-γgg-BP1 and γ-γgg-BP2, defined in Table 4.3. Given the final state particles, the dominant SM background is a single photon plus two QCD jets.

Before proceeding into the detailed analysis, we remark that it is useful to

impose parton-level "pre"-selection cuts to generate signal and background events in the appropriate region of phase space. These parton-level cuts are chosen such that there is always a final analysis cut, much stronger than the corresponding parton-level pre-selection cut. This allows us to remain conservative about the detector smearing effects. The robust features of our signal in this channel, which are useful to discriminate against the background, are a high transverse momentum for each of the two jets and the photon,[14] and a large invariant mass formed by the two jets. With these motivations, at the parton level, we apply $p_{T,j} > 150$ GeV for the two jets, $p_{T,\gamma} > 150$ GeV for the photon, and $M_{jj} > 500$ GeV for the jet pair. These cuts are presented in the cut flow Table 4.5. The effectiveness of these pre-selection cuts is reflected in their efficiency: the signal cross section reduces only marginally (65% and 58% for γ-γgg-BP1 and γ-γgg-BP2 data sets, respectively), while the γjj background gets reduced significantly (by 3.4×10^{-5}%).

After imposing these cuts, we streamline the parton-level signal and background events to Pythia and Delphes as per our general simulation scheme. As our simulation study is done at the detector level, we also consider three-jet events for which one of the jets is misidentified as an isolated photon. The ATLAS Collaboration has reported the photon fake rate to be around 10^{-4} [163]. A typical source is high-p_T neutral pions, which come from jets, decaying into two photons. We use Delphes with the default setup, which yields a similar fake rate. We find that most of the three-jet background can be removed by our choice of cuts, without affecting

[14] An alternative approach to reject background events would be to apply the cut on the photon energy. Since the photon comes from the decay of KK photon which is singly-produced at the leading order, in the photon energy distribution, events are likely to populate near the fixed energy value which would have been measured in the rest frame of the KK photon [164, 165].

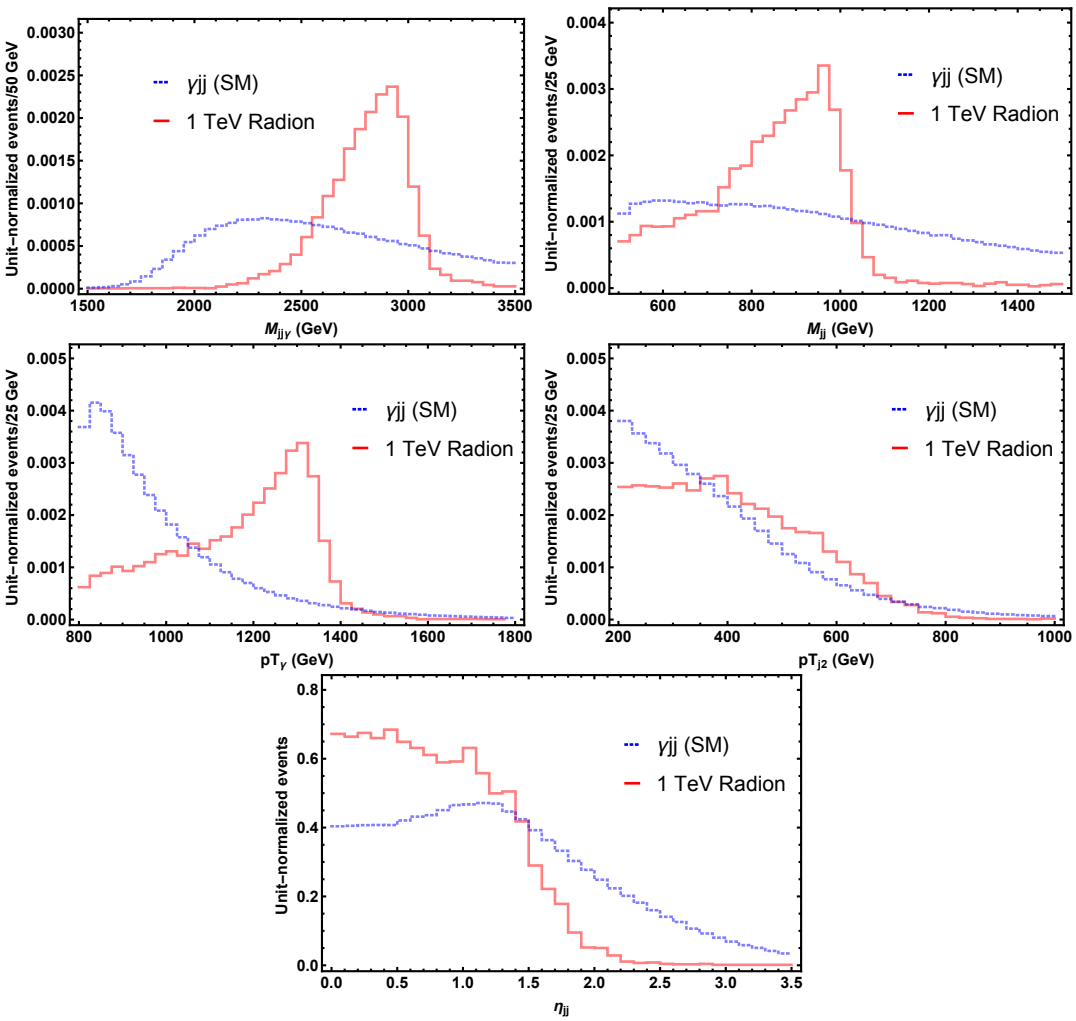

Figure 4.6: γ-γgg-BP1 benchmark point: Distributions of variables: $M_{jj\gamma}$ (top-left), M_{jj} (top-right), $p_{T,\gamma}$ (mid-left), p_{T,j_2} (mid-right) and η_{jj} (bottom) for signal (red solid) and background (blue dashed).

the final results significantly.

Defining N_γ and N_j as the number of photons and jets in the event, respectively, we only consider detector events with

$$N_\gamma \geq 1, \quad N_j \geq 2\,, \tag{4.49}$$

in order to focus on the relevant background events. As motivated earlier, the signal

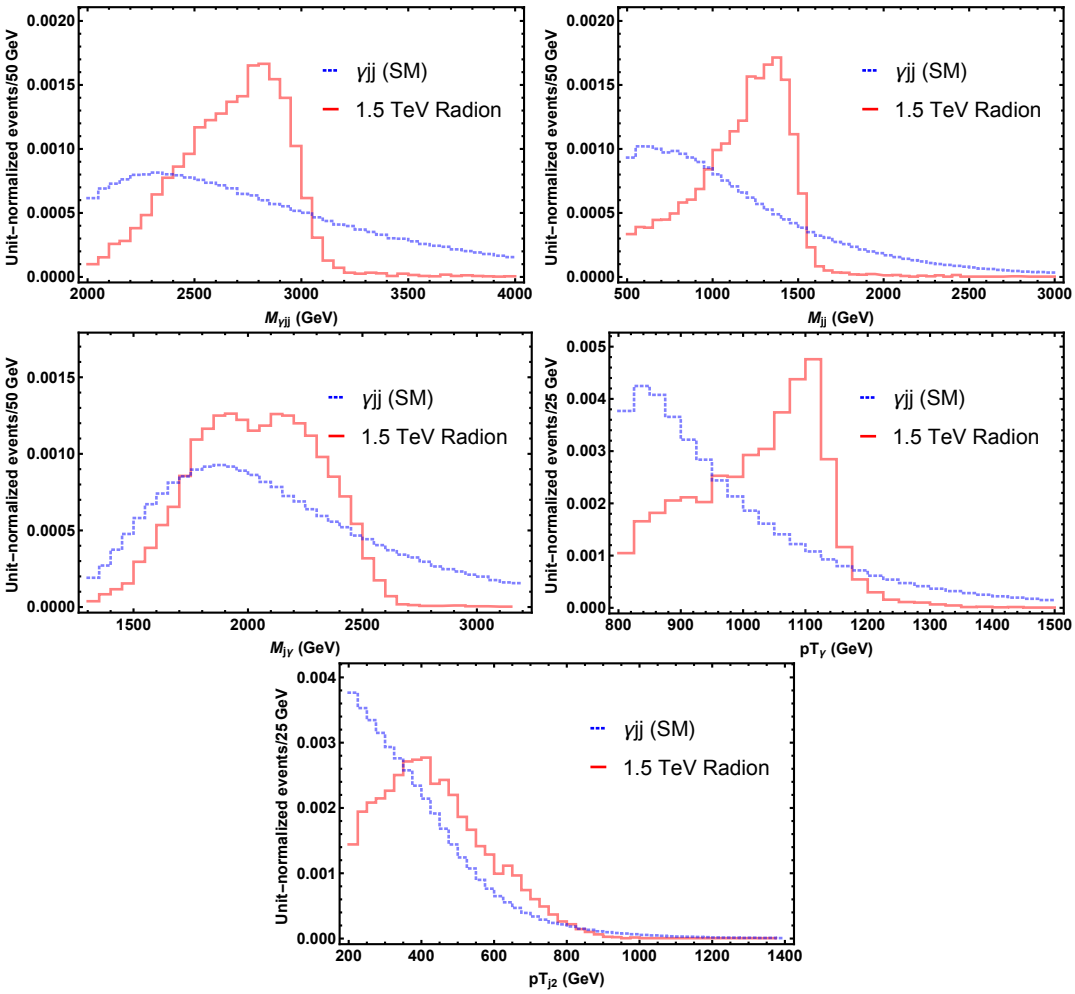

Figure 4.7: Distributions of variables for γ-γgg-BP2: $M_{jj\gamma}$ (top left), M_{jj} (top right), $M_{j\gamma}$ (mid left), $p_{T,\gamma}$ (mid right) and p_{T,j_2} (bottom) for signal (red) and background (blue).

events have *two* invariant mass variables that can be used to get rid of the background events. They essentially give rise to the masses of KK photon and radion, and we denote them by $M_{jj\gamma}$ and M_{jj}, respectively. In addition, the transverse momentum of the photon $p_{T\gamma}$ in the signal is very hard, allowing another independent way to suppress the background events. We also find that the transverse momentum of the second hardest jet, p_{T,j_2}, the absolute rapidity distance between the two hardest jets, η_{jj}, and the maximum of the invariant mass between a photon and the two energetic jets, $M_{j\gamma(\text{high})}(= \max[M_{j_1\gamma}, M_{j_2\gamma}])$ are further useful in reducing the background. In Figs. 4.6 (γ-γgg-BP1) and 4.7 (γ-γgg-BP2), we exhibit the unit-normalized distributions of signal and background events in the variables discussed so far. These events are after imposing the pre-selection cuts.

We then provide the final flow of signal and background events according to the cuts discussed so far in Table 4.5 in terms of their respective cross sections. From the cut flow, we observe that all the cuts are almost equally important to reduce the background. Defining our (statistical) significance as $S/\sqrt{B}$ with S and B being the number of signal and background events, respectively, we find that a moderate significance of 0.98σ (0.97σ) can be achieved for γ-γgg-BP1 (γ-γgg-BP2) at an integrated luminosity of 300 fb^{-1}. This small significance results primarily from a small rate for the signal as well as the presence of jets, which are smeared substantially, restricting the efficiencies of the invariant mass window cuts. Nevertheless, once we increase the statistics by a factor of 10, i.e., an integrated luminosity of 3000 fb^{-1}, we may achieve 3.10σ and 3.09σ for the two benchmark points.

Cuts	γ-γgg-BP1	γ-γgg-BP2	γjj
No cuts	0.20	0.29	(8.65×10^7)
$N_\gamma \geq 1, N_j \geq 2$, pre-selection cuts	0.10	0.13	18.56
$M_{jj\gamma} \in [2600, 3100]$ GeV	0.08	–	4.55
$M_{jj} \in [700, 1050]$ GeV	0.06	–	1.22
$p_{T,\gamma} \leq 1200$ GeV	0.03	–	0.28
$M_{jj\gamma} \in [2200, 3200]$ GeV	–	0.12	10.03
$M_{jj} \in [1000, 1600]$ GeV	–	0.10	4.55
$p_{T,\gamma} \in [950, 1200]$ GeV	–	0.07	1.66
$M_{j\gamma(\text{high})} \leq 2600$ GeV	–	0.07	1.54
S/B	0.10	0.05	–
$S/\sqrt{B}$ ($\mathcal{L} = 300$ fb^{-1})	0.98	0.97	–
$S/\sqrt{B}$ ($\mathcal{L} = 3000$ fb^{-1})	3.10	3.09	–

Table 4.5: Cut flows for signal and major background events in terms of their cross sections (in fb). The number in the parentheses for γjj is obtained with basic cuts ($p_{T,j} > 20$ GeV, $p_{T,\gamma} > 10$ GeV, $|\eta_j| < 5$, $|\eta_\gamma| < 2.5$, $\Delta R_{jj} > 0.4$, $\Delta R_{j\gamma} > 0.4$, $\Delta R_{\gamma\gamma} > 0.4$) at the generation level to avoid divergence. The pre-selection cuts ($p_{T,j} > 150$ GeV, $p_{T,\gamma} > 800$ GeV, $M_{jj} > 500$ GeV) are imposed at parton level to generate events in the relevant phase space, and are reimposed at the detector level.

4.5.2 KK gluon

We next consider the production and decay of KK gluons in our model. Due to a higher production cross section, there are multiple decay channels here that become relevant phenomenologically: the trijet, jet + diphoton, and jet + diboson (W/Z) decay modes. In all three, one regular jet comes from the decay of the KK gluon. The different radion decay modes give rise to the other two objects in the final state. Since the hierarchy in radion decay modes are dictated largely by the hierarchy in SM gauge couplings and multiplicity factors, the decay modes of the radion, in decreasing order of magnitude, are to jj, W/Z, and $\gamma\gamma$ final states.

For the case of radion decay to W/Z, there are multiple final states to consider.

Since $\mathrm{BR}(\varphi \to ZZ) \propto g_{Z_{\mathrm{KK}}}^{-4}$ as in eq. (4.17) and $g_{Z_{\mathrm{KK}}} = g_{W_{\mathrm{KK}}}/\sqrt{1 - g_{W_{\mathrm{KK}}}^2/g_{\gamma_{\mathrm{KK}}}^2}$ is necessarily larger than $g_{W_{\mathrm{KK}}}$, the ZZ mode is heavily suppressed compared to the WW mode. We therefore focus on the WWj channel. There are three final states of potential interest: fully hadronic JJj (where J denotes a hadronic merged jet coming from a boosted W), semileptonic $\ell\nu Jj$, and fully leptonic $\ell\nu\ell\nu j$. The fully leptonic final state is the cleanest, but has the smallest branching ratio. Moreover, it contains *two in*visible neutrinos manifesting themselves as a missing transverse energy, so it is impossible to reconstruct the radion resonance mass which is one of the crucial handles to suppress relevant background events.[15] The fully hadronic and semi-leptonic channels have similar branching fractions, and in existing LHC searches for simple diboson resonances have comparable sensitivity in this mass range [169]. We focus on the fully hadronic channel which allows a rather sharp feature in the reconstructed radion mass, which we shall demonstrate shortly.

It is worth noting that existing diboson resonance searches might eventually be sensitive to the diboson decay of the radion, however this is sensitive to the details of the experimental analysis. For example, the existing ATLAS diboson searches (e.g. [169]) will tend to reject events in which a diboson resonance is produced in association with a hard gluon-jet. This is because their analyses select only the hardest one or two fat jets as potential V-jet candidates in semi-leptonic and fully hadornic searches. In the benchmark scenarios considered in this chapter, the gluon jet produced directly in the decay of the KK gluon will typically be selected, and,

[15] One could instead try transverse mass variables (e.g., M_T, M_{T2} [166] or their variants) or even (3+1)-dimensional variables (e.g., M_2 [167,168]), but we do not pursue our study in this direction.

failing the V-tagging criteria, will be cause the event to be rejected from the analysis. CMS searches (e.g. [170]) however apply their V-tagging criteria *before* selecting the hardest V-jet candidates, which means that a hard QCD jet produced in association with the diboson resonance will not typically cause the event to be rejected. CMS diboson searches will therefore have some sensitivity to diboson resonances produced in a cascade decay of this kind, but will inevitably be less sensitive than a dedicated search which makes use of additional event characteristics.

4.5.2.1 Decay to trijet

We consider two benchmark points g-ggg-BP1 and g-ggg-BP2, and their model parameters are summarized in Table 4.3. Obviously, the dominant SM background comes from the three-jet QCD process. Again we need to consider pre-selection cuts to generate signal and background events in the relevant part of phase space. Our choice of mass spectra enforces the three jets to come with high transverse momenta and the three two-jet invariant masses to be large. We use these signal features, which are distinctive from typical background events, to establish the pre-selection cuts. With these motivations, at the parton level, we choose $p_{T,j} > 150$ GeV for the three jets and $M_{jj} > 500$ GeV for the three combinations of jet pairing. Their effectiveness is reflected in the efficiency: the signal cross section is reduced only marginally (88% and 92% for g-ggg-BP1 and g-ggg-BP2 benchmark points, respectively), whereas the three-jet QCD background is significantly suppressed by 5.5×10^{-3}%.

After generating parton-level signal and background events along with the pre-selection cuts, we feed them to PYTHIA and DELPHES as before. As the signal process of interest accompanies three jets in the final state, we select the events having

$$N_j \geq 3\,. \tag{4.50}$$

As discussed earlier, mass variables are useful in discriminating the signal events from the background ones. Let us first denote the three hardest jets (in decreasing order of p_T) as j_1, j_2, and j_3.

We emphasize here that depending on the benchmark points, different invariant mass combinations carry different potential in distinguishing the signal from the background. For example, in the case with radion mass of 1 TeV, the hardest jet in p_T mostly comes from the direct decay of the KK gluon because the mass gap between the radion and the KK gluon is quite large. As a result, $M_{j_2 j_3}$ has an invariant mass peak feature, corresponding to m_φ. On the contrary, the situation becomes completely reversed in the case of radion mass of 1.5 TeV. We find that $M_{j_1 j_3}$ and $M_{j_1 j_2}$ (partially) develop a resonance-like feature in their distributions because j_1 is mostly from the decay of the radion while the jet from the KK gluon decay can be either j_2 or j_3 event-by-event.

Therefore, $M_{j_2 j_3}$ shows quite a broad distribution. On top of these mass variables, the transverse momenta of the three jets are also useful in signal identification. In addition, the total invariant mass formed by all the visible particles, which we

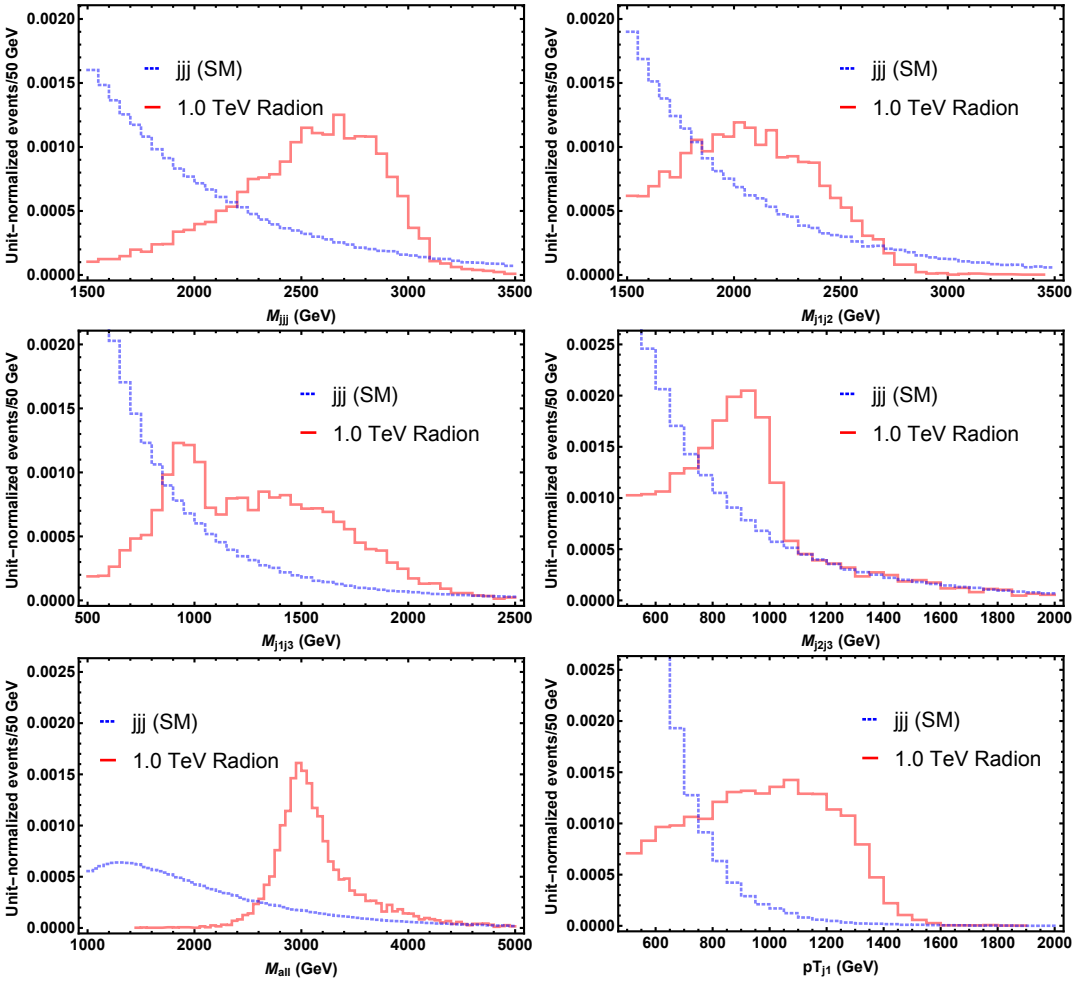

Figure 4.8: *g-ggg*-BP1 benchmark point: Distributions of variables: M_{jjj} (upper-left), $M_{j_1j_2}$ (upper-right), $M_{j_1j_3}$ (middle-left), $M_{j_2j_3}$ (middle-right), M_{all} (lower-left), p_{T,j_1} (lower-right) for signal (red solid histograms) and background (blue dashed histograms).

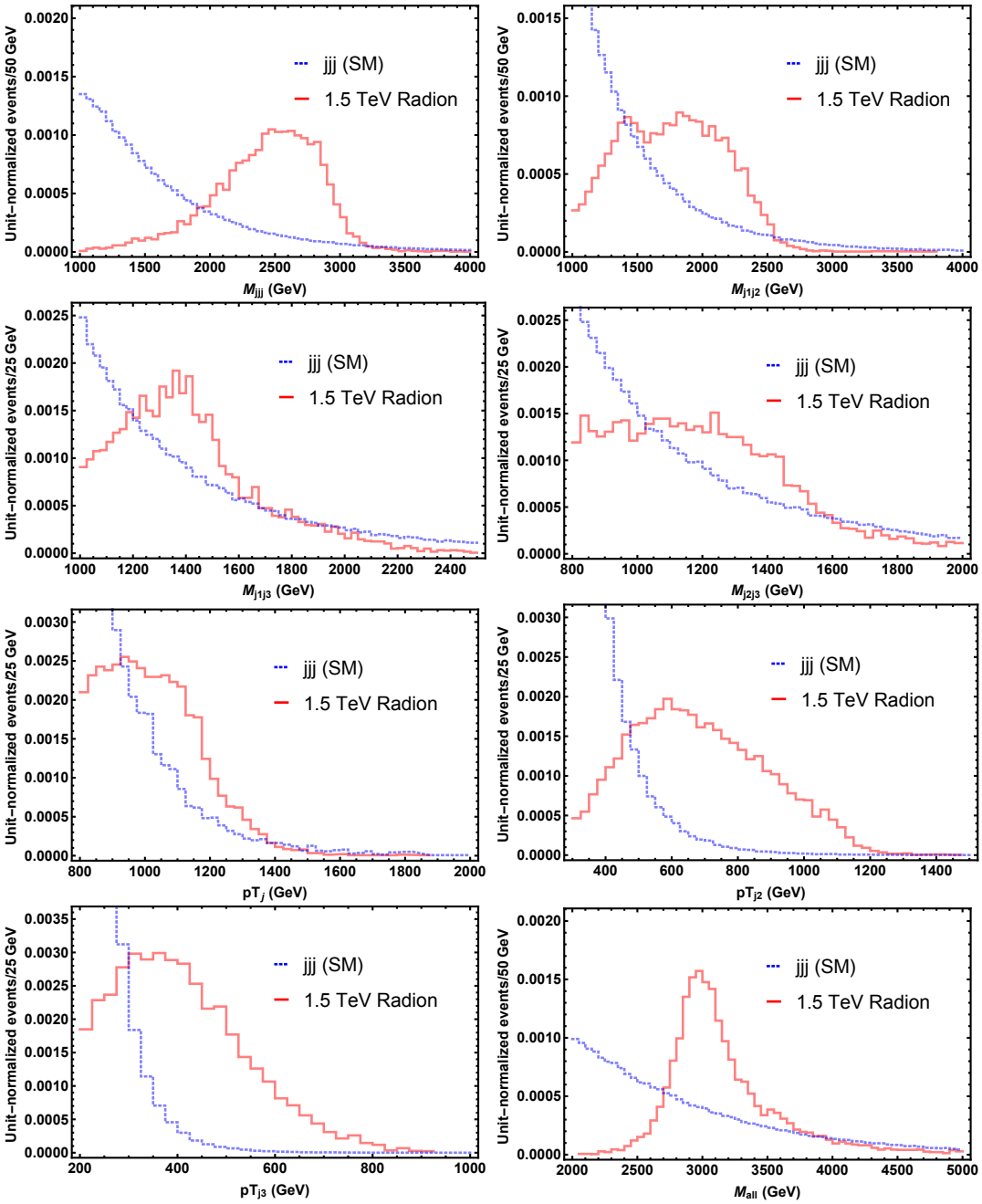

Figure 4.9: *g-ggg*-BP2 benchmark point: Distributions of variables: M_{jjj} (top-left), $M_{j_1j_2}$ (top-right), $M_{j_1j_3}$ (second row left), $M_{j_2j_3}$ (second row right), p_{T,j_1} (third row left), p_{T,j_2} (third row right), p_{T,j_3} (bottom-left) and M_{all} (bottom-right) (red solid histograms) and background (blue dashed histograms).

denote as M_{all}, also turns out to be beneficial in distinguishing the signal from the background. We show the unit-normalized distributions of signal and background events in the variables discussed thus far in Figs. 4.8 (g-ggg-BP1) and 4.9 (g-ggg-BP1), from which we develop our intuition for choosing a set of cuts for each benchmark point. These events are after imposing the pre-selection cuts.

As before, we provide our cut flow results for signal and background events in Table 4.6. Our data analysis suggests that we may achieve higher statistical significances of 3.49σ and 5.25σ for g-ggg-BP1 and g-ggg-BP2 benchmark points respectively, even at an integrated luminosity of 300 fb^{-1}. Definitely, the numbers here are greater than those for the KK photon in the previous section. This is expected mainly due to an increased rate for the signal (i.e., QCD coupling vs. QED coupling in the KK photon case), even though the three-jet background renders signal isolation challenging (compared to the 2 jets + photon background).

4.5.2.2 Decay to jet and diphoton

We next move our focus onto the jet + diphoton decay mode of the KK gluon, where the two photons come from the radion decay. As usual, we consider two representative benchmark points denoted by g-$g\gamma\gamma$-BP1 and g-$g\gamma\gamma$-BP2 (see Table 4.3 for model parameters).The dominant SM background for this decay mode comes from the $j\gamma\gamma$ process. However, it becomes important to take the effect of jet-faking photons at the detector level. To this end, we simulate the $jj\gamma$ process as well, and impose the same set of cuts to estimate its contribution to the total

Cuts	g-ggg-BP1	g-ggg-BP2	jjj
No cuts	29.33	46.60	(7.7×10^7)
$N_j \geq 3$ with pre-selection cuts	23.23	40.05	1.9×10^6
$M_{jjj} \in [2500, 3100]$ GeV	12.20	–	7.9×10^4
$M_{j_1 j_2} \in [1700, 2900]$ GeV	11.12	–	3.9×10^4
$M_{j_1 j_3} \in [850, 2100]$ GeV	9.96	–	1.9×10^4
$M_{j_2 j_3} \in [800, 1050]$ GeV	5.12	–	2015.28
$p_{T,j_1} \geq 1100$ GeV	2.73	–	266.41
$M_{all} \leq 3300$ GeV	1.98	–	94.53
$M_{jjj} \in [2400, 3100]$ GeV	–	22.31	1.0×10^5
$M_{j_1 j_2} \in [1300, 2400]$ GeV	–	19.57	4.8×10^4
$M_{j_1 j_3} \in [1100, 1700]$ GeV	–	13.82	1.0×10^4
$M_{j_2 j_3} \in [900, 1550]$ GeV	–	8.81	1564
$p_{T,j_1} \geq 900$ GeV	–	6.79	807.83
$p_{T,j_2} \geq 600$ GeV	–	6.20	644.54
$p_{T,j_3} \geq 300$ GeV	–	5.44	464.07
$M_{all} \in [2800, 3300]$ GeV	–	3.43	124.61
S/B	0.02	0.03	–
$S/\sqrt{B}$ ($\mathcal{L} = 300$ fb^{-1})	3.49	5.25	–
$S/\sqrt{B}$ ($\mathcal{L} = 3000$ fb^{-1})	11.03	16.60	–

Table 4.6: Cut flows for signal and major background events in terms of their cross sections (in fb). The number in the parentheses for jjj is obtained with basic cuts ($p_{T,j} > 20$ GeV, $p_{T,\gamma} > 10$ GeV, $|\eta_j| < 5$, $|\eta_\gamma| < 2.5$, $\Delta R_{jj} > 0.4$, $\Delta R_{j\gamma} > 0.4$, $\Delta R_{\gamma\gamma} > 0.4$) at the generation level to avoid divergence. The pre-selection cuts ($p_{T,j} > 150$ GeV, $M_{jj} > 300$ GeV) are imposed at the parton level as well to generate events in the relevant phase space, and are reimposed at the detector level.

background.[16] We once again need to employ pre-selection cuts to generate signal and background events in the relevant part of the phase-space. Motivated by our considerations earlier, we impose selections on the transverse momenta of the final objects. We require $p_T > 200$ GeV for the jet and $p_T > 200$ GeV for the photons at the parton level. We also impose a selection on the invariant mass of the two photons at parton level, requiring $M_{\gamma\gamma} > 750$ GeV. The values of these variables tend to

[16] We expect that the contribution from three-jet QCD events are small enough to be neglected, considering that two jets are simultaneously misidentified as photons, in combination with the set of selection cuts that we apply.

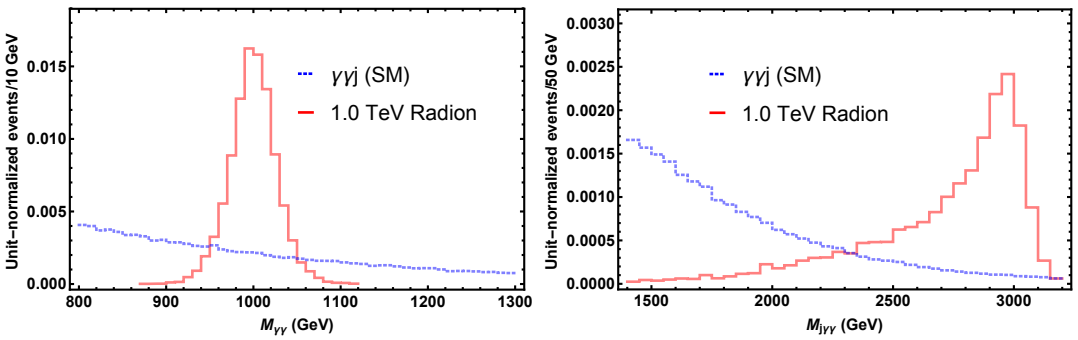

Figure 4.10: g-$g\gamma\gamma$-BP1 benchmark point: Distributions of variables: $M_{\gamma\gamma}$ (left) and $M_{j\gamma\gamma}$ (right) for signal (red solid histograms) and background (blue dashed histograms).

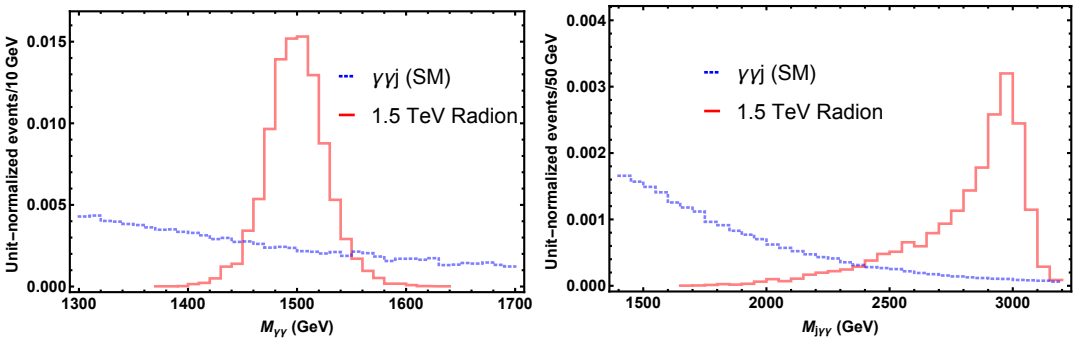

Figure 4.11: Distributions of variables for g-$g\gamma\gamma$-BP2 benchmark point: $M_{\gamma\gamma}$ (left) and $M_{j\gamma\gamma}$ (right) for signal (blue) and background (blue).

be much higher for the signal events than those for the background ones, allowing a clean way to generate relevant events. Again, their effectiveness is reflected in the efficiency: the signal cross section is reduced only marginally (78.2% and 87.8% for γ-γgg-BP1 and γ-γgg-BP2 benchmark points, respectively), while the jet + diphoton background is significantly suppressed by 1.8×10^{-3}%.

The parton-level signal and background events generated with the pre-selection cuts are fed into a sequence of PYTHIA and DELPHES. As mentioned before, we perform background simulation with $j\gamma\gamma$ and $jj\gamma$ processes. We find that the two background contribute to the total background at an equal level. As a parton-level

signal event contains two photons and a single jet, we restrict ourselves to the phase space involving

$$N_\gamma \geq 2, \;\; N_j \geq 1\,. \tag{4.51}$$

The unsmeared nature of the two photons in the final state makes clean signal identification possible. This is clearly supported by a sharp peak in the diphoton invariant mass distribution (see the left panels in Figs. 4.10 and 4.11). The other (resonant) invariant mass variable $M_{j\gamma\gamma}$ is broadened primarily due to the jet involved, but still provides a strong handle to distinguish the signal events from the background ones (see the right panels in Figs. 4.10 and 4.11).

Finally, the cut flow for this channel is presented in Table 4.5.2.3. Since it turns out that the data is essentially signal dominated, we conservatively adopt $S/\sqrt{S+B}$ as our figure of merit to estimate the statistical significance. We find a statistical significances of 4.3σ (5.4σ) for g-$g\gamma\gamma$-BP1 (g-$g\gamma\gamma$-BP2) benchmark point, even at an integrated luminosity of 300 fb^{-1}. This suggests that this could serve as the first discovery channel of gauge KK particles over the other ones in our study.

4.5.2.3 jet + diboson (W/Z-jets)

The fully hadronic analysis for WWj proceeds by requiring two merged jets consistent with coming from boosted W's and reconstructing the radion mass, and an additional gluon-induced jet which, combined with the reconstructed radion,

Cuts	g-$g\gamma\gamma$-BP1	g-$g\gamma\gamma$-BP2	$j\gamma\gamma$	$jj\gamma$
No cuts	0.17	0.19	(1.07×10^5)	(8.7×10^7)
$N_{j(\gamma)} \geq 1\,(2)$ with pre-selection cuts	0.10	0.13	1.35	1.60
$M_{\gamma\gamma} \in [950, 1350]$ GeV	0.10	–	0.2	0.13
$M_{j\gamma\gamma} \in [2100, 3200]$ GeV	0.09	–	0.02	0.02
$M_{\gamma\gamma} \in [1450, 1550]$ GeV	–	0.12	0.04	0.04
$M_{j\gamma\gamma} \in [2500, 3150]$ GeV	–	0.11	0.005	0.006
$S/\sum B$	2.25	10.0	–	–
$S/\sqrt{S+\sum B}$ ($\mathcal{L} = 300$ fb^{-1})	4.3	5.4	–	–
$S/\sqrt{S+\sum B}$ ($\mathcal{L} = 3000$ fb^{-1})	13.6	17.1	–	–

Table 4.7: Cut flows for signal and major background events in terms of their cross sections (in fb). The numbers in the parentheses for $j\gamma\gamma$ and $jj\gamma$ are obtained with basic cuts ($p_{T,j} > 20$ GeV, $p_{T,\gamma} > 10$ GeV, $|\eta_j| < 5$, $|\eta_\gamma| < 2.5$, $\Delta R_{jj} > 0.4$, $\Delta R_{j\gamma} > 0.4$, $\Delta R_{\gamma\gamma} > 0.4$) at the generation level to avoid divergence. The pre-selection cuts ($p_{T,j} > 200$ GeV, $p_{T,\gamma} > 200$ GeV, $M_{\gamma\gamma} > 750$ GeV) are imposed at the parton level to generate events in the relevant phase space, and are reimposed at the detector level.

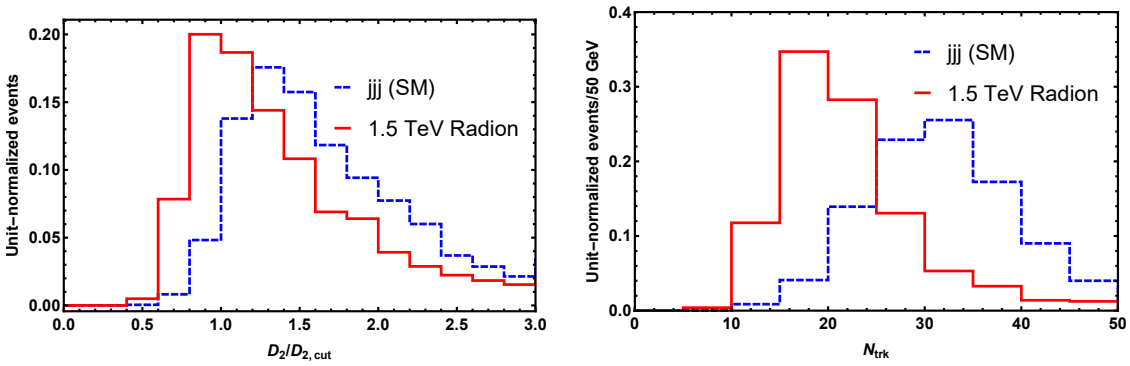

Figure 4.12: Distributions in N_{trk} (left) and D_2 (right) for signal (solid histograms) and background (dashed histograms) for radion mass of 1.5 TeV.

reproduces a KK gluon mass peak. The dominant background is SM jjj production, with two jets being mistagged as vector-boson jets.

The W-jets are selected according to the criteria described in Sec. 4.4, with a mass window requirement

$$65 \text{ GeV} < M_W < 100 \text{ GeV} . \tag{4.52}$$

Here we capitalize the mass symbol to distinguish it from the corresponding input mass. A second jet collection is made using the anti-k_t algorithm with radius parameter $R = 0.4$. Jets are kept if they have $|\eta| < 3$, are separated from W-candidates by $\Delta R > 0.8$, and both pairings of this jet with a W-candidate has invariant mass $M_{Jj} > 400$ GeV. The hardest remaining jet is the g-candidate.

Three-jet background events for the detector level analysis are simulated with the following parton level cuts: $p_{T,j} > 450$ GeV on the leading jet, $p_{T,j} > 250$ GeV on the remaining jets, $\Delta R_{jj} > 0.5$ between all jets, $M_{jj} > 250$ GeV between all jets. We additionally require a strong cut $M_{jjj} > 2000$ GeV in order to generate

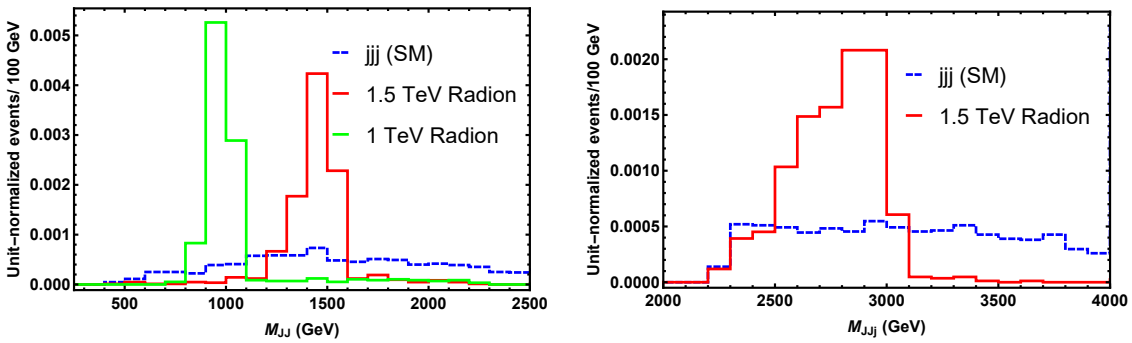

Figure 4.13: Distributions in M_{JJ} (left) and M_{JJj} (right) for signal (solid histograms) and background (dashed histograms).

a sufficiently large sample of events in the signal region. In contrast, signal WWj events are simulated with no parton-level cuts as before. In order to be consistent with the parton-level cuts applied to the background, events are retained for further analysis if they satisfy the following requirements:

$$p_{T,J_1} > 600 \text{ GeV}, \tag{4.53}$$

$$p_{T,J_2} > 300 \text{ GeV}, \tag{4.54}$$

$$p_{T,j} > 600 \text{ GeV}, \tag{4.55}$$

$$M_{JJj} > 2250 \text{ GeV}, \tag{4.56}$$

where J_1 and J_2 are the leading and the subleading merged jets. As discussed earlier, D_2 and N_{trk} are also useful in isolating signal from background.

In order to illustrate the discriminating power of the W-jet tagging observables used in this analysis, we present in Fig. 4.12 the distributions of D_2 and N_{trk} in selected events in event samples where the cuts on these distributions have not been applied.

Cuts	g-gVV-BP1	g-gVV–BP2	jjj
No cuts	1.6	2.6	(7.7×10^7)
Basic Cuts (with no V-tagging)	0.59	1.4	1.3×10^4
65 GeV $< M_J <$ 100 GeV	0.29	0.68	990
D_2 cut	7.5×10^{-2}	0.19	54
$N_{\rm trk} < 30$	6.0×10^{-2}	0.16	28
$p_{T,j} > 600$ GeV, $p_{T,J_1} > 600$ GeV	4.6×10^{-2}	0.11	9.4
$M_{JJj} \in [2500, 3100]$	3.8×10^{-2}	9.7×10^{-2}	4.8
$M_{JJ} \in [900, 1050]$ GeV	3.1×10^{-2}	–	0.17
$M_{JJ} \in [1350, 1600]$ GeV	–	7.8×10^{-2}	0.56
S/B	0.18	0.14	–
$S/\sqrt{B}$ ($\mathcal{L} = 300$ fb^{-1})	1.3	1.8	–
$S/\sqrt{B}$ ($\mathcal{L} = 3000$ fb^{-1})	4.0	5.7	–

Table 4.8: Cut flows for signal and major background events in terms their cross sections. The cross sections are in fb. The number in the parentheses for jjj is obtained with basic cuts ($p_{T,j} > 20$ GeV, $p_{T,\gamma} > 10$ GeV, $|\eta_j| < 5$, $|\eta_\gamma| < 2.5$, $\Delta R_{jj} > 0.4$, $\Delta R_{j\gamma} > 0.4$, $\Delta R_{\gamma\gamma} > 0.4$) at the generation level to avoid divergence. In the second row, the same basic cuts are imposed to both signal and background events.

In the left panel of Fig. 4.13, we see that the diboson pairs reproduce a sharp invariant mass peak at around the input radion mass. This radion peak is sharper than that for the $g_{\rm KK} \to jjj$ final state because in the latter case final state radiation from the gluons depletes them of energy, broadening the invariant mass peak. This effect is largely absent for the color-neutral W-jets. On the other hand, the JJj invariant mass is partially smeared due to final state radiation from the gluon. After isolating the two mass peaks, we find that 5σ discovery is possible with an integrated luminosity of 3000 fb^{-1} for radion mass of 1.5 TeV (see also the cut flow in Table 4.8).

4.5.3 KK W/Z: leptonic W + dijet

We finally consider the production of KK W/Z gauge bosons and collider signatures from their decays. They are also featured by a decent production cross section, so that a few channels deserve to be investigated. To secure enough statistics at the 14 TeV LHC, we lay our focus on the processes in which the radion decays into a gluon pair. The remaining SM particle in the final state is either W or Z gauge boson from the decay of the corresponding KK particle. Obviously, the hadronic channels come with higher cross sections than the leptonic ones. As mentioned earlier, hadronic gauge bosons appear as "single" boosted merged jets, the dominant SM background is the three-jet QCD process. Even if the tagging of merged jets (by the procedure described in Sec. 4.4) suppress the background, its huge production cross section overwhelms the signal cross section even with posterior cuts, which are also confirmed by our simulation study. We therefore focus on the final state involving a leptonic W and two jets in the rest of this section.[17]

The signal process of interest, mass spectra, and model parameter values are summarized in Table 4.3. As obvious from the signal process, the resulting final state contains two hard jets and an isolated lepton $\ell(= e, \mu)$ at the leading order. Defining N_ℓ and N_j as the number of isolated leptons and *non-b*-tagged jets, respectively, we

[17] We do not consider the channel with a leptonic Z since its associated cross section is too small to obtain enough statistics.

restrict ourselves to the events satisfying

$$N_\ell = 1 \text{ with } |\eta_\ell| < 2.5, \tag{4.57}$$

$$N_j \geq 2 \text{ with } |\eta_j| < 4. \tag{4.58}$$

It is clear that in our benchmark choices signal lepton and jets are rather hard, motivating us to further impose the following selection cuts for the lepton and the two hardest jets:

$$p_{T,\ell} > 150 \text{ GeV}, \tag{4.59}$$

$$p_{T,j_{h(s)}} > 400\,(200) \text{ GeV}, \; |\eta_{j_{h/s}}| < 2.5\,, \tag{4.60}$$

where $h(s)$ stands for the harder (softer) jet out of the two hardest jets as before. The existence of an invisible neutrino yields a large missing transverse momentum $\not{E}_T$ which is the opposite of the vectorial p_T sum of reconstructed objects in the event, comprised of the jets with p_T defined in (4.58). Since there is no other invisible particle, the unknown neutrino z-momentum can be reconstructed by requiring W mass shell condition up to two-fold ambiguity. For the detector-level events, we scan the W mass from 60 GeV to 100 GeV by an interval of 2 GeV and choose the solution whose input W mass is closest to the nominal W mass 80 GeV. Interestingly enough, we observe that both solutions yield the same values in relevant invariant mass variables, so we do not encounter two-fold ambiguity as long as invariant mass quantities are concerned. We later denote w as the resulting reconstructed W for

notational brevity.

Given the collider signature, the dominant SM background is irreducible Wjj, and jjj and $t\bar{t}$ could be potentially comparable. For the pure QCD background, a three-jet event would appear as a background one if one of three jets is misidentified as a lepton and mis-measurement of jets gives rise to a sizable missing transverse momentum. Although the associated process is featured by a huge production cross section, we anticipate that the tiny lepton-fake rate can significantly suppress this background. To ensure further reduction, we impose a rather hard missing transverse momentum cut which is expected to reject events whose $\not{E}_T$ is purely instrumental. In our analysis, we choose

$$\not{E}_T > 200\text{GeV}. \tag{4.61}$$

In addition, we require each jet to sufficiently distant in the azimuthal angle ϕ from the direction defined by the missing transverse momentum $\vec{\not{P}}_T$. This enables us to select the events in which the measured $\not{E}_T$ does not arise from mismeasured jets. For our study, we evaluate $\Delta\phi$ for the first two hardest jets and demand the same cut, following Ref. [152] which studied a similar signature:

$$\Delta\phi(\vec{\not{P}}_T, j_{h(s)}) > 2.0\,(0.8)\,. \tag{4.62}$$

We therefore expect that the three-jet background is well under control and negligible compared to the irreducible background. It turns out that our simulation study

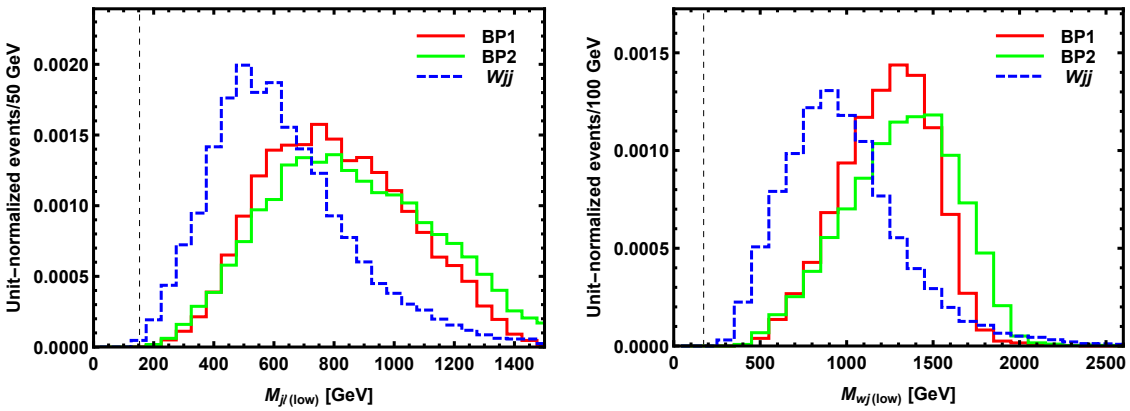

Figure 4.14: $M_{j\ell(\mathrm{low})}$ (left panel) and $M_{wj(\mathrm{low})}$ distributions (right panel) for W-Wgg-BP1 (red solid histogram), W-Wgg-BP2 (green solid histogram) and Wjj (blue dashed histogram) with events passing the selection criteria listed in-between (4.57) and (4.62) and the W reconstruction procedure. The black dashed lines mark $M_{bl}^{\max}$ value in the top quark decay and the top quark mass, respectively.

also supports this expectation. To the best of our knowledge, none of experimental papers have explicitly reported the rate for the lepton-faking jets. We assess it by comparing the relevant cross section reported in Ref. [171] and our simulated event sample, and find that the rate is of order 10^{-4}. Implementing the fake-object module into DELPHES, we generate three-jet events which are significantly reduced to be negligible by a set of our selection cuts.

On the other hand, getting a background event from the $t\bar{t}$ process depends on its decay mode. Due to the existence of an isolated lepton in the final state, dileptonic and semileptonic channels are relevant.

$$\text{Dileptonic:} \qquad t_1\bar{t}_2 \to b_1\ell_1^+\bar{b}_2\ell_2^- + \nu\bar{\nu} \tag{4.63}$$

$$\text{Semileptonic:} \qquad t_1\bar{t}_2 \to b_1\ell_1^+\bar{b}_2 q_2\bar{q}_2 + \nu \tag{4.64}$$

Here we assign the same number to all visible particles belonging to the same decay

leg just for convenience of the later argument. For the fully leptonic $t\bar{t}$ in (4.63), an event appear as a background with one of the two leptons (say, ℓ_2) missed or unaccepted. In contrast, any semi-leptonic $t\bar{t}$ events can be recorded as background events since we require $N_j \geq 2$.

Obviously, we can achieve an $\mathcal{O}(1)$ suppression of the background events stemming from $t\bar{t}$, vetoing the events with at least one b-tagged jet. However, this is not enough to make $t\bar{t}$ negligible due to its large production cross section. It turns out that $t\bar{t}$ background is subdominant, compared to Wjj [153, 154]. We note that the cuts in Refs. [153, 154] are softer than the corresponding ones in our analysis, so that $t\bar{t}$ would come back as a comparable background in the phase space resulting from the set of cuts that we require. Indeed, we find that various invariant mass variables play crucial roles in reducing the $t\bar{t}$ background as well. Considering first the dileptonic $t\bar{t}$ in (4.63) in which ℓ_2 is not recorded, we find that the following criteria available:

D-1. Since b_1-ℓ_1 invariant mass $M_{b_1\ell_1}$ is bounded by $M_{b_1\ell_1}^{\rm max}$ (= 153 GeV), for any dileptonic $t\bar{t}$ events $M_{j\ell({\rm low})} \equiv \min[M_{j_h\ell}, M_{j_s\ell}]$ should be smaller than $M_{b\ell}^{\rm max}$. The left panel in Fig. 4.14 exhibits $M_{j\ell({\rm low})}$ distributions for W-Wgg-BP1 (red solid histogram), W-Wgg-BP2 (green solid histogram) and Wjj (dashed blue histogram) at the detector level with events passing the cuts from (4.57) through (4.62) and the W reconstruction procedure described earlier. The black dashed line marks the position of $M_{b\ell}^{\rm max}$, from which we observe that more than 99.9% of signal events have a $M_{j\ell({\rm low})}$ value exceeding $M_{b\ell}^{\rm max}$.

D-2. Since the invisible momentum comes from a neutrino and a missing W, we often fail in reconstructing W with ℓ_1.

When it comes to semileptonic $t\bar{t}$, two cases are possible:

S-1. If one of the two hardest jets and ℓ_1 belong to the same decay side (e.g., $\ell_1 b_1 \bar{b}_2$, $\ell_1 b_1 q_2$, or $\ell_1 b_1 \bar{q}_2$), the invariant mass between b_1 and the reconstructed W should be the same as the top quark mass. Therefore, $M_{wj(\mathrm{low})} \equiv \min[M_{wj_h}, M_{wj_s}]$ does not exceed the top quark mass. The right panel in Fig. 4.14 shows $M_{wj(\mathrm{low})}$ distributions for W-Wgg-BP1 (red solid histogram), W-Wgg-BP2 (green solid histogram) and Wjj (blue dashed histogram) at the detector level with events satisfying the same criteria described in D-1. The black dashed line represent the location of the top quark mass. We observe that every single signal event has a $M_{wj(\mathrm{low})}$ value greater than 300 GeV.

S-2. If the two hardest jets belong to the second decay side (e.g., $\ell_1 \bar{b}_2 q_2$, $\ell_1 \bar{b}_2 \bar{q}_2$, or $\ell_1 q_2 \bar{q}_2$), the dijet invariant mass should be either the same as the W mass or smaller than $M_{bq}^{\max}$ (= 153 GeV). Since the dijet invariant mass window cut to be used later is much larger than those values, we do not expect any background contribution from this case.

From all these considerations thus far, we expect that $t\bar{t}$ is negligible as well, so we henceforth consider Wjj as the main background to signal events.

In this channel, invariant mass window cuts defined by the masses of KK W and radion are useful in separating signal events from background ones. The corresponding variables are M_{wjj} and M_{jj}. In addition, since the signal process

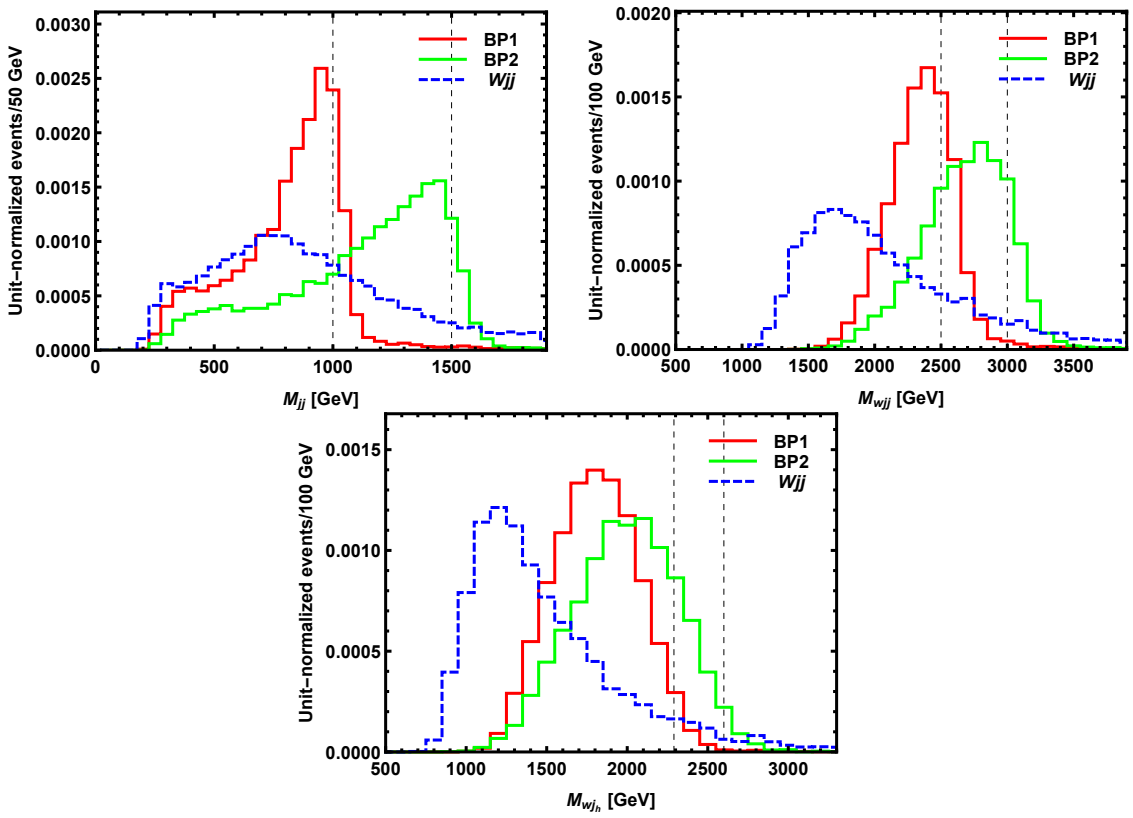

Figure 4.15: M_{jj} (upper left panel), M_{wjj} (upper right panel), and M_{wj_h} (bottom panel) distributions for W-Wgg-BP1 (red solid histogram), W-Wgg-BP2 (green solid histogram) and Wjj (blue dashed histogram) with events passing the selection criteria listed in-between (4.57) and (4.62) and the W reconstruction procedure. The black dashed lines mark the input radion mass, the input KK W mass, and the theoretical $M_{wj}^{\max}$ value, respectively.

Cuts	W-Wgg-BP1	W-Wgg-BP2	Wjj
No cuts	0.740	0.506	(43,600)
$N_\ell = 1$, $N_j \geq 2$ with basic cuts	0.478	0.339	14,500
$\not{E}_T > 200$ GeV	0.385	0.253	1,840
$p_{T,\ell} > 150$ GeV, $\lvert\eta_\ell\rvert < 2.5$	0.263	0.178	275
$p_{T,j_{h(s)}} > 400\,(200)$ GeV, $\lvert\eta_j\rvert < 2.5$	0.169	0.151	67.5
$\Delta\phi(\not{E}_T, j_{h(s)}) > 2.0\,(0.8)$	0.159	0.125	52.0
$M_w \in [60,\ 100]$ GeV	0.159	0.125	51.9
$M_{wj_s} > 300$ GeV	–	0.125	51.8
$M_{jj} \in [1150,\ 1550]$ GeV	–	0.0632	7.03
$M_{wjj} \in [2625,\ 3175]$ GeV	–	0.0515	1.18
$M_{wj_h} \in [1500,\ 2700]$ GeV	–	0.0496	0.903
$M_{wj_s} > 300$ GeV	0.159	–	51.8
$M_{jj} \in [675,\ 1025]$ GeV	0.104	–	16.8
$M_{wjj} \in [2175,\ 2625]$ GeV	0.0816	–	2.17
$M_{wj_h} \in [1375,\ 2250]$ GeV	0.0781	–	1.82
S/B	0.043	0.055	–
$S/\sqrt{B}$ ($\mathcal{L} = 300$ fb^{-1})	1.0	0.90	–
$S/\sqrt{B}$ ($\mathcal{L} = 3000$ fb^{-1})	3.2	2.9	–

Table 4.9: Cut flows for signal and major background events in terms their cross sections. The cross sections are in fb. The number in the parentheses for Wjj is obtained with basic cuts ($p_{T,j} > 100$ GeV, $|\eta_j| < 4$, $\Delta R_{jj} > 0.4, \not{E}_T > 60$ GeV) at the generation level to avoid divergence. In the second row, the same basic cuts are imposed to both signal and background events along with jet and lepton multiplicity requirements.

is characterized by a two-step cascade decay of a heavy resonance, the invariant mass formed by the reconstructed W and a jet is also useful as pointed out in Sec. 4.4.2. Two signal jets are not distinguishable here, motivating us to consider the prescriptions proposed in eqs. (4.45) and (4.46). In the channel of current interest, the two sets are translated as follows.

$$\text{Set 1:} \qquad M_{wj_h},\ \ M_{wj_s} \tag{4.65}$$

$$\text{Set 2:} \qquad M_{wj(\text{high})} = \max[M_{wj_h}, M_{wj_s}],\ \ M_{wj(\text{low})} = \min[M_{wj_h}, M_{wj_s}] \tag{4.66}$$

In this analysis, we choose Set 1 as it enables us to achieve slightly better signal sensitivity. We further restrict ourselves to M_{wj_h} along with M_{wjj} and M_{jj} as four variables are connected by the sum rule in eq. (4.44) which is translated as

$$M^2_{wjj} = M^2_{jj} + M^2_{wj_1} + M^2_{wj_2} = M^2_{jj} + M^2_{wj_h} + M^2_{wj_s}\,, \tag{4.67}$$

where W is assumed effectively massless. Fig. 4.15 demonstrates M_{jj} (upper left panel), M_{wjj} (upper right panel), and M_{wj_h} (bottom panel) distributions for W-Wgg-BP1 (red solid histogram), W-Wgg-BP2 (green solid histogram) and Wjj (blue dashed histogram) with events passing the selection criteria listed in-between (4.57) and (4.62) and the W reconstruction procedure. The black dashed lines mark the input radion mass, the input KK W mass, and the theoretical $M^{\rm max}_{wj}$ value, respectively. We clearly see that they can be utilized in the posterior analysis in order to further separate the signal events from the background ones. Of course, detailed invariant mass windows depend on the mass spectrum that we aim to look for, and we provide the cut flows for W-Wgg-BP1, W-Wgg-BP2, and the major SM background (i.e., Wjj) in Table 4.9. We observe that KK W in both benchmark points may manifest its existence by $\sim 3\sigma$ with an integrated luminosity of 3000 fb^{-1}.

Chapter 5: Conclusion

The LHC Run 1 complemented by electroweak/flavor/CP precision tests have thus far seen no deviations from the SM. In light of this we must conclude that the principle of Naturalness, that predicts new physics below the TeV scale, is either (i) at the cusp of discovery at the LHC, (ii) playing itself out in some exceptional dynamics (such as Twin Higgs theory [28]) that evades our standard experimental probes, or (iii) that the principle is compromised in some way. Our efforts must be directed at all these options. Higgs compositeness (AdS/CFT dual to warped extra-dimensions) within the LHC reach remains a strongly motivated possibility for (i), but requires some new refinement of the warped GIM mechanism. This thesis is directed instead to the option (iii) in the same, broad framework. Indeed, it is noteworthy that the *minimal* incarnation of this paradigm (see Fig. 2.1) can readily and elegantly fit the experimental facts if we take the related new physics to live at $\sim O(10)$ TeV, solving the "big hierarchy problem" between the electroweak and Planck scales, but leaving unexplained a "little hierarchy problem". It is not the modest associated fine-tuning that disturbs us here but the fact that the solution to the hierarchy problem would then lie out of LHC reach!

In the first part of this thesis, we have shown that a simple *extension* of the

above model can also readily fit all the experimental facts if the physics of naturalness is deferred until $\sim O(10)$ TeV. Namely, when different fields propagate different amounts into the IR of the extra dimension (see Fig. 3.2), there can naturally be lighter TeV-scale "vestiges" of the heavy naturalness physics within LHC reach, in the form of new spin-0,1,2 resonances, identified as KK excitations of the extra dimension or composites in the dual mechanism of vectorlike confinement. Although they would constitute a rich new physics close at hand, they escape the strong constraints from flavor/CP tests by virtue of their largely flavor-blind, gauge-mediated couplings to the standard model. We have described several striking features of their phenomenology in the 5D Randall-Sundrum framework and its AdS/CFT dual. In particular, search channels at the LHC such as dileptons, dijets and diphotons for the $\sim$ TeV-mass resonances acquire significance in this framework, cf. decays being dominated by top/Higgs in the minimal model of Fig. 2.1. In addition (and in contrast to the minimal model of Fig. 2.1), the radion and KK graviton (i.e., the gravitational sector) can be readily lighter than other states and, in part of the parameter space, can even lead to first discovery.

But flavor-blindness, however rich the physics, also suggests blindness to the solution to the hierarchy problem. Fortunately, we saw there are small deviations from flavor-blindness in resonance decays into top/Higgs rich final states. These processes thereby give a resonance-enhanced "preview" of Higgs compositeness at the LHC, even though the Higgs compositeness scale and its ultimate resolution of the hierarchy problem is out of LHC reach. This provides a pathway in which LHC discoveries might set the stage for even higher energy explorations. A roughly

comparable analogy within the supersymmetric paradigm is (mini-) Split SUSY [125, 126], in which the stops most directly relevant to the hierarchy problem lie above LHC reach (helping to explain the larger-than-expected Higgs boson mass) while spin-1/2 super-partners are significantly lighter. Seeing the lighter super-partners at the LHC with their SUSY-specific quantum numbers would also give a "preview" of the supersymmetric solution to the hierarchy problem, which could be fully confirmed by going to higher energy colliders.

In the second part of the thesis, we have also shown that there are other types of dramatic collider signals of light TeV-scale resonances. For concreteness, we considered the simplest possibility within the above extended framework, where we add only one more extra brane on top of the minimal/standard set up and only gauge and gravity fields have access to this additional space, while Higgs and matter fields are confined to the region of the bulk in-between the UV and an intermediate brane corresponding to a scale of $\gtrsim \mathcal{O}(10)$ TeV. We further assumed that *all* gauge fields live down to a few TeV. Such a geometry suppresses the usually dominant decay modes of lightest gauge/gravity KK particles into top/Higgs[1] for all KK modes, thereby allowing other decay modes, thus far overwhelmed by top/Higgs, to make their case; in short, the LHC phenomenology can be significantly altered as compared to the standard setup. For example, gauge KK particles can decay into the corresponding SM gauge boson, in association with a radion, with the latter decaying into various pairs of SM gauge bosons. Interestingly, using AdS/CFT

[1]Note that here by "Higgs" we mean the Higgs doublet, which includes the longitudinal W/Z as well as the physical Higgs.

duality between this warped model and the idea of composite SM Higgs, it can be argued that the above decay channel for KK gauge bosons is roughly the "analogue" of $\rho \to \pi\gamma$, followed by $\pi \to \gamma\gamma$ in QCD. Here, we studied in detail the LHC signals resulting from such cascade decays of gauge KK modes. It is clear that there is a plethora of final states possible from this decay (involving combinations of photons, ordinary jets, W/Z-jets, and leptons from W/Z decay). In this work, we focussed on several among them with significant rates.

Overall, we found that the prospects for evidence of these KK particles via the new cascade decay channel look bright, with the KK gluon being the best shot (due mostly to largest production cross-section), whereas KK photon/W/Z require higher luminosity (3000 fb^{-1}) for detection.

We are now well into LHC Run 2, and it is essential that theory lays out the most plausible and powerful mechanisms within reach. In the language of 4D strong dynamics we have shown that vectorlike confinement arising in the IR of Higgs compositeness is such a plausible form of new physics, already exciting at the LHC and able to pave the way for an even more ambitious program of discovery at future higher-energy colliders.

Chapter A: Details of choice of parameters

A.1 Matching at the intermediate/Higgs brane

We assume the same 5D Planck scale (M_5) throughout the bulk. However, in short, the bulk cosmological constant (CC) – and hence AdS curvature *scale* (k) – will be different in the matter/Higgs and gauge/gravity (only) bulks due to presence of (tension on) the intermediate/Higgs brane. In more detail, we define

$$\begin{aligned} \mathrm{CC}_{\mathrm{UV\ (IR)}} &\equiv 24 M_5^3 k^2_{\mathrm{UV\ (IR)}}, \\ k_{\mathrm{UV\ (IR)}} &\equiv \frac{1}{R^{\mathrm{AdS}}_{\mathrm{UV\ (IR)}}} \end{aligned} \tag{A.1}$$

where "UV" and "IR" denote the bulks on the two sides of the Higgs brane and R^{AdS} is the AdS curvature radius. Solving Einstein's equations across the the Higgs brane (with tension, T_{Higgs}) gives [127]:

$$T_{\mathrm{Higgs}} = 12 M_5^3 \left(k_{\mathrm{IR}} - k_{\mathrm{UV}}\right) \tag{A.2}$$

Since we require $T_{\rm Higgs} > 0$ in order to avoid a branon (brane-bending degrees of freedom, denoted by Y) ghost [128], we see that

$$k_{\rm UV} \;<\; k_{\rm IR} \tag{A.3}$$

i.e., curvature scale *increases* in the IR. Let us consider in the following how this new feature modifies the usual choice of parameters.

A.2 Implications of above matching

Consider the gravity sector of the model first. Clearly, we then have two different $g_\star^{\rm grav}$'s on the two sides of the Higgs brane:

$$\frac{g_{\star\,{\rm IR}}^{\rm grav}}{g_{\star\,{\rm UV}}^{\rm grav}} \;=\; \sqrt{\frac{k_{\rm IR}^3}{k_{\rm UV}^3}} \tag{A.4}$$

As usual, we have bulk gravity becoming strongly coupled at [129]

$$\Lambda_{\rm strong}^{\rm grav} \;\sim\; k\left(\frac{16\pi^2}{g_\star^{{\rm grav}\,2}}\right)^{1/3} \tag{A.5}$$

Suppose we would like to have at least $N_{\rm KK}^{\rm min}$ number of weakly-coupled KK modes (i.e., that much gap between 5D cut-off and curvature scale as our control parameter). Then we must have

$$g_\star^{\rm grav} \;\lesssim\; \sqrt{\frac{16\pi^2}{N_{\rm KK}^{{\rm min}\,3}}} \tag{A.6}$$

from the condition that $\Lambda^{\rm grav}_{\rm strong} \gtrsim N^{\rm min}_{\rm KK} k$. Note that this is required in each of the two bulks, i.e., for both $g^{\rm grav}_{\star\,{\rm IR,\,UV}}$. Of course, in order to avoid large hierarchies amongst fundamental/5D parameters (for example, between k and M_5), we would also impose that $g^{\rm grav}_\star$ is *not* $\ll 1$.

Moving onto *gauge* sector, we similarly have

$$\frac{g^{\rm gauge}_{\star\,{\rm IR}}}{g^{\rm gauge}_{\star\,{\rm UV}}} \;=\; \sqrt{\frac{k_{\rm IR}}{k_{\rm UV}}} \tag{A.7}$$

The strong coupling scale is given by :

$$\Lambda^{\rm gauge}_{\rm strong} \;\sim\; k \frac{16\pi^2}{N_{\rm SM}\; 3\; g^{\rm gauge\;2}_\star} \tag{A.8}$$

where $N_{\rm SM}$ denotes size of the SM gauge group (take it here to be 3 for color) and factor of 3 in denominator above (i.e., enhancement of loop expansion parameter) comes from counting helicities of spin-1 field. So, the associated request (i.e, imposing $\Lambda^{\rm gauge}_{\rm strong} \gtrsim N^{\rm min}_{\rm KK} k$) is

$$g^{\rm gauge}_\star \;\lesssim\; \frac{4\pi}{3\sqrt{N^{\rm min}_{\rm KK}}} \tag{A.9}$$

for each of the two bulks.

On the other hand, fitting to the observed/SM gauge coupling gives *lower* limits on $g^{\rm gauge}_\star$ as follows (note that there is no analog of Landau pole for gravity, hence no lower limit on $g^{\rm grav}_\star$ on this count). Consider the running of the SM gauge couplings from the UV cut-off to the IR shown in Eq. (3.11). Plugging in the low-

energy values of $g_{\rm SM}$ and $b_{\rm SM}$ into Eq. (3.11), we find (assuming $\Lambda_{\rm Higgs} \sim 10$ TeV and $\Lambda_{\rm IR} \sim$ few TeV)

$$g_{\star\,\rm UV}^{\rm gauge} \;\gtrsim\; 3 \tag{A.10}$$

from the requirement that $1/g_{\rm UV}^2 > 0$, i.e., Landau poles for SM gauge couplings are at/above $\sim 10^{15}$ GeV. However, $g_{\star\,\rm IR}^{\rm gauge}$ mostly unconstrained, since it contributes over a (much) smaller hierarchy.

Finally, there is another requirement that the strong coupling scale of the Y self-interactions be (at least modestly) above the curvature scale, i.e.,

$$\mathcal{L} \;\ni\; (\partial_\mu Y)^2 + \frac{(\partial_\mu Y)^4}{T_{\rm Higgs}} \tag{A.11}$$

results in

$$\Lambda_{\rm strong}^{\rm branon} \;\sim\; \left(16\pi^2 T_{\rm Higgs}\right)^{1/4} \tag{A.12}$$

So we need [as usual, imposing $\Lambda_{\rm strong}^{\rm branon} \gtrsim N_{\rm KK}^{\rm min} k$ and using Eq. (A.2)]

$$g_\star^{\rm grav\,IR} \;\lesssim\; \left[\frac{192\pi^2}{N_{\rm KK}^{\rm min\;4}}\left(1 - \frac{k_{\rm UV}}{k_{\rm IR}}\right)\right]^{1/2} \tag{A.13}$$

We can check that the following choices of couplings *barely* satisfy *all* the above

needs (including giving observable LHC signals):

$$g^{\rm grav}_{\star\,\rm UV} < g^{\rm grav}_{\star\,\rm IR} \lesssim 3 \quad \text{and} \quad g^{\rm gauge}_{\star\,\rm UV} \sim 3; \;\; g^{\rm gauge\,2}_{\star\,\rm IR} \approx g^{\rm gauge\,2}_{\star\,\rm UV}\Big[1 + O(0.1)\Big] \tag{A.14}$$

for a *minimal* request of

$$N^{\rm min}_{\rm KK} \;\; \sim \;\; 2 \tag{A.15}$$

(and corresponding to $k_{\rm IR}/k_{\rm UV} \approx 1 + O(0.1)$).

Note that $g^{\rm gauge}_{\star\,\rm IR}$ and $g^{\rm gauge}_{\star\,\rm UV}$ are "forced" to be close to each other, due to a *combination* of perturbativity (upper bound on $g^{\rm gauge}_{\star\,\rm UV}$) and Landau pole (lower bound) constraints. One possibility to relieve this tension is to reduce the UV-IR hierarchy, for example, lower the UV scale to the flavor scale of $\sim 10^5$ TeV [130], while keeping IR scale $\sim$ TeV: from Eq. (3.11), we see that $g^{\rm gauge}_{\star\,\rm UV} \gtrsim 2$ might then be allowed (keeping both $g^{\rm gauge}_{\star}$'s at/below ~ 3 for perturbativity).

Chapter B: Two Dilaton system

Here we discuss the CFT dual of stabilization of the model with one intermediate brane studied in the main text. In short, as usual, we start with a CFT at a UV cut-off $\Lambda_{\rm UV}$. This CFT confines, i.e., scale invariance is broken, at $\Lambda_{\rm int}$, which is to be identified with $\Lambda_{\rm Higgs}$, i.e., scale of the Higgs brane in the specific model, but here we would like to keep the notation more general. As already mentioned, this scale can be parametrized by the VEV of dilaton/radion field [denoted by $\Phi_{\rm int}$ of mass dimension +1, fluctuations around which correspond to the physical dilaton ($\varphi_{\rm int}$)], i.e.,

$$\Phi_{\rm int} \quad \sim \quad \Lambda_{\rm int} + a g^{\rm grav}_{\star\,{\rm UV}} \varphi_{\rm int}. \tag{B.1}$$

The departure from the standard (i.e., minimal model of Fig. **??**) script involves the resulting (daughter) theory (i.e., below $\Lambda_{\rm int}$) flowing to a new fixed point. This "IR" CFT then confines at an even lower scale $\Lambda_{\rm IR}$, corresponding to the VEV of *another* field, $\Phi_{\rm IR}$ (associated with a second dilaton, $\varphi_{\rm IR}$).

In more detail, in order to stabilize the two inter-brane separations (dual to determining the various mass scale hierarchies), we perturb the (UV) CFT by adding

a *single* scalar operator (dual to the GW field) in the UV:

$$\mathcal{L}\left(\Lambda_{\rm UV}\right) \;\ni\; \mathcal{L}_{\rm CFT\ UV} + \lambda\, \Lambda_{\rm UV}^{\epsilon_{\rm UV}}\, \mathcal{O}_{\rm GW}^{\rm UV} \tag{B.2}$$

where scaling *and* naive/engineering dimension of $\mathcal{O}_{\rm GW}^{\rm UV}$ is $(4-\epsilon_{\rm UV})$ (i.e., λ above is dimension*less*). As usual, we assume that there is only one scalar operator with scaling dimension close to 4, rest of them being irrelevant (hence being dropped from the Lagrangian). We flow to $\Lambda_{\rm int}$ (as usual, promoting appropriately Λ's to Φ's throughout):

$$\begin{aligned}\mathcal{L}\left(\Lambda_{\rm int}\right) \;\ni\; & \mathcal{L}_{\rm CFT\ IR} + \left(\partial_\mu \Phi_{\rm int}\right)^2 + \lambda' \Phi_{\rm int}^4 + d_1 \lambda\, \Phi_{\rm int}^4 \left(\frac{\Phi_{\rm int}}{\Lambda_{\rm UV}}\right)^{-\epsilon_{\rm UV}} + \\ & \left[d_2 \lambda \left(\frac{\Phi_{\rm int}}{\Lambda_{\rm UV}}\right)^{-\epsilon_{\rm UV}} + \tilde{\lambda}\right] \Phi_{\rm int}^{\epsilon_{\rm IR}}\, \mathcal{O}_{\rm GW}^{\rm IR}\end{aligned} \tag{B.3}$$

where $d_{1,\,2}$ are $O(1)$ factors.

Let us elaborate on the various terms above. The first three terms above (in first line) are as discussed earlier (i.e., for the usual minimal model). Whereas, the first *new* term (in second line above) comes from using the interpolation:

$$\mathcal{O}_{\rm GW}^{\rm UV}\left(\Lambda_{\rm int}\right) \;\sim\; \mathcal{O}_{\rm GW}^{\rm IR} \Phi_{\rm int}^{\epsilon_{\rm IR}-\epsilon_{\rm UV}} + ... \tag{B.4}$$

in the RG evolved *explicit* conformal symmetry breaking term in Eq. (B.2). Here, (with obvious choice of notation) $\mathcal{O}_{\rm GW}^{\rm IR}$ is an operator of the *IR* CFT of scaling dimension $(4-\epsilon_{\rm IR})$: again, we assume that there exists only one such operator. On

the other hand, the second term in second line of Eq. (B.3) arises from *spontaneous* conformal symmetry breaking at the scale $\Lambda_{\rm int}$, i.e., even if $\lambda\, O^{\rm UV}_{\rm GW}$ were "absent". Given above assumption about scaling dimensions of scalar operators of the *IR* CFT, it is clear that both terms in second line above must involve the *same* operator (as the leading term), i.e., coupling of $\Phi_{\rm int}$ to *other* scalar operators of the IR CFT will be irrelevant.

Finally, i.e., RG flowing to the far IR scale of $\Lambda_{\rm IR}$ and adding (for a second time) the usual term consistent with the (IR) conformal symmetry, we obtain the complete potential for the two scalar fields (Φ's):

$$\begin{aligned}\mathcal{L}\left(\Lambda_{\rm IR}\right) \;\ni\; & \left(\partial_\mu \Phi_{\rm int}\right)^2 + \lambda' \Phi_{\rm int}^4 + d_1 \lambda \Phi_{\rm int}^4 \left(\frac{\Phi_{\rm int}}{\Lambda_{\rm UV}}\right)^{-\epsilon_{\rm UV}} + \\ & \left(\partial_\mu \Phi_{\rm IR}\right)^2 + \tilde{\lambda}' \Phi_{\rm IR}^4 + \left[d_3 \lambda \left(\frac{\Phi_{\rm int}}{\Lambda_{\rm UV}}\right)^{-\epsilon_{\rm UV}} + d_4 \tilde{\lambda}\right] \left(\frac{\Phi_{\rm IR}}{\Phi_{\rm int}}\right)^{-\epsilon_{\rm IR}} \Phi_{\rm IR}^4 \qquad \text{(B.5)}\end{aligned}$$

We have to minimize the above potential in order to determine the scales $\Lambda_{\rm int}$ and $\Lambda_{\rm IR}$ in terms of $\Lambda_{\rm UV}$ and the scaling dimensions [we can assume that the various λ's are $O(1)$]. As usual, we assume $\epsilon_{\rm UV,\,IR}$ are *modestly* smaller than 1. In this case, we can proceed with the minimization in steps as follows. At "leading-order" (LO), it is reasonable to assume that $\langle \Phi_{\rm int} \rangle \sim \Lambda_{\rm int}$ is mostly determined (as in the minimal two brane case) by first line of Eq. (B.5) (i.e., potential for $\Phi_{\rm int}$ by itself) to be:

$$\Lambda_{\rm int} \;\sim\; \left(-d_1 \frac{\lambda}{\lambda'}\right)^{1/\epsilon_{\rm UV}} \Lambda_{\rm UV} \qquad \text{(B.6)}$$

with

$$m^2_{\varphi_{\rm int}} \sim \epsilon_{\rm UV}\Lambda^2_{\rm int}. \tag{B.7}$$

Similarly, plugging $\Phi_{\rm int} = \Lambda_{\rm int}$ (i.e., a fixed value) into second line of Eq. (B.5), i.e., effective potential for $\Phi_{\rm IR}$, will give (again, as usual):

$$\Lambda_{\rm IR} \sim \left(-\frac{1}{\tilde{\lambda}'}\left(d_4\tilde{\lambda} - \frac{d_3}{d_1}\lambda'\right)\right)^{1/\epsilon_{\rm IR}}\Lambda_{\rm int} \tag{B.8}$$

with

$$m^2_{\varphi_{\rm IR}} \sim \epsilon_{\rm IR}\Lambda^2_{\rm IR}. \tag{B.9}$$

As a (partial) consistency check of the above procedure (for obtaining the values of VEV's), we can consider the mixing (if you will, the NLO) term involving *both* the dilatons arising from the last two terms of second line of Eq. (B.5), where $\Phi_{\rm int}$ can be thought of as fluctuations around $\Lambda_{\rm int}$:

$$\Delta m^2_{\varphi_{\rm int}\varphi_{\rm IR}} \sim O\left(\epsilon_{\rm IR},\ \epsilon_{\rm UV}\right)\frac{\Lambda^3_{\rm IR}}{\Lambda_{\rm int}}. \tag{B.10}$$

We see that this results in a mixing angle between two dilatons of $\sim \epsilon\left(\Lambda_{\rm IR}/\Lambda_{\rm int}\right)^3$, i.e., small enough. As a further check, we can show that the first derivatives of the *full* potential in Eq. (B.5) at above values of VEV's vanish, up to terms suppressed by (powers of) $\Lambda_{\rm IR}/\Lambda_{\rm int}$, i.e., the actual VEV's are close enough to those obtained by the

above “piece-wise” minimization of the potential. Hence, to a good approximation, we can “decouple” the two dilaton systems (as already assumed in the main text).

Bibliography

[1] S. Weinberg, "The Quantum theory of fields. Vol. 1: Foundations,";

S. Weinberg, "The quantum theory of fields. Vol. 2: Modern applications."

[2] C. N. Yang, Asia Pac. Phys. Newslett. **01**, 27 (2012). doi:10.1142/S2251158X12000045

[3] D. B. Chitwood *et al.* [MuLan Collaboration], Phys. Rev. Lett. **99**, 032001 (2007) doi:10.1103/PhysRevLett.99.032001 [arXiv:0704.1981 [hep-ex]].

[4] G. Aad *et al.* [ATLAS Collaboration], Phys. Lett. B **716**, 1 (2012) doi:10.1016/j.physletb.2012.08.020 [arXiv:1207.7214 [hep-ex]].

[5] S. Chatrchyan *et al.* [CMS Collaboration], Phys. Lett. B **716**, 30 (2012) doi:10.1016/j.physletb.2012.08.021 [arXiv:1207.7235 [hep-ex]].

[6] G. Aad *et al.* [ATLAS and CMS Collaborations], Phys. Rev. Lett. **114**, 191803 (2015) doi:10.1103/PhysRevLett.114.191803 [arXiv:1503.07589 [hep-ex]].

[7] V. Khachatryan *et al.* [CMS Collaboration], Eur. Phys. J. C **75**, no. 5, 212 (2015) doi:10.1140/epjc/s10052-015-3351-7 [arXiv:1412.8662 [hep-ex]].

[8] V. Khachatryan *et al.* [CMS Collaboration], Phys. Rev. D **92**, no. 1, 012004 (2015) doi:10.1103/PhysRevD.92.012004 [arXiv:1411.3441 [hep-ex]].

[9] G. Aad *et al.* [ATLAS Collaboration], Eur. Phys. J. C **75**, no. 10, 476 (2015) Erratum: [Eur. Phys. J. C **76**, no. 3, 152 (2016)] doi:10.1140/epjc/s10052-015-3685-1, 10.1140/epjc/s10052-016-3934-y [arXiv:1506.05669 [hep-ex]].

[10] G. F. Giudice, In *Kane, Gordon (ed.), Pierce, Aaron (ed.): Perspectives on LHC physics* 155-178 doi:10.1142/9789812779762_0010 [arXiv:0801.2562 [hep-ph]].

[11] G. 't Hooft, C. Itzykson, A. Jaffe, H. Lehmann, P. K. Mitter, I. M. Singer and R. Stora, NATO Sci. Ser. B **59**, pp.1 (1980). doi:10.1007/978-1-4684-7571-5

[12] C. Patrignani *et al.* [Particle Data Group], Chin. Phys. C **40**, no. 10, 100001 (2016). doi:10.1088/1674-1137/40/10/100001

[13] L. Susskind, Phys. Rev. D **20**, 2619 (1979). doi:10.1103/PhysRevD.20.2619

[14] E. Witten, Nucl. Phys. B **188**, 513 (1981). doi:10.1016/0550-3213(81)90006-7

[15] S. Dimopoulos and H. Georgi, Nucl. Phys. B **193**, 150 (1981). doi:10.1016/0550-3213(81)90522-8

[16] D. B. Kaplan and H. Georgi, Phys. Lett. **136B**, 183 (1984). doi:10.1016/0370-2693(84)91177-8

[17] D. B. Kaplan, H. Georgi and S. Dimopoulos, Phys. Lett. **136B**, 187 (1984). doi:10.1016/0370-2693(84)91178-X

[18] T. Banks, Nucl. Phys. B **243**, 125 (1984). doi:10.1016/0550-3213(84)90389-4

[19] H. Georgi, D. B. Kaplan and P. Galison, Phys. Lett. **143B**, 152 (1984). doi:10.1016/0370-2693(84)90823-2

[20] H. Georgi and D. B. Kaplan, Phys. Lett. **145B**, 216 (1984). doi:10.1016/0370-2693(84)90341-1

[21] M. J. Dugan, H. Georgi and D. B. Kaplan, Nucl. Phys. B **254**, 299 (1985). doi:10.1016/0550-3213(85)90221-4

[22] N. Arkani-Hamed, S. Dimopoulos and G. R. Dvali, Phys. Lett. B **429**, 263 (1998) doi:10.1016/S0370-2693(98)00466-3 [hep-ph/9803315].

[23] I. Antoniadis, N. Arkani-Hamed, S. Dimopoulos and G. R. Dvali, Phys. Lett. B **436**, 257 (1998) doi:10.1016/S0370-2693(98)00860-0 [hep-ph/9804398].

[24] L. Randall and R. Sundrum, Phys. Rev. Lett. **83**, 3370 (1999) doi:10.1103/PhysRevLett.83.3370 [hep-ph/9905221].

[25] L. Randall and R. Sundrum, Phys. Rev. Lett. **83**, 4690 (1999) doi:10.1103/PhysRevLett.83.4690 [hep-th/9906064].

[26] N. Arkani-Hamed, A. G. Cohen and H. Georgi, Phys. Rev. Lett. **86**, 4757 (2001) doi:10.1103/PhysRevLett.86.4757 [hep-th/0104005].

[27] N. Arkani-Hamed, A. G. Cohen and H. Georgi, Phys. Lett. B **513**, 232 (2001) doi:10.1016/S0370-2693(01)00741-9 [hep-ph/0105239].

[28] Z. Chacko, H. S. Goh and R. Harnik, Phys. Rev. Lett. **96**, 231802 (2006) doi:10.1103/PhysRevLett.96.231802 [hep-ph/0506256].

[29] G. Burdman, Z. Chacko, H. S. Goh and R. Harnik, JHEP **0702**, 009 (2007) doi:10.1088/1126-6708/2007/02/009 [hep-ph/0609152].

[30] P. W. Graham, D. E. Kaplan and S. Rajendran, Phys. Rev. Lett. **115**, no. 22, 221801 (2015) doi:10.1103/PhysRevLett.115.221801 [arXiv:1504.07551 [hep-ph]].

[31] N. Arkani-Hamed and S. Dimopoulos, JHEP **0506**, 073 (2005) doi:10.1088/1126-6708/2005/06/073 [hep-th/0405159].

[32] For a review, see O. Aharony, S. S. Gubser, J. M. Maldacena, H. Ooguri and Y. Oz, Phys. Rept. **323**, 183 (2000) [hep-th/9905111].

[33] For the duality of gravity and bulk gauge fields, see, for example, N. Arkani-Hamed, M. Porrati and L. Randall, JHEP **0108**, 017 (2001) [hep-th/0012148].

[34] R. Rattazzi and A. Zaffaroni, JHEP **0104**, 021 (2001) doi:10.1088/1126-6708/2001/04/021 [hep-th/0012248].

[35] For duality of bulk fermions, see, for example, R. Contino and A. Pomarol, JHEP **0411**, 058 (2004) [hep-th/0406257].

[36] R. Contino, Y. Nomura and A. Pomarol, Nucl. Phys. B **671**, 148 (2003) doi:10.1016/j.nuclphysb.2003.08.027 [hep-ph/0306259].

[37] T. Gherghetta, hep-ph/0601213.

[38] H. Davoudiasl, S. Gopalakrishna, E. Ponton and J. Santiago, New J. Phys. **12**, 075011 (2010) doi:10.1088/1367-2630/12/7/075011 [arXiv:0908.1968 [hep-ph]].

[39] C. Csaki, In *Shifman, M. (ed.) et al.: From fields to strings, vol. 2* 967-1060 [hep-ph/0404096].

[40] C. Csaki, J. Hubisz and P. Meade, hep-ph/0510275.

[41] R. Sundrum, hep-th/0508134.

[42] E. Ponton, doi:10.1142/97898143901630007 arXiv:1207.3827 [hep-ph].

[43] W. D. Goldberger and M. B. Wise, Phys. Rev. Lett. **83**, 4922 (1999) [arXiv:hep-ph/9907447].

[44] D. B. Kaplan, Nucl. Phys. B **365**, 259 (1991). doi:10.1016/S0550-3213(05)80021-5. For AdS dual of this idea, see [35].

[45] For a review, see, for example, G. Panico and A. Wulzer, Lect. Notes Phys. **913**, pp.1 (2016) doi:10.1007/978-3-319-22617-0 [arXiv:1506.01961 [hep-ph]].

[46] K. Agashe, R. Contino and A. Pomarol, Nucl. Phys. B **719**, 165 (2005) doi:10.1016/j.nuclphysb.2005.04.035 [hep-ph/0412089].

[47] M. J. Strassler, hep-th/0309122.

[48] S. Kachru, D. Simic and S. P. Trivedi, JHEP **1005**, 067 (2010) doi:10.1007/JHEP05(2010)067 [arXiv:0905.2970 [hep-th]].

[49] For a recent summary, see, for example, K. Agashe *et al.*, arXiv:1309.7847 [hep-ph].

[50] K. Agashe, A. Delgado, M. J. May and R. Sundrum, JHEP **0308**, 050 (2003) [arXiv:hep-ph/0308036].

[51] K. Agashe, R. Contino, L. Da Rold and A. Pomarol, Phys. Lett. B **641**, 62 (2006) [arXiv:hep-ph/0605341].

[52] M. Carena, E. Ponton, J. Santiago and C. E. M. Wagner, Nucl. Phys. B **759**, 202 (2006) [arXiv:hep-ph/0607106].

[53] M. S. Carena, E. Pontón, J. Santiago and C. E. M. Wagner, Phys. Rev. D **76**, 035006 (2007) [arXiv:hep-ph/0701055].

[54] C. Delaunay, O. Gedalia, S. J. Lee, G. Perez and E. Ponton, Phys. Rev. D **83**, 115003 (2011) [arXiv:1007.0243 [hep-ph]].

[55] T. Gherghetta and A. Pomarol, Nucl. Phys. B **586**, 141 (2000) [hep-ph/0003129].

[56] S. J. Huber and Q. Shafi, Phys. Lett. B **498**, 256 (2001) [arXiv:hep-ph/0010195].

[57] S. J. Huber, Nucl. Phys. B **666**, 269 (2003) [hep-ph/0303183].

[58] K. Agashe, G. Perez and A. Soni, Phys. Rev. D **71**, 016002 (2005) [arXiv:hep-ph/0408134].

[59] C. Csaki, A. Falkowski and A. Weiler, JHEP **0809**, 008 (2008) doi:10.1088/1126-6708/2008/09/008 [arXiv:0804.1954 [hep-ph]].

[60] M. Blanke, A. J. Buras, B. Duling, S. Gori and A. Weiler, JHEP **0903**, 001 (2009) [arXiv:0809.1073 [hep-ph]].

[61] M. Bauer, S. Casagrande, U. Haisch and M. Neubert, JHEP **1009**, 017 (2010) [arXiv:0912.1625 [hep-ph]].

[62] B. Keren-Zur, P. Lodone, M. Nardecchia, D. Pappadopulo, R. Rattazzi and L. Vecchi, Nucl. Phys. B **867**, 394 (2013) [arXiv:1205.5803 [hep-ph]].

[63] A. L. Fitzpatrick, G. Perez and L. Randall, Phys. Rev. Lett. **100**, 171604 (2008) doi:10.1103/PhysRevLett.100.171604 [arXiv:0710.1869 [hep-ph]].

[64] C. Csaki, A. Falkowski and A. Weiler, Phys. Rev. D **80**, 016001 (2009) doi:10.1103/PhysRevD.80.016001 [arXiv:0806.3757 [hep-ph]].

[65] M. Redi and A. Weiler, JHEP **1111**, 108 (2011) doi:10.1007/JHEP11(2011)108 [arXiv:1106.6357 [hep-ph]].

[66] R. Barbieri, D. Buttazzo, F. Sala, D. M. Straub and A. Tesi, JHEP **1305**, 069 (2013) doi:10.1007/JHEP05(2013)069 [arXiv:1211.5085 [hep-ph]].

[67] D. M. Straub, JHEP **1308**, 108 (2013) [arXiv:1302.4651 [hep-ph]].

[68] M. Konig, M. Neubert and D. M. Straub, Eur. Phys. J. C **74**, 2945 (2014) [arXiv:1403.2756 [hep-ph]].

[69] C. Csaki and L. Randall, JHEP **1607**, 061 (2016) doi:10.1007/JHEP07(2016)061 [arXiv:1603.07303 [hep-ph]].

[70] M. Aaboud *et al.* [ATLAS Collaboration], arXiv:1606.03833 [hep-ex].

[71] V. Khachatryan *et al.* [CMS Collaboration], arXiv:1606.04093 [hep-ex].

[72] L. Vecchi, Phys. Lett. B **727**, 130 (2013) doi:10.1016/j.physletb.2013.08.006 [arXiv:1206.4701 [hep-ph]].

[73] G. Panico and A. Pomarol, JHEP **1607** (2016) 097 doi:10.1007/JHEP07(2016)097 [arXiv:1603.06609 [hep-ph]].

[74] See, for example, A. Carmona, E. Ponton and J. Santiago, JHEP **1110**, 137 (2011) doi:10.1007/JHEP10(2011)137 [arXiv:1107.1500 [hep-ph]].

[75] C. Kilic, T. Okui and R. Sundrum, JHEP **0807**, 038 (2008) doi:10.1088/1126-6708/2008/07/038 [arXiv:0802.2568 [hep-ph]].

[76] C. Kilic, T. Okui and R. Sundrum, JHEP **1002**, 018 (2010) doi:10.1007/JHEP02(2010)018 [arXiv:0906.0577 [hep-ph]].

[77] Y. Bai and R. J. Hill, Phys. Rev. D **82**, 111701 (2010) doi:10.1103/PhysRevD.82.111701 [arXiv:1005.0008 [hep-ph]].

[78] J. Garriga and A. Pomarol, Phys. Lett. B **560**, 91 (2003) [hep-th/0212227].

[79] For non-supersymmetric versions, see, for example, S. Raby, S. Dimopoulos and L. Susskind, Nucl. Phys. B **169**, 373 (1980). doi:10.1016/0550-3213(80)90093-0.

[80] For supersymmetric cases, see, for example, I. R. Klebanov and M. J. Strassler, JHEP **0008**, 052 (2000) doi:10.1088/1126-6708/2000/08/052 [hep-th/0007191].

[81] R. Franceschini *et al.*, JHEP **1603**, 144 (2016) doi:10.1007/JHEP03(2016)144 [arXiv:1512.04933 [hep-ph]].

[82] Y. Nakai, R. Sato and K. Tobioka, Phys. Rev. Lett. **116**, no. 15, 151802 (2016) doi:10.1103/PhysRevLett.116.151802 [arXiv:1512.04924 [hep-ph]].

[83] M. Low, A. Tesi and L. T. Wang, JHEP **1603**, 108 (2016) doi:10.1007/JHEP03(2016)108 [arXiv:1512.05328 [hep-ph]].

[84] K. Harigaya and Y. Nomura, Phys. Lett. B **754**, 151 (2016) doi:10.1016/j.physletb.2016.01.026 [arXiv:1512.04850 [hep-ph]].

[85] E. Molinaro, F. Sannino and N. Vignaroli, arXiv:1512.05334 [hep-ph].

[86] B. Bellazzini, R. Franceschini, F. Sala and J. Serra, JHEP **1604**, 072 (2016) doi:10.1007/JHEP04(2016)072 [arXiv:1512.05330 [hep-ph]].

[87] See, for example, J. Barnard, T. Gherghetta, T. S. Ray and A. Spray, JHEP **1501**, 067 (2015) doi:10.1007/JHEP01(2015)067 [arXiv:1409.7391 [hep-ph]].

[88] J. Barnard, P. Cox, T. Gherghetta and A. Spray, JHEP **1603**, 003 (2016) doi:10.1007/JHEP03(2016)003 [arXiv:1510.06405 [hep-ph]].

[89] H. Davoudiasl, J. L. Hewett and T. G. Rizzo, JHEP **0308**, 034 (2003) doi:10.1088/1126-6708/2003/08/034 [hep-ph/0305086].

[90] A. Carmona, Phys. Lett. B **760**, 502 (2016) doi:10.1016/j.physletb.2016.07.040 [arXiv:1603.08913 [hep-ph]].

[91] A. Falkowski and J. F. Kamenik, Phys. Rev. D **94**, no. 1, 015008 (2016) doi:10.1103/PhysRevD.94.015008 [arXiv:1603.06980 [hep-ph]].

[92] B. M. Dillon and V. Sanz, arXiv:1603.09550 [hep-ph].

[93] J. L. Hewett and T. G. Rizzo, arXiv:1603.08250 [hep-ph].

[94] A. Kobakhidze, K. L. McDonald, L. Wu and J. Yue, arXiv:1606.08565 [hep-ph].

[95] B. M. Dillon, C. Han, H. M. Lee and M. Park, arXiv:1606.07171 [hep-ph].

[96] T. Konstandin, G. Nardini and M. Quiros, Phys. Rev. D **82**, 083513 (2010) doi:10.1103/PhysRevD.82.083513 [arXiv:1007.1468 [hep-ph]].

[97] Y. Eshel, S. J. Lee, G. Perez and Y. Soreq, JHEP **1110**, 015 (2011) doi:10.1007/JHEP10(2011)015 [arXiv:1106.6218 [hep-ph]].

[98] Z. Chacko, R. K. Mishra and D. Stolarski, JHEP **1309**, 121 (2013) doi:10.1007/JHEP09(2013)121 [arXiv:1304.1795 [hep-ph]].

[99] Z. Chacko and R. K. Mishra, Phys. Rev. D **87**, no. 11, 115006 (2013) doi:10.1103/PhysRevD.87.115006 [arXiv:1209.3022 [hep-ph]].

[100] See, for example, K. Agashe, R. Contino and R. Sundrum, Phys. Rev. Lett. **95**, 171804 (2005) doi:10.1103/PhysRevLett.95.171804 [hep-ph/0502222].

[101] C. Csaki, J. Hubisz and S. J. Lee, Phys. Rev. D **76**, 125015 (2007) doi:10.1103/PhysRevD.76.125015 [arXiv:0705.3844 [hep-ph]].

[102] Z. Chacko, R. K. Mishra, D. Stolarski and C. B. Verhaaren, Phys. Rev. D **92**, no. 5, 056004 (2015) doi:10.1103/PhysRevD.92.056004 [arXiv:1411.3758 [hep-ph]].

[103] For simplified discussion (using elementary-composite sectors), see, for example, R. Contino, T. Kramer, M. Son and R. Sundrum, JHEP **0705**, 074 (2007) [hep-ph/0612180].

[104] G. Panico, L. Vecchi and A. Wulzer, arXiv:1603.04248 [hep-ph].

[105] T. Flacke, B. Gripaios, J. March-Russell and D. Maybury, JHEP **0701**, 061 (2007) doi:10.1088/1126-6708/2007/01/061 [hep-ph/0611278].

[106] C. Vafa and E. Witten, Phys. Rev. Lett. **53**, 535 (1984). doi:10.1103/PhysRevLett.53.535.

[107] C. Vafa and E. Witten, Nucl. Phys. B **234**, 173 (1984). doi:10.1016/0550-3213(84)90230-X.

[108] CMS Collaboration, CMS-PAS-EXO-16-027.

[109] The ATLAS collaboration, ATLAS-CONF-2016-059.

[110] CMS Collaboration, CMS-PAS-EXO-16-032.

[111] See, for example, D. Stolarski and R. Vega-Morales, Phys. Rev. D **86**, 117504 (2012) doi:10.1103/PhysRevD.86.117504 [arXiv:1208.4840 [hep-ph]].

[112] CMS Collaboration, CMS-PAS-EXO-16-031.

[113] The ATLAS collaboration, ATLAS-CONF-2016-045.

[114] The ATLAS collaboration [ATLAS Collaboration], ATLAS-CONF-2016-061.

[115] CMS Collaboration [CMS Collaboration], CMS-PAS-EXO-15-006.

[116] D. Pappadopulo, A. Thamm, R. Torre and A. Wulzer, JHEP **1409**, 060 (2014) doi:10.1007/JHEP09(2014)060 [arXiv:1402.4431 [hep-ph]].

[117] The ATLAS collaboration, ATLAS-CONF-2016-062.

[118] The ATLAS collaboration, ATLAS-CONF-2016-055.

[119] V. Khachatryan *et al.* [CMS Collaboration], Phys. Rev. D **93**, no. 1, 012001 (2016) doi:10.1103/PhysRevD.93.012001 [arXiv:1506.03062 [hep-ex]].

[120] CMS Collaboration [CMS Collaboration], CMS-PAS-B2G-15-002.

[121] R. M. Harris and S. Jain, Eur. Phys. J. C **72**, 2072 (2012) doi:10.1140/epjc/s10052-012-2072-4 [arXiv:1112.4928 [hep-ph]].

[122] K. Agashe, A. Belyaev, T. Krupovnickas, G. Perez and J. Virzi, Phys. Rev. D **77**, 015003 (2008) doi:10.1103/PhysRevD.77.015003 [hep-ph/0612015].

[123] R. S. Chivukula, A. Farzinnia, J. Ren and E. H. Simmons, Phys. Rev. D **87**, no. 9, 094011 (2013) doi:10.1103/PhysRevD.87.094011 [arXiv:1303.1120 [hep-ph]].

[124] H. Georgi and Y. Nakai, arXiv:1606.05865 [hep-ph].

[125] A. Arvanitaki, N. Craig, S. Dimopoulos and G. Villadoro, JHEP **1302**, 126 (2013) doi:10.1007/JHEP02(2013)126 [arXiv:1210.0555 [hep-ph]].

[126] N. Arkani-Hamed, A. Gupta, D. E. Kaplan, N. Weiner and T. Zorawski, arXiv:1212.6971 [hep-ph].

[127] I. I. Kogan, S. Mouslopoulos, A. Papazoglou and L. Pilo, Nucl. Phys. B **625**, 179 (2002) doi:10.1016/S0550-3213(02)00009-3 [hep-th/0105255].

[128] R. Sundrum, Phys. Rev. D **59**, 085009 (1999) doi:10.1103/PhysRevD.59.085009 [hep-ph/9805471].

[129] Z. Chacko, M. A. Luty and E. Ponton, JHEP **0007**, 036 (2000) doi:10.1088/1126-6708/2000/07/036 [hep-ph/9909248].

[130] H. Davoudiasl, G. Perez and A. Soni, Phys. Lett. B **665**, 67 (2008) doi:10.1016/j.physletb.2008.05.024 [arXiv:0802.0203 [hep-ph]].

[131] K. Agashe, P. Du, S. Hong and R. Sundrum, JHEP **1701**, 016 (2017) doi:10.1007/JHEP01(2017)016 [arXiv:1608.00526 [hep-ph]].

[132] S. J. Huber and Q. Shafi, Phys. Rev. D **63**, 045010 (2001) doi:10.1103/PhysRevD.63.045010 [hep-ph/0005286].

[133] S. J. Huber, C. A. Lee and Q. Shafi, Phys. Lett. B **531**, 112 (2002) doi:10.1016/S0370-2693(02)01368-0 [hep-ph/0111465].

[134] C. Csaki, J. Erlich and J. Terning, Phys. Rev. D **66**, 064021 (2002) doi:10.1103/PhysRevD.66.064021 [hep-ph/0203034].

[135] J. L. Hewett, F. J. Petriello and T. G. Rizzo, JHEP **0209**, 030 (2002) doi:10.1088/1126-6708/2002/09/030 [hep-ph/0203091].

[136] K. Agashe, C. Y. Chen, H. Davoudiasl and D. Kim, Phys. Rev. D **91**, no. 7, 076002 (2015) doi:10.1103/PhysRevD.91.076002 [arXiv:1412.6215 [hep-ph]].

[137] C. Bini, R. Contino and N. Vignaroli, JHEP **1201**, 157 (2012) doi:10.1007/JHEP01(2012)157 [arXiv:1110.6058 [hep-ph]].

[138] CMS Collaboration [CMS Collaboration], CMS-PAS-EXO-16-015.

[139] The ATLAS collaboration [ATLAS Collaboration], ATLAS-CONF-2016-070.

[140] The ATLAS collaboration [ATLAS Collaboration], ATLAS-CONF-2014-006.

[141] A. Alloul, N. D. Christensen, C. Degrande, C. Duhr and B. Fuks, Comput. Phys. Commun. **185**, 2250 (2014) doi:10.1016/j.cpc.2014.04.012 [arXiv:1310.1921 [hep-ph]].

[142] J. Alwall *et al.*, JHEP **1407**, 079 (2014) doi:10.1007/JHEP07(2014)079 [arXiv:1405.0301 [hep-ph]].

[143] R. D. Ball *et al.*, Nucl. Phys. B **867**, 244 (2013) doi:10.1016/j.nuclphysb.2012.10.003 [arXiv:1207.1303 [hep-ph]].

[144] T. Sjostrand, S. Mrenna and P. Z. Skands, JHEP **0605**, 026 (2006) doi:10.1088/1126-6708/2006/05/026 [hep-ph/0603175].

[145] M. Cacciari and G. P. Salam, Phys. Lett. B **641**, 57 (2006) doi:10.1016/j.physletb.2006.08.037 [hep-ph/0512210].

[146] M. Cacciari, G. P. Salam and G. Soyez, Eur. Phys. J. C **72**, 1896 (2012) doi:10.1140/epjc/s10052-012-1896-2 [arXiv:1111.6097 [hep-ph]].

[147] J. de Favereau *et al.* [DELPHES 3 Collaboration], JHEP **1402**, 057 (2014) doi:10.1007/JHEP02(2014)057 [arXiv:1307.6346 [hep-ex]].

[148] Y. L. Dokshitzer, G. D. Leder, S. Moretti and B. R. Webber, JHEP **9708**, 001 (1997) doi:10.1088/1126-6708/1997/08/001 [hep-ph/9707323].

[149] M. Wobisch and T. Wengler, In *Hamburg 1998/1999, Monte Carlo generators for HERA physics* 270-279 [hep-ph/9907280].

[150] J. M. Butterworth, A. R. Davison, M. Rubin and G. P. Salam, Phys. Rev. Lett. **100**, 242001 (2008) doi:10.1103/PhysRevLett.100.242001 [arXiv:0802.2470 [hep-ph]].

[151] S. H. Lim, C. Han, D. Kim, M. Kim, K. Kong and M. Park, arXiv:1609.06205 [hep-ph].

[152] G. Aad *et al.* [ATLAS Collaboration], JHEP **1411**, 118 (2014) doi:10.1007/JHEP11(2014)118 [arXiv:1407.0583 [hep-ex]].

[153] G. Aad *et al.* [ATLAS Collaboration], Eur. Phys. J. C **75**, no. 2, 82 (2015) doi:10.1140/epjc/s10052-015-3262-7 [arXiv:1409.8639 [hep-ex]].

[154] CMS Collaboration [CMS Collaboration], CMS-PAS-SMP-16-005.

[155] The ATLAS collaboration [ATLAS Collaboration], ATL-PHYS-PUB-2015-033.

[156] Larkoski, Andrew J. and Moult, Ian and Neill, Duff JHEP **1412**, 009 (2014) doi:10.1007/JHEP12(2014)009 [arXiv:1409.6298 [hep-ph]].

[157] Larkoski, Andrew J. and Moult, Ian and Neill, Duff JHEP **1605**, 117 (2016) doi:10.1007/JHEP05(2016)117 [arXiv:1507.03018 [hep-ph]].

[158] C. G. Lester, M. A. Parker and M. J. White, JHEP **0601**, 080 (2006) doi:10.1088/1126-6708/2006/01/080 [hep-ph/0508143].

[159] C. G. Lester, M. A. Parker and M. J. White, JHEP **0710**, 051 (2007) doi:10.1088/1126-6708/2007/10/051 [hep-ph/0609298].

[160] M. Burns, K. T. Matchev and M. Park, JHEP **0905**, 094 (2009) doi:10.1088/1126-6708/2009/05/094 [arXiv:0903.4371 [hep-ph]].

[161] P. S. B. Dev, D. Kim and R. N. Mohapatra, JHEP **1601**, 118 (2016) doi:10.1007/JHEP01(2016)118 [arXiv:1510.04328 [hep-ph]].

[162] D. Kim, K. T. Matchev and M. Park, JHEP **1602**, 129 (2016) doi:10.1007/JHEP02(2016)129 [arXiv:1512.02222 [hep-ph]].

[163] G. Aad *et al.* [ATLAS Collaboration], arXiv:0901.0512 [hep-ex].

[164] K. Agashe, R. Franceschini and D. Kim, Phys. Rev. D **88**, no. 5, 057701 (2013) doi:10.1103/PhysRevD.88.057701 [arXiv:1209.0772 [hep-ph]].

[165] C. Y. Chen, H. Davoudiasl and D. Kim, Phys. Rev. D **89**, no. 9, 096007 (2014) doi:10.1103/PhysRevD.89.096007 [arXiv:1403.3399 [hep-ph]].

[166] C. G. Lester and D. J. Summers, Phys. Lett. B **463**, 99 (1999) doi:10.1016/S0370-2693(99)00945-4 [hep-ph/9906349].

[167] R. Mahbubani, K. T. Matchev and M. Park, JHEP **1303**, 134 (2013) doi:10.1007/JHEP03(2013)134 [arXiv:1212.1720 [hep-ph]].

[168] W. S. Cho, J. S. Gainer, D. Kim, K. T. Matchev, F. Moortgat, L. Pape and M. Park, JHEP **1408**, 070 (2014) doi:10.1007/JHEP08(2014)070 [arXiv:1401.1449 [hep-ph]].

[169] M. Aaboud *et al.* [ATLAS Collaboration], JHEP **1609**, 173 (2016) doi:10.1007/JHEP09(2016)173 [arXiv:1606.04833 [hep-ex]].

[170] CMS Collaboration, CMS-PAS-B2G-16-021 (2016).

[171] V. Khachatryan *et al.* [CMS Collaboration], JHEP **1504**, 025 (2015) doi:10.1007/JHEP04(2015)025 [arXiv:1412.6302 [hep-ex]].